

**NISTIR 4973**

---

---

# A Computer Model of the Smoldering Ignition of Furniture

---

---

Henri E. Mitler  
George Walton

Building and Fire Research Laboratory  
Gaithersburg, Maryland 20899

QC  
100  
.U56  
4973  
1992



United States Department of Commerce  
Technology Administration  
National Institute of Standards and Technology



NISTIR-IR 00  
100  
1056  
1093  
1097  
1102

**NISTIR 4973**

---

---

# A Computer Model of the Smoldering Ignition of Furniture

---

---

Henri E. Mitler  
George Walton

September 1992  
Building and Fire Research Laboratory  
National Institute of Standards and Technology  
Gaithersburg, MD 20899



**U.S. Department of Commerce**  
Barbara Hackman Franklin, *Secretary*  
**Technology Administration**  
Robert M. White, *Under Secretary for Technology*  
National Institute of Standards and Technology  
John W. Lyons, *Director*



## Table of Contents

	<u>Page</u>
List of Tables .....	iv
List of Figures .....	v
Abstract .....	1
1. Introduction .....	1
2. Ignition Dynamics .....	3
2a. Surface Heat Source .....	3
2b. Heat Transfer .....	5
2c. Time to Ignition .....	7
2d. Pyrolysis of the substrate .....	7
2e. Gas Diffusion .....	9
2f. Boundary Conditions for Gases .....	10
2g. An Approximation to Oxygen Diffusion .....	12
3. Numerics .....	
3a. Introduction .....	16
3b. Boundary Conditions .....	18
3c. Air Gap .....	19
3d. Variable Grid .....	20
3e. Variable Thermal Properties .....	22
3f. Pyrolysis .....	22
3g. Time Integration .....	22
4. Experiments .....	24
4a. Experimental Arrangement .....	24
4b. Material Data .....	25
4b.1 Fabric .....	25
4b.2 Char .....	26
4b.3 Reaction kinetic parameters .....	26
4b.4 Heat of combustion .....	28
4b.5a Foam .....	28
4b.5b PU Foam kinetic parameters .....	28
5. Results and Discussion .....	29
5a. Inert Case .....	29
5b. Results with pyrolysis .....	29
6. Summary .....	33
7. References .....	35

Table of Contents (continued)

	<u>Page</u>
Appendix A Conduction Algorithm Tests .....	55
Appendix B TMPSUB2 User's Guide .....	64
Appendix C Analysis of numerical errors produced by having a runaway reaction rate .....	85
Appendix D Analysis of Ignition Experiment .....	89
Appendix E Thermophysical Data for Cotton .....	92

List of Tables

	<u>Page</u>
Table 1. Ignition delay times . . . . .	25
Table 2. Calculated vs experimental ignition delay times for the four fluxes . . . . .	32
Table 3. Surface temperatures which would be attained by the substrate at the measured ignition times if the substrate had been inert . . . . .	32

## List of Figures

	<u>Page</u>
Figure 1. One dimensional conduction . . . . .	37
Figure 2. Air gap heat transfer model . . . . .	38
Figure 3. Substrate coordinate system . . . . .	39
Figure 4. Schematic of heat source for ignition tests . . . . .	40
Figure 5. Flux profile from heat source, as measured by a total heat flux gauge . . . . .	41
Figure 6. Time required to ignite the fabric, for different (initial) heat flux exposures. Crosses correspond to the discussion in the text. Filled circles correspond to to a different set of experiments . . . . .	42
Figure 7. Peak surface temperatures of substrate as a function of time, for the four exposures . . . . .	43
Figure 8. Peak surface temperatures of substrate exposed to $Q = 25 \text{ kW/m}^2$ , as a function of $t$ , for a. Material assumed to be inert b. Thermal degradation only c. Oxidative pyrolysis as well d. Char oxidation also included, as well e. Only <u>one</u> reaction: oxidative pyrolysis . . . . .	44
Figure 9. Temperature and density of central cell (subscript 0), adjacent cells (subscript 1), and cells in next ring around center (subscript 2), as functions of time . . . . .	45
Figure 10. Temperature of central surface cell (i.e., peak temperature) for three different grid sizes: 1.25, 0.50, and 0.25-mm cubes. Char oxidation was purposely left out . . . . .	46
Figure 11. Peak temperature for the 25 and 34.5 $\text{kW/m}^2$ cases, assuming (a) no pyrolysis, and (b) all three pyrolytic reactions . . . . .	47
Figure 12. Peak temperature for the 18 $\text{kW/m}^2$ case, with the same assumptions as in Fig. 11 . . . . .	48

List of Figures (continued)

	<u>Page</u>
Figure 13. Peak temperature for the 18 kW/m <sup>2</sup> case, for several values of mean O <sub>2</sub> mass fraction, <math>\langle y \rangle</math> . . . . .	49
Figure 14. Peak temperature for the 18 kW/m <sup>2</sup> case, with various assumptions for the pyrolysis: Curve a, no pyrolysis curve b, "standard" pyrolysis; curve c, double the char oxidation rate; Curve d, double the oxidative pyrolysis rate; Curve e, 1.2 time the oxidative pyrolysis rate; Curve f, 1.1 times the oxidative pyrolysis rate . . . . .	50
Figure 15. Peak temperature as a function time, for all four cases, using the best set of input data . . . . .	51
Figure 16. Total heat flux impinging on gauge, with and without purge flow . . . . .	52
Figure 17. Calculated heat transfer coefficient, as a function of the temperature T <sub>g</sub> of the impinging purge gas jet . . . . .	53
Figure 18. Thermal conductivity of cotton as a function of temperature, as measured by different workers . . . . .	54



# A COMPUTER MODEL OF THE SMOLDERING IGNITION OF FURNITURE

Henri E. Mitler and George Walton

Building and Fire Research Laboratory  
National Institute of Standards and Technology

September 1992

## ABSTRACT

This paper describes a user-friendly computer model, TMPSUB2. This model calculates the temperature field throughout a solid (but porous) substrate which can undergo exothermic pyrolysis, when it is exposed to an arbitrary (localized) heat flux which can move uniformly, such as that of a smoldering cigarette. TMPSUB2 has successfully simulated the thermal runaway signifying smoldering ignition of the substrate when it is exposed to a set of external heating fluxes. The processes taken into consideration are three-dimensional heat conduction in the substrate, pyrolysis of the latter, and the diffusion of air into it at the top surface. TMPSUB2 also takes into account the fact that the substrate consists of two layers (a foam pad covered by a fabric), with the possibility of an air gap between them, up to three pyrolytic reaction steps, and with temperature-dependent thermophysical constants. TMPSUB2 solves the equations describing the physics and chemistry of the heating and ignition process numerically; the results have been compared with a set of ignition experiments, and have been found to be semi-quantitatively correct, both for the ignition temperature and for the time to ignition. Analysis of the experiments indicates that the substrate, which consists of a thin fabric layer over a thick foam padding, behaves as a thermally thin layer. Use of TMPSUB2 shows that smoldering ignition would result from a stationary hot spot of intensity and dimension simulating a quietly smoldering cigarette. A users' guide is included.

Key Words: Computer models; furniture fires; ignition; mathematical modeling; pyrolysis; smoldering

## 1. INTRODUCTION

Over 1600 people die each year (see ref.[1]) from fires started by smoking materials (cigarettes, matches, etc.), and many times that number are hurt and/or disfigured; most of those fires are established in upholstered furniture. As a result, Congress passed the Cigarette Safety Act of 1984; its goal was to determine whether safer (from the point of view of fires!) cigarettes were technically feasible. One of the tasks under that Act was to model mathematically the behavior of upholstered furniture and of the cigarette, when a smoldering cigarette is dropped onto it. The result was two prototype programs, TEMPSUB (for TEMPerature of a SUBstrate) and CIG25 (see ref [2]). One of the tasks under the Fire

Safe Cigarette Act of 1990 (P.L. 101-352) is to "Conduct laboratory studies on and computer modeling of ignition physics to develop valid, "user-friendly" predictive capability." In order to do this, two (new) models were to be developed: one for the ignition of the substrate (an advance over TEMPSUB), and another for the quiescent smoldering of a cigarette which is resting on the substrate (an improvement on CIG25). In this paper, the first model is described; the cigarette model will follow.

Consider what is involved in developing this computer model: we must simulate the behavior of a (typical) substrate when it is subjected to a heat flux. In order to do that, the physics and chemistry of the process must first be understood. It is then expressed as a set of equations describing the behavior; these equations must then be solved, with the appropriate data and boundary conditions. The solution method is numerical, and the data input is to a computer.

This program serves to calculate the temperature of the upholstered furniture as a function of time and position, when it is exposed to a prescribed heating flux. This flux can be highly peaked at a point, vary with time, and move at a constant (specified) rate over the top surface of the furniture, assumed to be horizontal. The radiative and convective heat losses from the surface are given correctly. If and when the temperature rate of rise at a given location suddenly "accelerates" to a value high enough that the surface glows (that is,  $T > 500^{\circ}\text{C}$  or so), we can say that smoldering ignition has occurred. The ambient oxygen level can be set at whatever value one wishes. The program will not tell us whether flaming ignition takes place. It also does not treat the case where the flux is applied in a crevice, such as is formed between the seat cushion and the seat back. The program does not take oxygen diffusion within the cushion explicitly into account; hence in certain threshold situations, where a small change in oxygen concentration determines whether ignition does or does not take place, the results are ambiguous and not to be trusted. Note that it is often difficult to obtain the needed kinetic and/or thermophysical parameters for the material; or, when available, to know how accurate they are. Therefore this caveat must also be made: even if the program were perfect, its results are only as good as the input parameters which are supplied. On the other hand, it should accurately reproduce (or predict) trends.

Here is a brief overview of the dynamics: For the purpose of this work, the "upholstered furniture" will be taken to be the flat, horizontal cushioned seat -- that is, the substrate is a cushion consisting of fabric-covered foam padding. Assume that there is a localized source of heat on the cushion. The temperature of the cushion will then rise, locally. In order for ignition to occur, a number of conditions must be met; the principal one is that the temperature of the cushion must rise, in this region, to a critical temperature for the initiation of smoldering. This is generally referred to as the ignition temperature. It will be shown, however, that this temperature is not unique, even for a well-defined material: it depends also on the magnitude of the incident (igniting) flux. The temperature of the substrate will be calculated, nevertheless; for, as will be shown, the temperature history will determine whether ignition does or does not take place.

In order to calculate the temperature as a function of time and position, it is necessary to know the heat flux from the cigarette (as it is affected by its contact with the chair), how this heat flux distribution moves with time, and how the seat cushion responds to that "insult." We wish to find whether the cushion will in fact reach its ignition temperature, to begin with. It may be necessary to know some other things as well, such as the effect of the presence of the cigarette on the oxygen concentration in the cushion; that will be dealt with at a later time. Thus the first task is to examine the thermal response of the cushion to a specified flux distribution. This is done in the next section. In section 3, the numerical solution method is presented, and some of the physics is revisited in this (numerical) context. In section 4 we discuss a set of experiments where a mock-up was ignited, give the measured ignition times, and give the input data required to make computer runs. The results of these runs are given and then

discussed in Section 5, validating the model to some degree. Section 6 summarizes the work. For the reader interested in a more extensive discussion, see the references cited here, especially the bibliography in [2]. A copy of the program on disk may be obtained from the authors, as well as a listing of the program and the program itself.

## 2. IGNITION DYNAMICS

The equations describing the relevant physical processes taking place in the substrate will be written in this section. They will mostly be written in general form to start, and then particularized to our problem. The assumptions made in the model are summarized and displayed in Table 1.

Table 1. What is, and is not, in the substrate model

---

### IN

- two porous layers with an air gap
- 3-d heat conduction
- variable (prescribed) thermophysical properties
- correct (nonlinear) boundary conditions
- endothermic (non-oxidative) pyrolysis
- exothermic (oxidative) pyrolysis
- char oxidation
- arbitrary (prescribed) moving heat source
- variable grid on a moving coordinate system
- (approximate) radiative heat transfer within the material
- Impinging air flow, when wanted

### NOT IN

- oxygen diffusion
  - melting and/or regression of the foam
- 

The most appropriate place to begin (perhaps) is with the heat source; that will be described in subsection 2a. The equation describing heat diffusion in a solid is given and discussed in subsection 2b; it is solved for a very simple, special case in section 2c, for later use. Pyrolysis of the substrate is discussed in section 2d, and the diffusion of gases (a process very similar to the diffusion of heat) in section 2e. The principal gas of interest here is oxygen. Although we do not explicitly include its movement in the substrate, those expressions are necessary for estimating the rate at which oxygen can enter the reactive zone in the substrate, from outside. That boundary condition and its consequences is discussed in subsection 2f.

### 2a. Surface Heat Source

The process is initiated by external heating of the surface. Thus, it is necessary to specify the heat gains at the bounding surfaces of the cushion. The cushion is assumed to be a rectangular parallelepiped; therefore a Cartesian coordinate system is employed. For the top surface, we have: first, the localized heat flux from the glowing tip of the cigarette or other heat source; the flux consists of two parts, one due to convection ( $\phi_c$ ) and one due to radiation ( $\phi_r$ ):

$$\phi_{in} = \phi_c + \phi_r \quad (1)$$

$\phi_{in}$  is the heating flux reaching the surface. For a cigarette, these fluxes are strong functions of position, since the glowing tip is only a few millimeters in extent. With this formulation,  $\phi_r$  can be expressed in the approximate form

$$\phi_r \sim \Omega \epsilon_{cig} \sigma T_{cig}^4 + (1 - \Omega) \sigma T_a^4 \quad (2)$$

where  $\Omega = \Omega(r)$  is the shape, or view, factor of the cigarette as seen by the substrate at the point  $r$ . It is only approximate in this form, because the cigarette surface temperature,  $T_{cig}$ , varies strongly with position.

The convective flux is given by

$$\phi_c(x, y, t) = h[T_{cig}(x, y, t) - T_s(x, y, t)] \quad (3)$$

where  $h$  is the heat transfer coefficient,  $T_s$  is the surface temperature of the substrate, which is explicitly shown to be a function of position and time, and where  $T_{cig}$  is the cigarette surface temperature, also a function of position and time. **It is important to point out here that in this version of the substrate model, the source flux must be specified by the user.**

It is equally necessary to specify the heat losses. If the existence of the cigarette is neglected for the moment, so that the view factors need not be considered, then

$$\phi_{out} = h(T_s - T_a) + \epsilon \sigma T_s^4 \quad (4)$$

where the first term is the convective cooling term and the second is the radiative cooling term. In contrast to the source term, these losses are explicitly included in the program. Here, the dependence of  $T_s$  on  $x$ ,  $y$ , and  $t$  has not been shown explicitly.  $\epsilon$  is the emissivity of the surface and  $\sigma$  is the Stefan-Boltzmann constant (note: we have used  $\epsilon$  where sometimes  $\alpha$ , the absorptivity of the surface, should be used. When there is thermal equilibrium between the radiation field and the hot surface, then  $\alpha = \epsilon$ . We have assumed the latter, for simplicity). Evidently, the loss rate from the cushion surface increases as it heats up.  $h$  is determined by the laws of fluid flow, as well as the thermal properties of air; the simplest way to find  $h$ , however, is to use well-known expressions, usually derived from correlations. This will be further discussed below.

Along with the partial differential equation (12), we must have boundary conditions: for the top surface, the net flux entering the surface at each point is connected to the net flux according to

$$\phi_{net}(x, y, t) = -\kappa \left( \frac{\partial T(x, y, z, t)}{\partial z} \right)_{z=0} \quad z=0, \quad t>0 \quad (5)$$

where

$$\phi_{net} \equiv \phi_{in} - \phi_{out} \quad (6)$$

When the cigarette lies on the substrate, the mean convective heating flux over the heating region is given by

$$\phi_c = h_{in}(\bar{T}_{cig} - T_s) \quad (7)$$

If  $h_q$  is the heat transfer coefficient for quiescent air, then the surface heat loss for the areas away from the cigarette is

$$\phi_{out} = h_q(T_s - T_a) \quad (8)$$

The boundary condition is greatly simplified if we can say that Eq(8) is valid over the entire surface. That is readily achieved by using the model convective heating flux  $\phi_c^*$ ,

$$\phi_c^* = h_{in}(\bar{T}_{cig} - T_s) + h_q(T_s - T_a) \quad (9)$$

$h_{in}$  is found as follows: the mean initial convective flux from a cigarette was measured to be 37 kW/m<sup>2</sup>. Taking the mean value of the cigarette surface temperature to be about  $\langle T \rangle_{cig} \approx 450^\circ\text{C}$ , the mean heat transfer coefficient in this area is  $h_{in} \approx (37000/430) = 86 \text{ W/m}^2\text{-K}$ .  $h_q$  is found from Table 7-1 of ref [2a]: the Nusselt number for a heated, horizontal, upward-facing surface is

$$Nu = 0.54(Ra)^{1/4} \quad (10)$$

where Ra is the Rayleigh number. Since  $h = \kappa Nu/L$ , where L is the characteristic dimension of the surface, we find

$$h = 0.54 \kappa \left[ \frac{g \beta (T_s - T_a)}{\alpha \nu L} \right]^{1/4} \quad (11)$$

where  $\beta$  is the volumetric coefficient of (gas) expansion. Taking the value for  $T_s = 500 \text{ K} \approx 227^\circ\text{C}$  as an approximate mean temperature of the surface, and  $L = 7 \text{ mm}$ , we find

$$h_q = 9.7 \text{ W/m}^2\text{-K}$$

For the other surfaces, the boundary conditions (b.c.) can be expressed in different forms, depending on whether the slab for which we are making calculations is exposed to the air, or is embedded within the cushion. If the slab were the entire cushion -- that is, the other five surfaces are exposed to the air, then the b.c. would be that the heat fluxes  $\kappa \partial T / \partial x$ ,  $\kappa \partial T / \partial y$ ,  $\kappa \partial T / \partial z$ , are given by terms of exactly the same form as (4), except that h is different for the vertical and the downward-facing horizontal surface. On the other hand, the numerical calculation we are using makes using the entire cushion prohibitively large. We therefore consider a subsection abstracted from the whole cushion, and the other five faces are surrounded by more foam. If that foam were a perfectly insulating material, then the b.c. at those faces is the adiabatic condition; that is, no flux crosses the surfaces:  $\kappa \partial T / \partial x = \kappa \partial T / \partial y = \kappa \partial T / \partial z = 0$ . This eliminates any heat losses from the slab, and makes the calculated temperatures somewhat higher than they really are. A simpler b.c. is to assume that the temperature at the five faces is constant and unchanging, remaining at the original (usually ambient) temperature. This produces a larger temperature gradient than actually prevails, and errs in the opposite direction. That is the default b.c. used in the calculation, but which of the two b.c.'s is used is determined by an input parameter.

## 2b. Heat Transfer

The partial differential equation which describes the conduction of heat in a solid, when there is no radiation heat transfer, does so by giving the rate of change of temperature at every point within the solid. It is (see, for example, [3])

$$\rho \frac{\partial cT}{\partial t} = \text{div}(\kappa \text{grad} T) + S \quad (12)$$

where  $T$ , which is a function of position and of time, is the variable for which we are trying to find a solution. The other symbols in this equation are:  $\rho$  is the density of the solid,  $c$  its specific heat,  $\kappa$  its thermal conductivity, and  $S$  is any volumetric heat source or sink.  $\rho$ ,  $c$ ,  $\kappa$ , and  $S$  may vary with position and with  $T$ . Because these may vary in Eq(12), it is conceptually simple to consider a substrate which consists of layers of material. Indeed, it will be straightforward to implement this in practice, as well. Note that because we only have derivatives of  $T$ ,  $T$  need not be the absolute temperature: it may be taken to be that relative to a convenient reference temperature. In other places, such as in Eq(2), it must be taken to be absolute (i.e., in degrees Kelvin).

The first term on the right-hand side describes the diffusion of heat in the solid. If there is any release of heat -- usually by combustion -- at the (interior) point in question, it is given by  $S(x,y,z,t)$ . A general expression for  $S$  is

$$S = \sum_i R_i H_{ci} + L_v \frac{\partial \rho}{\partial t} \quad (13)$$

where  $R_i$  is the reaction rate (in  $\text{kg}/\text{m}^3\text{-s}$ ) and  $H_{ci}$  is the heat of combustion (in  $\text{J}/\text{kg}$ ), for the  $i$ th reaction. If there is endothermic pyrolysis or evaporation, we have the last term on the right-hand side as well, where  $L_v$  is the latent heat of evaporation or pyrolysis. An explicit expression for  $R_i$  will be given in Section 2b.

Since the furniture (apart from the frame) consists of a fabric-covered pad, it is clear that the program must take at least two layers (with different properties) into account. Therefore the program was written so as to permit different values for the relevant thermophysical constants  $\rho$ ,  $c$ , and  $\kappa$  in each layer. In fact, generally there is not perfectly intimate thermal contact between the fabric covering and the padding; there is a small but sometimes significant intervening air gap. Normally, one would place a node within this gap, in order to take a third layer into account; because of the thinness of the gap, and other technical difficulties, however, a different treatment of the effect of this air gap has been devised: the gap can be represented in terms of its "thermal resistance" (see Section 3c.). This has been programmed and successfully tested.

In writing Eq.(12), we have made the simplifying assumption that the cushion is totally opaque; that is, there is no radiative transfer of heat through the cushion. If there were, the equation describing heat transfer through the solid would become still more complicated. However, the fabric and foam can each be thought of as porous, consisting of solid parts interspersed with void spaces. Then taking forward radiation transfer in those spaces, it is possible to incorporate a first approximation to (one-d) radiation transfer, as shown by Kunii [4]

$$\kappa(T) = (1 - \Phi^{2/3})\kappa_s + \Phi^{1/3}(\kappa_g + 2h_r D_p/3) \quad (14)$$

where  $\Phi$  is the void fraction, and  $\kappa_s$  and  $\kappa_g$  are the solid and gas-phase thermal conductivities, respectively; they are each functions of  $T$ .  $D_p$  is the mean pore diameter, and

$$h_r = 4\epsilon\sigma T^3 \quad (15)$$

Eq.(14) was Eq.(5-50) in ref[2]. Finally, we must note that at a given temperature, the thermal conductivity is proportional to the density (also see Section 3e):

$$\kappa(\rho) = (\rho/\rho_a)\kappa(\rho_a) \quad (16)$$

### 2c. Time to Ignition

An experimental test for the time to ignition is described in Section 4. We can readily make an order-of-magnitude estimate for this time, based on Eq(12): For the very special case that the substrate is initially at the uniform temperature  $T_o$ , that it is homogeneous, isotropic, inert, and semi-infinite, that the thermophysical characteristics  $\rho$ ,  $c$ , and  $\kappa$  of the material are independent of the temperature, and (finally) that the problem is one-dimensional (i.e., the incident flux is the same everywhere on the plane  $z = 0$ , resulting in the slab being subjected to the uniform net heating flux  $\phi_{net}(t)$ ), then Eq(12) can be solved analytically and explicitly, and it can be shown ([3], p.76) that the surface temperature is given by

$$T_s(t) = T_o + \frac{1}{\sqrt{\pi\kappa\rho c}} \int_0^t \frac{\phi_{net}(t') dt'}{\sqrt{t-t'}} \quad (17)$$

For the still simpler (unrealistic) case  $\phi_{net} = \text{constant}$ , this can be immediately integrated, and we obtain

$$T(t) = T_o + \frac{2\phi_{net}\sqrt{t}}{\sqrt{\pi\kappa\rho c}} \quad (18)$$

When the left-hand side reaches the ignition temperature  $T_{ig}$ , the time elapsed must be the time in the right-hand side of the equation, and

$$t_{ig} = \frac{\pi\kappa\rho c}{4} \left( \frac{T_{ig} - T_o}{\phi_{net}} \right)^2 \quad (19)$$

Although not a single one of the simplifying assumptions required to obtain Eq(19) is valid, this expression is nevertheless very useful as a guide to the form of the dependence of  $t_{ig}$ . In particular, we will use Eq(19) in order to make sense out of the experimental observations, in Section 5a.

(We can, if desired, get a somewhat more realistic result by relaxing one of the assumptions above: it is possible to write, starting with Eq.(17), an explicit expression for  $T_s(t)$  for the case where the net flux is not constant, but results from some impressed external flux, diminished by a Newtonian (i.e., linear) cooling loss; that is, where we can write  $\phi_{loss} = h^*(T_s - T_s)$ ; see ref[5]).

### 2d. Pyrolysis of the substrate

As described above, we assume that the substrate consists of a thin fabric covering a relatively thick foam pad, with a very thin air gap between them. Each of the two materials will heat up and can pyrolyze. In this section we describe how these reactions are calculated. Pyrolytic reactions can generally be expressed in the Arrhenius form

$$R_p(T, \rho_f, \rho_o) = A \rho_f^m \rho_{ox}^n e^{-E_A/RT} \quad \text{kg/m}^3 \cdot \text{s} \quad (20)$$

where  $\rho_f$  is the density of the fuel and  $\rho_{ox}$  that of oxygen;  $E_A$  is the activation energy for the reaction, and  $R$  is the universal gas constant (not to be confused with the reaction rate  $R_p$  in Eq(20)). It is sometimes convenient to define an "activation temperature"  $T_A$ :

$$T_A \equiv E_A/R \quad (21)$$

In the remainder of the paper,  $R$  is used only to represent a reaction rate. All the quantities in Eq.(20) except the preexponential factor  $A$  are at the location  $(x,y,z)$  within the porous solid and at the time  $t$ ; this dependence is not shown explicitly in order to minimize the complexity of the expression. Similarly, the subscript  $i$ , corresponding to  $i$ th "reaction" has been suppressed from  $R$ ,  $A$ ,  $\rho_f$ ,  $m$ ,  $n$ , and  $E_A$ . If the reactions were truly elemental Arrhenius reactions, then  $m = n = 1$ . However, Eq. (20) is really a model equation, and therefore  $m$  and  $n$  are purely empirical parameters (just as  $A$  and  $E_A$  are), and need not be integers.

Oxidative as well as non-oxidative pyrolysis (thermal decomposition) of materials have been included. The former reactions are generally exothermic, while the latter are generally endothermic. There may be several oxidative reactions as well as several non-oxidative ones; char oxidation, when it takes place, is the last step. In this model a maximum of three reactions is permitted for each material. The oxidative reactions are exothermic; we assume that the rate of each step (reaction) is adequately described by an Arrhenius equation of the form (20).

It had been hoped that the different pyrolysis steps take place at sufficiently different temperatures, that the reaction sequence for the ignition of the fabric could be taken to consist of a small number of steps which follow each other sequentially. That would correspond to the equations taking the form

$$R_p = \sum_i R_{pi} = \sum_i A_i (\rho - \rho_i)^{s_i} \rho_{ox}^{n_i} \exp(-T_i/T) \quad (22)$$

where  $\rho_i$  is the density of the fuel at the end of the  $i^{\text{th}}$  reaction step. When the reaction produces a gaseous species which escapes, the reaction rate is given by

$$R_p = -\frac{\partial \rho}{\partial t} \quad (23)$$

More generally, if species  $i$  is reacting and producing species  $j$ , then

$$\frac{\partial \rho_i}{\partial t} = -R_i = -\frac{\partial \rho_j}{\partial t} \quad (24)$$

We will here discuss only the pyrolysis of the fabric, which is of principal interest: when smoldering ignition is produced, it is almost always first initiated in the fabric. Pyrolysis of the foam is discussed briefly in Section 4b. The fabric of particular interest is cotton duck; cotton is principally cellulose.

Analysis of the reaction kinetics of a cellulosic paper by Kashiwagi and Nambu [6] showed that it could be described by three reactions, all of which will proceed simultaneously (though obviously at different rates). That means that the equations describing the creation and destruction of different fuel species must

be included. Virgin material goes to char, via two pathways: degradation and oxidative pyrolysis; each gram produces  $n_c$  grams of char. The char then goes to ash, via char oxidation; each gram of char produces  $n_a$  grams of ash. Thus one gram of material produces  $n_a n_c$  grams of ash. The governing equations are:

$$\dot{\rho}_v = -R_d - R_{op} \quad (25a)$$

$$\dot{\rho}_c = n_c(R_d + R_{op}) - R_{co} \quad (25b)$$

and

$$\dot{\rho}_a = n_a R_{co} \quad (25c)$$

The density of the solids is

$$\rho_s = \rho_v + \rho_c + \rho_a \quad (25d)$$

Hence

$$\dot{\rho}_s = -(1 - n_c)(R_d + R_{op}) - (1 - n_a)R_{co} \quad (25e)$$

The subscripts denote:

a = ash	op = oxidative pyrolysis
c = char	s = solid
co = char oxidation	v = virgin material
d = degradation	

Besides the surface heat source described in section 2a, there are also internal heat sources (and sinks), given by Eq(13). The heats of combustion must be supplied by the user of the model; those for cotton are given in sections 4b.3 and 4b.4. The global kinetic constants given by Kashiwagi and Nambu are listed in Section 4.b.1. If the reaction rate of one or more exothermic reactions becomes high, for any reason, the rate at which energy is being generated will exceed the rate at which it is lost, and a "thermal runaway" will ensue (very similar to a chain reaction!). During the runaway, the rate of pyrolysis (and of heating) is limited by the availability of oxygen. Since  $O_2$  has 0.001 times the density of the local fuel, it would immediately be exhausted, but for the supply which (a) diffuses in from adjoining cells, and that which (b) diffuses in (or is convected in) from the surface.

## 2e. Gas Diffusion

As oxygen is depleted in the regions where combustion (oxidative pyrolysis, char oxidation) is taking place, the concentration gradient which results will induce diffusion of oxygen into those regions, from the surface as well as from adjacent, oxygen-rich regions, assuming the medium is porous and permits diffusion. Similarly, the gaseous (and other) products which are generated -- mainly  $CO_2$  -- build up in local concentration, and diffuse away.

The equations which describe the rate of change of species concentration are analogous to Eq. (12) for the diffusion of heat; assuming no convection, the  $i$ th species density is governed by

$$\frac{\partial \rho_i}{\partial t} = \text{div}(D_{i0} \text{grad } \rho_i) + S_i \quad (26)$$

where  $D_{i0}$  is the diffusion coefficient for species  $i$  in the background "o", and  $S_i$  is the source/sink term.

If the diffusion coefficient increases with  $T$ , as it normally does, then the  $\text{CO}_2$  diffusion, for example, will take place preferentially towards the hot regions -- that is, towards the surface. The migration of gases is expected to have a minor effect on the heat transfer, and hence on the temperature distribution, from this effect. However, the diffusion of oxygen is important: the rate at which oxygen enters the reacting region sets the limit on the reaction rate.

A porous medium is one consisting of solid particles embedded in a gaseous medium. Put in a different way, a gas molecule cannot penetrate any of the solid phase, but is able to traverse the entire medium, either because of a pressure difference, or merely from the "random walk" which constitutes diffusion. The diffusivity of a gas species in such a medium is really the diffusivity of those gas molecules through a gaseous medium consisting of the same or some other gas, where the solid volumes are excluded. That is the **effective** diffusivity.

It has been found experimentally (Szekely, ref[7]) that, approximately,

$$D_{eff} = D_o \Phi^n \quad (27)$$

where  $\Phi$  is the fractional void space; this is also referred to as the "porosity" in the literature. The relationship is strongly dependent on the structure of the (granular) material; thus, Fig. 2.4 from ref [7] shows that for particles of mica,

$$D_{eff}/D_o = \Phi^{10.3} \quad (27a)$$

whereas for sand, a bed of glass spheres, carborundum powder, and table salt,

$$D_{eff}/D_o = 0.677 \Phi^{1.18} \quad (27b)$$

for  $\Phi < 0.7$ . As shown in Appendix E,  $\Phi \approx 0.6$  for the cotton fabric that will be our main focus of interest; hence Eq.(27b) is the relationship to be used.

Here  $D_o$  is the diffusivity of  $\text{O}_2$  in  $\text{N}_2$ . From Eq.(16.3-1) of Bird et al (ref [8]), we find that for  $\text{O}_2$  in  $\text{N}_2$ , the temperature dependence is

$$D_o(T) = 0.199 \left( \frac{T}{293.16} \right)^{1.823} \text{ cm}^2/\text{sec} \quad (28)$$

## 2f. Boundary Conditions for Gases

There are two cases of interest: first, when the air above the substrate is quiescent, and second, when -- as was the case in the experiment to be described in Section 4 -- there is a stream of air impinging on the substrate. We first obtain a general expression:

When the air above the substrate is quiescent, and there are oxidative reactions taking place in the substrate, the concentration of oxygen molecules in the air decreases towards the surface, through a boundary layer. The maximum possible reaction rate is obtained by assuming  $y_s = 0$ , as can be seen from Eq(29). On the other hand, this is clearly not possible, since we must have a finite concentration at the surface in order to get any reactions at all. It is possible to obtain a value for  $y_s$  analytically, if one makes the simplifying assumptions of an isothermal substrate and a first-order reaction rate (ref [8a]).

Mass transfer is a (molecular) transport phenomenon, just as is heat (momentum) transfer. Thus, analogous to the first term on the right-hand side of Eq.(4), the mass transfer of oxygen across the surface of the solid can be written as

$$\dot{m}_{O_2}'(x,y) = k_{gas}[Y_a - Y_s(x,y)] \quad (29)$$

where  $Y_a$  is the ambient oxygen mass fraction and  $Y_s$  that at the solid surface; the  $x,y$  dependence of the latter has been put in explicitly in order to emphasize the origin of the spatial dependence of  $\dot{m}_o'$ .

The velocity at which oxygen enters the surface is

$$V_o = D \left( \frac{\partial Y}{\partial x} \right)_s = \gamma (Y_a - Y_i) \quad (30)$$

(see ref[2], p.159-160) where  $D$  is the diffusion coefficient inside the solid. Thus

$$k_{gas} = \rho_a \gamma \quad (31)$$

In TMPSUB (see [2], Eq.(5-64), from ref [9]) the following equation was used:

$$\gamma_b = 6.38 \times 10^{-3} \left[ \frac{T^{2.75} (T - T_a)(T + 123.6)}{R T_a} \right]^{1/4} \quad \text{cm/sec} \quad (32)$$

On the other hand, in this paper we obtain  $\gamma$  in a different way; we will afterwards use Eq(32) in order to compare the results. The way  $\gamma$  is obtained is as follows: Because of the similar origin of mass and heat transfer, one can often use the Reynolds-Colburn analogy [10]. It is not difficult to show, from the treatment in Chap.3 of [10], that the Reynolds-Colburn analogy leads to

$$\gamma = \frac{h Pr^{2/3}}{\rho c_p Sc^{2/3}} \quad \text{m/sec} \quad (33)$$

where  $h$  is the heat transfer coefficient appropriate to the problem,  $Pr$  is the Prandtl number,  $Sc$  is the Schmidt number ( $Sc = \nu/D$ ), and  $\nu$  is the kinematic viscosity.

Case A. Quiescent air.

Here we have

$$h = \kappa Nu/l_c \quad (34)$$

where  $\kappa$  is the thermal conductivity,  $l_c$  is a characteristic dimension for the problem, and  $Nu$  is the Nusselt number. We can thus rewrite Eq.(33) as

$$\gamma = \frac{\alpha}{l_c} Nu \left( \frac{Pr}{Sc} \right)^{2/3} \quad (35)$$

In quiescent air, there is a constant movement of molecules in all directions; the flow in any one direction is exactly compensated by the flow in the opposite direction, normally. If, however, the gas is near a boundary which "absorbs" some of these molecules (as is the case for oxygen impinging on a reactive

substrate) then evidently the return flow is smaller, and hence the impinging flow is not completely nullified. The result is that there is a gradual decrease in the concentration of those molecules as the surface is approached. This region is referred to as the "boundary layer."

The quantities in Eq.(35) are to be evaluated at some characteristic (mean) temperature of the boundary layer. That temperature can be taken to be the mean between  $T_a$  and  $T_s$ . For quiescent air, with the surface horizontal and facing upward,  $l_c$  is the boundary layer thickness. The expression for the Nusselt number is given in section 2a.

### Case B. Impinging air

The Nusselt number for this case is given by Eq.(D10), Appendix D. Inserting that into Eq.(35), we obtain

$$\gamma = 0.767 \frac{\alpha}{l_c} \sqrt{Re} Pr^{1.07} Sc^{-2/3} \quad (36)$$

where  $\alpha$  is the thermal diffusivity of air,  $Re \equiv u_o l_c / \nu$  is the Reynolds number and  $u_o$  is the incoming velocity of the impinging flow.

We now show that when oxygen consumption is significant, it takes place in a very narrow layer; this is analogous to the flame sheet approximation for combustion in air. As a result, we may take the concentration of oxygen in that layer to be some appropriate average value, rather than having to actually program in the species diffusion equations, via Eq(26).

### 2g. An Approximation to Oxygen Diffusion

In this section, it is shown that a reasonable approximation to the overall reaction rate can be obtained without explicitly solving the gas diffusion equation, Eq.(26), for the diffusion of oxygen in the substrate. This is the approximation made in the model.

In the experiment to be discussed in Section 4, a jet of air is directed downward at the substrate. Hence there is no boundary layer in this case, and the oxygen concentration just outside the surface is 21%. When the reaction rate is low, the oxygen concentration in the top of the substrate will not be much affected by the slow reactions. When the reaction rate becomes high, on the other hand, the mean oxygen concentration in that thin layer becomes low; it cannot get too low, however, since (as discussed in Section 2f), the reaction rate would then fall. Hence a quasi-steady state is established. Thus, in the "runaway" phase, the reaction rate must be given by the boundary condition Eq(29).

We will now argue that when significant oxidative pyrolysis is taking place,

- (a) taking a constant value for the oxygen concentration ( $[O_2]$ ) in the substrate is a valid approximation,
- (b) most of the pyrolysis occurs in the surface layer, and that therefore
- (c) we obtain an adequate approximation to the pyrolysis rate, without explicitly including the oxygen diffusion equations:

When the surface temperature is relatively low, there is negligible pyrolysis, and the oxygen distribution  $[O_2](x)$  in the substrate is approximately uniform. When  $T_s$  has risen to the point that perceptible pyrolysis is taking place at and near the surface, the  $[O_2]$  profile in the substrate dips as the surface is approached from below (i.e., from within); it must reach a minimum and then rise again at the surface,

because of the diffusion of oxygen from outside. When the temperature reaches values so high that  $[O_2]$  is pulled down to negligible values near (but not at) the surface, the principal source of oxygen in the reaction zone is from the air diffusing in from the surface; the region where there is significant oxidative reaction is then highly localized near the surface, with  $[O_2]$  being highest at the surface, and falling rapidly until it reaches negligible values. The characteristic oxygen penetration distance is  $\delta$ , and it is clear that  $\delta$  is a steeply falling function of  $T$ . (At some further distance in, the oxygen must diffuse towards the surface from other (deeper, or peripheral) parts of the porous substrate, because of the concentration gradient, so that the profile must rise again as we go deeper -- it can do so because at that depth the temperature has fallen sufficiently to "freeze out" the (oxidative) reaction rate -- i.e., it is negligibly small).

Suppose that  $T_s$  is high enough to drive  $[O_2]$  to near-zero at some depth. Then we may write, crudely,

$$Y(x) \sim Y_s e^{-x^2/\delta^2} \quad (37)$$

with  $Y_s$  = surface value of  $[O_2]$ , and  $\delta$  = characteristic penetration depth. If we write the reaction rate in the form

$$R[x, T(x)] = Y(x)^n F[x, T(x)] \equiv Y^n G(x) \quad (38)$$

then the total reaction rate per unit area is

$$\dot{m}'' = \int_0^\infty Y(x)^n G(x) dx \quad (39)$$

where  $G(x)$  is a fairly steep (decreasing) function of  $x$ . We may further write (still very crudely)

$$G(x) \sim G_0 e^{-x^2/\theta^2} \quad (40)$$

Then

$$\dot{m}'' \sim \int_0^\infty Y_s^n e^{-nx^2/\delta^2} G_0 e^{-x^2/\theta^2} dx = G_0 Y_s^n \frac{\sqrt{\pi}}{2} \left( \frac{1}{\theta^2} + \frac{n}{\delta^2} \right)^{-1/2} \quad (41)$$

We can also use the mean-value theorem, and write the integral in Eq(41) as

$$\int_0^\infty \bar{Y}^n G_0 e^{-x^2/\theta^2} dx = \bar{Y}^n G_0 \theta \sqrt{\pi}/2 \quad (42)$$

Then

$$\bar{Y}^n = Y_s^n \left( 1 + \frac{n\theta^2}{\delta^2} \right)^{-1/2} \quad (43)$$

We now need an estimate for  $\theta/\delta$ . Clearly, the reaction rate must be significant for a distance comparable to the penetration depth  $\delta$ : else, if the reactions "froze" before  $[O_2]$  becomes negligible,  $[O_2]$  would not fall below some appreciable value. Moreover, the reaction rate cannot be significant below that depth, precisely because there is so little oxygen below. Thus  $\theta \approx \delta$ . For  $n$ , we take  $n_0 = 0.5$ , as given in [6]. Then Eq.(43) yields

$$\bar{Y} = 2Y_s/3 \quad (44)$$

Next, consider the effect of discretizing the equations (see section 3). If  $\delta > \Delta x$ , then assuming that the reaction takes place in the top cells only, clearly underestimates the reaction rate. However, when  $\delta$  is

large, the total reaction rate is very low. That is, while the fractional error is large, the absolute error is small, and (we shall show) typically negligible.

Assume, for the sake of simplicity, only one oxidation reaction. Assume, also, that the temperature and reaction rate are uniform in a thin sheet of depth  $\delta$  at the surface, where  $T$  is maximum (this is essentially what is implicitly assumed in the numerical calculation). Then if the stoichiometric fuel/oxygen ratio is  $r$ , the fuel burnup rate is

$$R\delta = \dot{m}_f'' = r \dot{m}_{ox}'' \quad (45)$$

where  $R$  is the reaction rate ( $\text{g/cm}^3\text{sec}$  or  $\text{kg/m}^3\text{s}$ ). If  $\delta$  is greater than the thickness of the surface cell, then evidently the reaction rate in the top layer is limited to  $R\Delta z$ ; whereas if  $\delta < \Delta z$ , Eq.(45) gives the limit. Thus the reaction rate in the top cell is

$$R_{\text{top}}\Delta z = \min[R\Delta z, r \dot{m}_{ox}''] \quad \text{g/cm}^2\text{-sec} \quad (46)$$

Note that when the reaction rate is so high that  $\delta < \Delta z$ , the concentration at the bottom face of the top cell(s) is close to zero; therefore a reasonable value to take for  $[\text{O}_2]$  in the cell is on the order of the mean value, 11%, (or 0.12 for the mass fraction); or, according to Eq.(44),  $\langle Y \rangle \approx \frac{2}{3}(0.2318) = 0.15$

We now make a calculation to find a typical value for  $\delta$ . As is clear from Eq.(45), we must begin by calculating a reaction rate  $R$ . In order to find  $R$ , we must anticipate some results from section 4b.3: using Eqs(79) and (80), we find that

$$R_{\text{op}} = \rho_v k_{\text{op}} = \rho_v 1.5 \times 10^{14} Y^{0.5} (W_d/W_o)^{1.3} \exp(-160/RT)$$

and

$$R_{\text{co}} = \rho_c k_{\text{co}} = \rho_c 3.4 \times 10^{11} Y^{0.78} (W_c/W_o) \exp(-160/RT)$$

The meaning of the subscripts is made clear in the list below Eq.(25e). These rates are in  $\text{kg/m}^3\text{-min}$ . We must choose characteristic values for  $\rho_v$ ,  $Y$ ,  $W_d/W_o$ ,  $\rho_c$ ,  $W_c/W_o$ , and  $T$ , in order to get estimates. Reasonable values are

$$W_d = W_o/2, \quad W_c = W_o/4, \quad \text{and} \quad Y \approx 0.11$$

For  $\rho_v$  and  $\rho_c$ , we assume that the volumes are unchanged, so that

$$\rho_v/\rho_o = W_d/W_o \quad \text{and} \quad \rho_c/\rho_o = W_c/W_o$$

Finally, we take  $\rho_o = 1560 \text{ kg/m}^3$ . We then find that

$$k_{\text{op}} = 2.02 \times 10^{13} \exp(-160/RT) \text{ min}^{-1}$$

and

$$k_{\text{co}} = 1.52 \times 10^{10} \exp(-160/RT) \text{ min}^{-1}$$

The universal gas constant  $R = 8.31447 \text{ J/mol-K}$ , so that the activation temperature for both reactions is  $T_A = 160,000/R = 19244 \text{ K}$ . For a temperature in the vicinity of the ignition temperature, say,  $400^\circ\text{C} = 673.16 \text{ K}$ , we then have

$$k_{op} = 7.77 \text{ min}^{-1} \quad \text{and} \quad k_{co} = 0.00584 \text{ min}^{-1},$$

yielding

$$\begin{aligned} R_{op} &= \rho_v k_{op} = 101 \text{ kg/m}^3\text{-s} \\ \text{and} \quad R_{co} &= \rho_c k_{co} = 0.038 \text{ kg/m}^3\text{-s}. \end{aligned}$$

Thus at 400°C, with these assumptions for  $\rho_v$  and  $\rho_c$ , oxidative pyrolysis takes place more than 2600 times faster than does char oxidation, and we may therefore take

$$R = R_{op} = 101 \text{ kg/m}^3\text{-s}$$

Next, we need to have the rate at which oxygen enters the medium,  $\dot{m}_{ox}''$ . Eqs(29) and (31) give the required value. For the ignition experiment, the appropriate expression to use to find  $\gamma$  is Eq.(36). The temperature at which the various quantities must be evaluated is that of the purging gas. Examination of Table D1 in Appendix D shows that  $T_g$  is quite high. Assume  $T_g = 800 \text{ K}$ . Eq(28) yields  $D_o(800) = 1.24 \text{ cm}^2/\text{sec}$ . Then the Schmidt number is  $Sc = 0.663$ , and

$$\gamma \approx 8.10 \times 10^{-5} \sqrt{Re} / \ell_c \text{ m/s}$$

(with  $\ell_c$  in meters). The characteristic air velocity for calculating Re is given by Eq(D15) in Appendix D; finally, the characteristic length  $\ell_c$  is the standoff distance,  $\delta$ . With  $\delta = 5.4 \text{ mm}$ , we find  $Re = 11.06$  and  $\gamma = 4.99 \text{ cm/sec}$ .

(Incidentally, if we had quiescent air at 800 K, Muaramatsu's expression, Eq(32), yields  $\gamma_b \approx 2.35 \text{ cm/sec}$ ).

Finally, taking  $Y_a = 0.232$  and  $Y_s = 0$ , Eqs(29) and (31) then yield

$$\dot{m}_{ox}'' \approx 13.6 \text{ g/m}^2\text{-s}$$

We must also have  $r$  (the stoichiometric fuel/oxygen ratio), in order to use Eq(45) to get the penetration depth  $\delta$ . The stoichiometric air/fuel mass ratio for wood is  $S = 5.78$ , close enough to that for cellulose. Hence  $r \approx 0.746$ , and we find  $\delta = 0.10 \text{ mm}$ . Thus the penetration depth  $\delta$  is indeed much smaller than the layer thickness  $\Delta x$  (which is of the order 0.5 mm).

For  $T_s = 300^\circ\text{C}$ , on the other hand, we find  $k_{op} = 0.053 \text{ min}^{-1}$ , so that  $R_{op} = 1.38 \text{ kg/m}^3\text{-s}$ . Then  $\delta \approx 7.3 \text{ mm}$ , several times  $\Delta x$ , but the resulting mass-loss rate is only  $0.043 \text{ g/m}^2\text{-s}$ , which is indeed negligible.

For the case of quiescent air above the substrate, the mean value for the oxygen concentration to be used in the top cell during the runaway, is midway between the value at the top surface (i.e., at the bottom of the boundary layer), and at the bottom of the top cell (presumably, close to zero).

The only time that we cannot justifiably make the simplification that the oxygen concentration in the top layer is either that at the top surface or half (or 2/3ds) that value (during runaway), is when the reaction rate is intermediate between the very low values and the runaway value. This period should be relatively short, and the error introduced by these simplifications should not be large.

### 3. NUMERICS

In general, it is not possible to solve Eq.(12) analytically, in spite of the simplifying assumption of no radiation heat transfer, and even for the case  $S=0$ . That is, to write down an explicit expression which gives  $T$  in terms of the inputs. This is so, because of the nonlinear and nonuniform boundary conditions. It is therefore necessary to resort to a numerical procedure, which is that incorporated in TMPSUB2.

#### 3a. Introduction

The development of TMPSUB2 centers around the capability to simulate transient heat transfer. A one-dimensional heat conduction problem provides the simplest example to illustrate transient simulation methods. Figure 1 shows a portion of a one-dimensional conduction problem in which the material has been divided into thin layers. This example will be described by physical instead of mathematical arguments following the description given by Clausing (ref[11], pp.157-213).

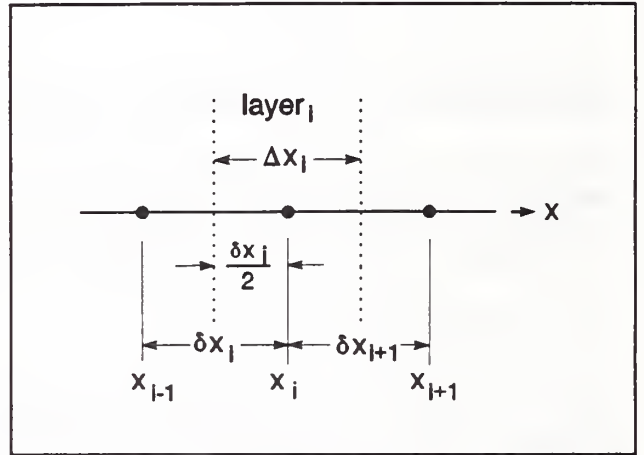


Figure 1. One Dimensional Conduction

The figure focuses on a representative layer of material of thickness  $\Delta x_i$  centered in a node at coordinate  $x_i$ . This material layer is represented by a single temperature  $T_i$  and a corresponding thermal conductivity  $\kappa_i$ , density  $\rho_i$ , and specific heat  $c_i$ . Assume this layer has a surface area of magnitude  $A$  in the Y-Z plane. The distance between nodes  $i$  and  $i-1$  is given by  $\delta x_i (= x_i - x_{i-1})$ . Subscripts  $i$  and  $n$  refer to positions in space and time, respectively. Subscript  $n$  is temporarily suppressed until it becomes necessary to consider time, in the following equations.

The instantaneous internal energy of layer  $i$  is given by:

$$U_i = \rho c \Delta V T_i = \rho c \Delta x_i A T_i \equiv C_i T_i \quad (47)$$

where  $T$  is the absolute temperature. This equation also serves to define the heat capacity,  $C$ , assigned to node  $i$ . Heat is transferred to and from layer  $i$  by three methods:

(1) conduction from layer  $i-1$  at the rate

$$q_{i-} = (T_{i-1} - T_i) \kappa_{i-} A / \delta x_i = K_{i-} (T_{i-1} - T_i) \quad (48)$$

(2) conduction from layer  $i+1$  at the rate

$$q_{i+} = (T_{i+1} - T_i) \kappa_{i+} A / \delta x_{i+1} = K_{i+} (T_{i+1} - T_i) \quad (49)$$

and (3) internal heat generation or radiation absorbed within the layer,  $S_i$ .

Eqs(48) and (49) define the thermal conductance,  $K$ , in each direction. The possibility of a thermal conductivity which varies with position is explicitly taken into account here using labels  $+$  and  $-$ :  $\kappa_{i-}$  and  $\kappa_{i+}$ . A good first order approximation for  $\kappa_{i-}$  is the harmonic average of  $\kappa_i$  and  $\kappa_{i-1}$ :

$$\kappa_{i-} = \frac{2\kappa_i\kappa_{i-1}}{\kappa_i + \kappa_{i-1}} \quad (50)$$

with a similar expression for  $\kappa_{i+}$ .

The change in internal energy of this layer between time  $t_n$  and time  $t_{n+1}$  is given to first order in  $\Delta t$  by

$$\Delta U_{i,n-n+1} = C_{i,n+1}T_{i,n+1} - C_{i,n}T_{i,n} = \Delta t(q_{i-} + q_{i+} + q_i) \quad (51)$$

where the time dependence has now been put in explicitly. There are several common solutions to Eq. (51) depending on when the heat gains are evaluated. One solution involves evaluating at time  $n$ :

$$C_{i,n+1}T_{i,n+1} = C_{i,n}T_{i,n} + \Delta t[K_{i-}(T_{i-1,n} - T_{i,n}) + K_{i+}(T_{i+1,n} - T_{i,n}) + S_{i,n}] \quad (52)$$

which is the standard Euler explicit time integration formula. "Explicit" means that  $T_{i,n+1}$  can be directly computed from values known at time  $n$ . On the other hand, evaluating at time  $n+1$  gives:

$$C_{i,n+1}T_{i,n+1} = C_{i,n}T_{i,n} + \Delta t[K_{i-}(T_{i-1,n+1} - T_{i,n+1}) + K_{i+}(T_{i+1,n+1} - T_{i,n+1}) + S_{i,n+1}] \quad (53)$$

which is Euler's standard implicit time integration formula. "Implicit" means that  $T_{i,n+1}$  is computed from other values also evaluated at time  $n+1$ . These values depend implicitly on each other and must be computed by a solution of simultaneous equations.

Clausing ([11], p.190) also gives a discussion of stability in terms of thermodynamic laws. Rearranging Eq.(52) to solve for  $T_{i,n+1}$  gives

$$T_{i,n+1} = (K_{i-,n}T_{i-1,n} + K_{i+,n}T_{i+1,n} + S_{i,n})\Delta t / C_{i,n+1} + T_{i,n}[C_{i,n} - (K_{i-,n} + K_{i+,n})\Delta t] / C_{i,n+1} \quad (54)$$

where the time subscript,  $n$ , has been added to the  $K$  terms to indicate exactly when these values are evaluated. For the sake of argument, assume  $C_{i,n+1} = C_{i,n} (=C_i)$  for simplicity. There is no solution if  $C_i = 0$ . If  $C_i$  is sufficiently small or  $\Delta t$  sufficiently large, then  $(K_{i-,n} + K_{i+,n})\Delta t / C_i > 1$ , and as  $T_{i,n}$  increases  $T_{i,n+1}$  must decrease, and vice versa. This is thermodynamically impossible. It shows up in a numerical solution as oscillations, i.e. "instability", in the node temperatures at each time step. These oscillations tend to quickly increase to totally meaningless values. In general, the smaller the thermal mass of the element, the smaller the time step needed for a stable explicit solution. This suggests a simple technique to determine the minimum stable time step for any element in the system.

Thus, rearranging the implicit Eq(53) to solve for  $T_{i,n+1}$  gives

$$T_{i,n+1} = \frac{C_{i,n}T_{i,n} + \Delta t(K_{i-,n+1}T_{i-1,n+1} + K_{i+,n+1}T_{i+1,n+1} + S_{i,n+1})}{C_{i,n+1} + \Delta t(K_{i-,n+1} + K_{i+,n+1})} \quad (55)$$

This equation shows none of the computational or thermodynamic problems of Eq.(54) indicating that the standard implicit method is stable for all time steps.

The spatial discretization error (for a uniform grid) for the standard explicit and standard implicit methods is proportional to  $(\Delta x)^2$  (for a variable grid, the accuracy is reduced somewhat; see Section 3d). The time discretization error is proportional to  $\Delta t$ .

The standard explicit and standard implicit methods err in opposite directions. Therefore, a more accurate solution can be obtained by combining the two methods. Expressing this combination generally in terms of a parameter  $\beta$  gives:

$$\Delta U_{i,n-n+1} = \Delta t [(1-\beta)(q_{i-,n} + q_{i+,n} + S_{i,n}) + \beta(q_{i-,n+1} + q_{i+,n+1} + S_{i,n+1})] \quad (56)$$

where  $0 \leq \beta \leq 1$ .

- $\beta = 0$  corresponds to the standard explicit method,
- $\beta = 1/2$  corresponds to the Crank-Nicholson method,
- $\beta = 2/3$  corresponds to the Galerkin method, and
- $\beta = 1$  corresponds to the standard implicit method.

For  $\beta \geq 1/2$  this method is unconditionally stable, although the solution may be oscillatory. For  $\beta > 3/4$  (approximately) the solution is stable and non-oscillatory. For  $\beta = 1/2$ , the time discretization error is proportional to  $(\Delta t)^2$ .

The methods presented above extend directly into three dimensions. For a Cartesian coordinate system and a cell of dimensions  $\Delta x_i$  by  $\Delta y_j$  by  $\Delta z_k$ , Eq.(51) can be rewritten to account for conduction from the six adjacent cells in the 3-D system:

$$\Delta U_{i,j,k} = \Delta t (q_{i-,j,k} + q_{i+,j,k} + q_{i,j-,k} + q_{i,j+,k} + q_{i,j,k-} + q_{i,j,k+} + S_{i,j,k}) \quad (57)$$

where

$$q_{i-} = (T_{i-1,j,k} - T_{i,j,k}) \kappa_{i-} \Delta y_j \Delta z_k / \delta x_i$$

$$q_{i+} = (T_{i+1,j,k} - T_{i,j,k}) \kappa_{i+} \Delta y_j \Delta z_k / \delta x_{i+1}$$

$$q_{j-} = (T_{i,j-1,k} - T_{i,j,k}) \kappa_{j-} \Delta x_i \Delta z_k / \delta y_j$$

$$q_{j+} = (T_{i,j+1,k} - T_{i,j,k}) \kappa_{j+} \Delta x_i \Delta z_k / \delta y_{j+1}$$

$$q_{k-} = (T_{i,j,k-1} - T_{i,j,k}) \kappa_{k-} \Delta x_i \Delta y_j / \delta z_k$$

$$q_{k+} = (T_{i,j,k+1} - T_{i,j,k}) \kappa_{k+} \Delta x_i \Delta y_j / \delta z_{k+1}$$

and  $S_{i,j,k}$  represents other heat added directly to the cell.

### 3b. Boundary Conditions

Special treatment is required for cells on the boundaries of the region being modeled. In particular, the nodes which represent the cells are placed on the boundary, rather than at the center. Referring to the one-dimensional example in Figure 1, the surface layer is only half as thick as the others.

An adiabatic boundary condition (b.c.) is handled by setting the appropriate heat flux terms in Eq(45) to zero. A constant temperature (isothermal) b.c. is handled by leaving the temperature unchanged.

The surface of the substrate ( $z=0$  plane; see Fig. 3) transfers heat to the environment by convection and by radiation. The convective heat gain for cell  $i,j,1$  is given by

$$(S_c)_{i,j,1} = (T_a - T_{i,j,1})h \Delta x_i \Delta y_j \quad (58)$$

where  $T_a$  is the temperature of the surrounding (ambient) air, and  $h$  is the heat transfer coefficient. A positive value of  $S_c$  represents a heat gain by the cell. The radiative heat gain is given by

$$(S_r)_{i,j,1} = \sigma \epsilon (T_a^4 - T_{i,j,1}^4) \Delta x_i \Delta y_j \quad (59)$$

where

$T_a$  is the temperature of the surrounding surfaces,

$\sigma$  is the Stefan-Boltzmann constant, and

$\epsilon$  is the emissivity of the fabric (assuming that  $\alpha$ , the absorptivity, =  $\epsilon$ ).

The temperatures in Eq(59) must be absolute (Kelvin) temperatures. In TMPSUB2 the temperature of the surrounding surfaces is assumed equal to the air temperature. (Note that Eq(59) can be rewritten in an apparently linear form similar to Eq(58):

$$(S_r)_{i,j,1} = [\sigma \epsilon (T_a + T_{i,j,1})(T_a^2 + T_{i,j,1}^2)](T_a - T_{i,j,1}) \Delta x_i \Delta y_j \quad (59a)$$

This form will be useful further on.

The heat flux from a smoldering cigarette to the fabric is represented by the following pair of equations:

$$\phi_s(x, y, t) = \phi_{\max} \exp \left[ - \left( \frac{x - x_o - vt}{\sigma_{x+}} \right)^2 - \frac{y^2}{\sigma_y^2} \right] \quad (x \geq x_o + vt) \quad (60a)$$

and

$$\phi_s(x, y, t) = \phi_{\max} \exp \left[ - \left( \frac{x - x_o - vt}{\sigma_{x-}} \right)^2 - \frac{y^2}{\sigma_y^2} \right] \quad (x < x_o + vt) \quad (60b)$$

This heat flux is converted to a heat gain,  $S_s$ , by multiplying the flux at the position of the node by the cell surface area. These values are adjusted slightly so that their (discrete) sum is equal to the total heat flux represented by Eq.(40a,b):

$$\int_{-\infty}^{\infty} \int_{-\infty}^{\infty} \phi_s dx dy = \frac{\pi}{2} \phi_m \sigma_y [\sigma_{x+} + \sigma_{x-}] \quad (60c)$$

### 3c. Air Gap

Since the furniture (apart from the frame) consists of fabric-covered padding, it is clear that the program must take at least two layers (with different properties) into account. Therefore the program was written so as to permit different values for the relevant thermophysical constants  $\rho$ ,  $c$ , and  $\kappa$  at each node. In fact, generally there is not perfectly intimate thermal contact between the fabric covering and the padding: there is a small but sometimes significant intervening air gap. Normally, one would place a node within this gap, in order to take a third layer into account; because of the thinness of the gap, and other technical difficulties, however, a different treatment of the effect of this air gap has been devised: the gap can be represented in terms of its "thermal resistance".

The optional air gap between the fabric and the padding is modeled by assuming one-dimensional heat transfer. Figure 2 shows the basic configuration and nomenclature for an air gap of thickness  $s$  between cells  $i,j,k$  and  $i,j,k+1$ .  $s$  is small relative to the separation between the cells,  $\delta_{k+1}$ . Although pyrolysis of the fabric and the possible melting and/or pyrolysis of the padding may well change the dimensions of the air gap, the simplifying assumption is nevertheless made here that the air gap has fixed and uniform dimensions. The heat transfer between these cells is given by

$$q_{i,j,k+} = K(T_{i,j,k} - T_{i,j,k+1}) \quad (61)$$

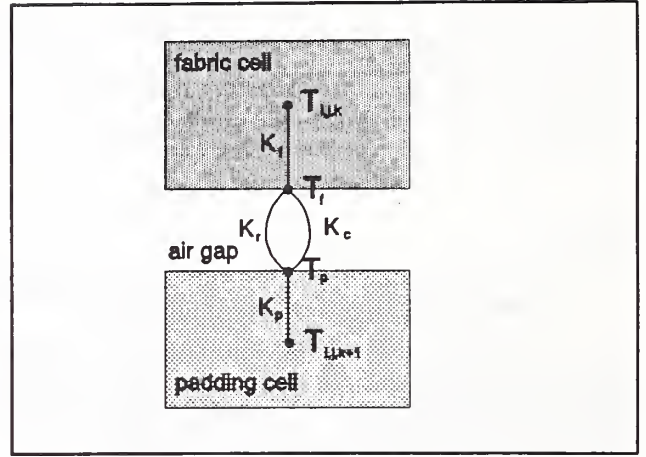


Figure 2. Air Gap Heat Transfer Model

where  $K$  is an implicit function of  $q_{i,j,k+}$ ,  $T_{i,j,k}$ , and  $T_{i,j,k+1}$ .

The overall heat transfer coefficient is given by

$$K = \frac{1}{\frac{1}{K_f} + \frac{1}{K_p} + \frac{1}{K_r + K_c}}$$

where the fabric conductance is

$$K_f = 2 \Delta x_i \Delta y_j \kappa_{i,j,k} / \delta_{k+1} ,$$

the padding conductance is

$$K_p = 2 \Delta x_i \Delta y_j \kappa_{i,j,k+1} / \delta_{k+1} ,$$

the fabric (bottom) surface temperature is

$$T_f = T_{i,j,k} - q_{i,j,k+} / \kappa_{i,j,k} ,$$

the padding surface temperature is

$$T_p = T_{i,j,k+1} + q_{i,j,k+} / \kappa_{i,j,k+1} ,$$

the radiant conductance is

$$K_r = \frac{\sigma \Delta x_i \Delta y_j (T_f + T_p)(T_f^2 + T_p^2)}{\frac{1}{\epsilon_f} + \frac{1}{\epsilon_g} - 1} ,$$

and the convective conductance is

$$K_c = \Delta x_i \Delta y_j \kappa_{air} / s .$$

The conductance of the air,  $\kappa_{air}$ , is evaluated at the average of  $T_f$  and  $T_p$ . These equations are solved to give  $K$  and  $q_{i,j,k+}$  during the overall process used to compute cell temperatures.

### 3d. Variable Grid

The heat from the cigarette spreads into the substrate by conduction. In order to correctly estimate the temperatures near the peak, it is important that conduction to the outer boundaries (at  $x=0$ ,  $x=x_{max}$ ,

$y=y_{\max}$ , and  $z=z_{\max}$ ) be negligible, since it cannot be known *a priori*. This requires a relatively large region relative to the size of the cigarette heat flux pattern. However, setting  $\Delta x$ ,  $\Delta y$ , and  $\Delta z$  sufficiently small to achieve the desired accuracy in the conduction calculation can result in an extremely large number of cells ( $N = (x_{\max}/\Delta x) \cdot (y_{\max}/\Delta y) \cdot (z_{\max}/\Delta z)$ ) with correspondingly large memory requirements and computation time.

The heating flux from a smoldering cigarette rises from negligible values to a high peak, on the order of  $60 \text{ kW/m}^2$  over a region only a few millimeters in extent. In order to follow this faithfully, the region must be covered by a mesh which is fine enough so that there are no changes from one mesh point to another large enough to produce numerical inaccuracies or instabilities. Thus, the required size of the grid is inversely proportional to the temperature gradient, where steep temperature gradients occur only near the point of peak heat flux.

Therefore, a variable grid is used. This grid consists of a few constant-width cells near the peak followed by cells of regularly increasing size to the outer boundaries. The increase in cell size is based on geometric progression, and can be different for each axis. Thus, for example,  $\Delta y_{j+1} = R_y \Delta y_j$  ( $R_y \geq 1$ ). The general effect of this variable grid is shown in figure 3. This is easy to implement in Eq.(45) which explicitly incorporates the grid sizes. The variable grid gives results which are less accurate than a constant grid. A benchmark test indicates that the results for  $R = 1.23$  differ by  $< 0.11\%$  at  $t=100$  sec. from those obtained for the constant grid case, with still smaller errors for  $R$  closer to unity (see Table A1, Appendix A).

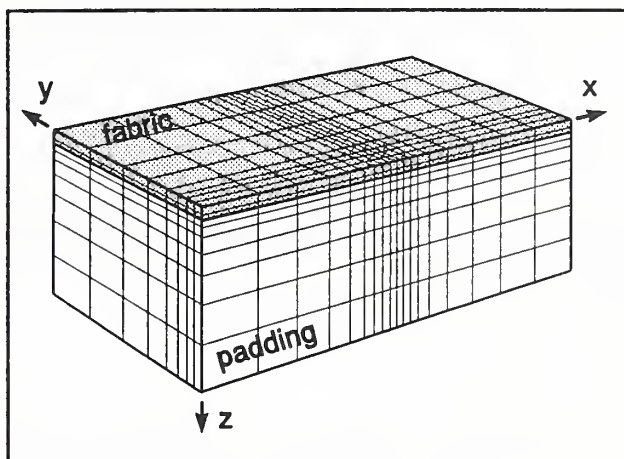


Figure 3. Substrate Coordinate System

The general effect of this variable grid is shown in figure 3. This is easy to implement in Eq.(45) which explicitly incorporates the grid sizes. The variable grid gives results which are less accurate than a constant grid. A benchmark test indicates that the results for  $R = 1.23$  differ by  $< 0.11\%$  at  $t=100$  sec. from those obtained for the constant grid case, with still smaller errors for  $R$  closer to unity (see Table A1, Appendix A).

Note: In choosing a grid, the user determines four items, in each coordinate direction: the width of the constant-width cells in the fine-grid region, the number of such cells, the total number of nodes along that axis, and the total width in that direction. The program then does the arithmetic, and finds the corresponding value of  $R_i$ . If that is  $< 1$ , an error message will be returned. Likewise, if too many grid points result from the attempted selection, an error message will result.

The point of peak heat flux moves as the cigarette smolders. TMPSUB2 adjusts the x-coordinates to keep the fine grid region centered on that peak. This adjustment is made by:

- (1) computing the new x-coordinates of the shifted grid,
- (2) computing a cubic spline curve for the temperature in each row of cells in the old grid, and
- (3) using the curve to compute the cell temperatures in each row at the new grid positions.

The standard explicit algorithm for solving Eq.(12), without pyrolysis included, was checked in several ways, principally by comparing its predictions against known analytical solutions (see Appendix A). These checks showed that the numerical procedure, and the computer program for implementing it, are correct, effective, and accurate.

### 3e. Variable Thermal Properties

The conductivity and specific heat of the substrate materials are known to vary with temperature. TMPSUB2 allows the user to describe this variation. The values entered for  $\kappa$  and  $c$  are converted to cubic spline curves giving  $\kappa(T)$  and  $c(T)$ . The conductivity is further adjusted within the program to take into account the fact that the thermal conductivity is proportional to the density:

$$\kappa = \rho \kappa(T) / \rho_0, \quad (62)$$

where  $\rho_0$  is the original density (recall that the assumption of constant  $\kappa$ ,  $\rho$ , and  $c$ , in section 2c, was a special case used only in order to obtain Eqs(17) to (19)).

### 3f. Pyrolysis

Consider pyrolysis from the finite difference viewpoint. We begin with a cell having constant volume,  $\Delta V (= \Delta x \Delta y \Delta z)$  and temporarily ignore the subscripts  $i,j,k$ . This cell contains a mass  $\rho_v \Delta V$  of virgin (unpyrolyzed) material, a mass  $\rho_c \Delta V$  of char, and a mass  $\rho_a \Delta V$  of ash.\* The numerical method must keep track of the density of each material as a function of time; in this program, this is done via the difference equation

$$\rho_{x,n+1} = \rho_{x,n} + \Delta t \dot{\rho}_{x,n+\beta} \quad (63)$$

where the subscript  $x$  may be  $v$ ,  $c$ , or  $a$ , and  $\beta$  indicates the type of time integration, as discussed above.

$\dot{\rho}_x$  is modeled using Eqs.(25a,b,c). Note that  $\rho_a = \rho_c = 0$  and  $\rho_s = \rho_v = \rho_0$  at  $t = 0$ .

Some material is converted to gases during pyrolysis; the rate at which gases are created is given by Eq.(25e). The gases are lost from the cell, and they carry away all the energy they contain -- i.e., there is an enthalpy loss which does not affect the temperature of the remaining mass. Moreover, since the gas diffusion equations have not been explicitly included, any possible loss of heat from the escaping hot gases to the cooler solid in other regions of the substrate is ignored. Thus, the rate of heat gain in the cell due to pyrolysis is (almost exactly) given by

$$S_p = \Delta V (R_d H_d + R_{op} H_{op} + R_{co} H_{co} + \dot{\rho}_s c T) \quad \text{Watts} \quad (64)$$

The  $R_i$  are given in Section 2c, and  $d\rho_s/dt$  is given by Eq(25e).

### 3g. Time Integration

A choice must be made for the time integration method. Following the discussion of Belytschko (ref[12], pp.55, 419, 445), the advantages of explicit time integration are:

- (1) Fewer calculations per time step.
- (2) Algorithm logic and structure are simple; this implies that it is good for testing new ideas.
- (3) Complex nonlinearities are easily handled.
- (4) It requires little core storage compared to implicit methods using direct elimination procedures.

---

\* That is, the densities are here defined on a bulk basis.

(5) It is very reliable in terms of accuracy and completing the computation.

The only notable disadvantage is that explicit time integration is only conditionally stable so that a very large number of time steps may be required.

With regard to accuracy, since implicit methods are unconditionally stable, they can easily be used with too large a time step, leading to significant time integration errors. The stability requirements for explicit time integration force the time step to be so small that the time integration error is almost always smaller than the spatial discretization error. Of course, it is also possible to use a spatial discretization that is much too large.

The addition of pyrolysis to the model required significantly smaller cells in the region of interest, and therefore required significantly longer execution time. Hence a better method than explicit time integration was required. The following method attributed to Saul'yev as described by Larkin [13] and Clausing [11] was adopted:

Again consider the one dimensional presentation of Fig 1. Assume that the calculation of cell temperatures is proceeding in the positive x direction. Then at cell i,  $T_{i-1,n+1}$  is a known quantity and can be used in computing  $T_{i,n+1}$ . Eq.(51) becomes

$$\Delta U_{i,n-n+1} \equiv C_{i,n+1} T_{i,n+1} - C_{i,n} T_{i,n} = \Delta t (q_{i-,n+1} + q_{i+,n} + S_{i,n+\beta}) \quad (65a)$$

During the next time step, calculate cell temperatures in the negative x direction. In that case Eq.(51) becomes

$$\Delta U_{i,n-n+1} \equiv C_{i,n+1} T_{i,n+1} - C_{i,n} T_{i,n} = \Delta t (q_{i-,n} + q_{i+,n+1} + S_{i,n+\beta}) \quad (65b)$$

Both Eqs(65a) and (65b) are unconditionally stable because of the inclusion of the implicit terms; operating together, the truncation errors during successive time steps tend to cancel leading to an  $O(\Delta t^2)$  algorithm. This method is directly expanded into 2 or 3 dimensions by adding the j and k position indices and the  $q_{j-}$ ,  $q_{j+}$ ,  $q_{k-}$ , and  $q_{k+}$  heat gains. The key factor is that it is only necessary to solve implicitly for one cell temperature at a time. There are no time consuming simultaneous equations to be solved. Tests indicate that this method is very accurate except for the possibility of some small oscillations as with the Crank-Nicholson method.

A question remains on when to evaluate  $S_i$ ,  $C_i$ , and  $\kappa_i$  (which is implicit in the q's) in Eqs(65a). Numerical errors are minimized by evaluating  $S_i$  at time step  $n + 1/2$ . These terms are all functions of temperature in the TMPSUB2 program. Furthermore, they are such complicated functions that the equations cannot be solved directly. The following equation must be solved implicitly for  $T_{i,j,k,n+1}$ .

$$U_{i,j,k,n+1} = U_{i,j,k,n} + \Delta t (q_{i-,j,k,n+1} + q_{i+,j,k,n} + q_{i,j-,k,n+1} + q_{i,j+,k,n} + q_{i,j,k-,n+1} + q_{i,j,k+,n} + S_{i,j,k,n+\beta}) \quad (66)$$

where

$$U_{i,j,k,m} = \rho_{i,j,k,m} \Delta V_{i,j,k} c_{i,j,k,m} T_{i,j,k,m}$$

with  $m = n$  and  $n+1$ . The total solid density in the cell is the sum of the virgin, char, and ash densities [Eq(25d)] and is a function of time due to the pyrolysis reactions:

$$\rho_{i,j,k,n+\beta} = (\rho_v + \rho_c + \rho_a)_{i,j,k,n} + \beta \Delta t (\dot{\rho}_v + \dot{\rho}_c + \dot{\rho}_a)_{i,j,k,n+\beta} \quad (67)$$

The cell pyrolysis for the time step is evaluated at  $T = (T_n + T_{n+1}) / 2$ , and component densities also at  $\beta = 1/2$ . Eq.(66) was rewritten in a form allowing numerical solution by a standard secant method (ref [14], pp 299-306). This completes the outline of Larkin's method. The net result of using Larkin's method is that the time step is no longer limited by grid size, and pyrolysis is modeled in a reasonable execution time.

## 4. EXPERIMENTS

### 4a. Experimental Arrangement

The next step is to compare the results predicted by TMPSUB2 with experimental results, in which an electrical heater was substituted for a cigarette. The schematic of an experiment designed to measure time to ignition is shown in figure 4. This consists of the heater element from an automobile cigarette lighter, fitted with a concentric jacket to permit an air purge. The purpose of the air purge is to keep evolved products from the sample from being ignited to flaming, rather than to merely smolder. The heating element is raised to varying temperatures, all of them high enough for the element to be glowing (500 - 900°C). The purging jet comes through the jacket, past the face of the element, and then out normal to it, toward the sample; it picks up a good deal of heat as it travels through the device. The resulting flux distribution beneath the heating element is shown in figure 5. As we would expect, it is axially symmetric; it is well fitted by a Gaussian profile. Note that the higher the temperature the disk is heated to, the higher is the peak flux.

The measured flux to the gauge is not the same as what the substrate sees, however, because the latter heats up, whereas the flux gauge does not; call the former  $\phi_g$  and the latter,  $\phi_s$ . It follows from Eq(3) that

$$\phi_g = \phi_{rad} + \phi_c = \phi_{rad} + h(T_g - T_c) \quad (68)$$

where  $T_g$  is the temperature of the hot purging gas,  $T_c$  that of the (cold) gauge, and  $\phi_s \equiv \phi_{in}$ . For the case where the substrate is being heated, however, the convective contribution goes down:

$$\phi_s = \phi_{rad} + h[T_g - T_s(t)] \quad (69)$$

where  $T_s(t)$  is the temperature of the substrate, which increases continuously. Thus the total flux decreases monotonically. Although we do not know the gas temperature  $T_g$ , we do not need it; for, we can combine Eqs.(68) and (69) to obtain

$$\phi_s(t) = \phi_g - h[T_s(t) - T_c] \quad (70)$$

The heat transfer coefficient  $h$  was discussed in Section 2. It is found for this experimental configuration in Appendix D. Analysis of the experimental results, given in Appendix D, yields a number of values important for this experiment, including  $h$  and the disk temperatures; the results are shown in Table D1;  $h$  is found to be a weak function of  $\phi_{ext}$ .

When a mock-up consisting of flexible PU foam covered by #12 cotton duck was placed in position under the heat source, smoldering ignition occurred after a certain amount of time; the ignition delay depends on the intensity of the flux, as indicated qualitatively by Eq.(19), Section 2b. The experimentally-obtained ignition delays are plotted in figure 6 as a function of the peak heat flux.

Analysis of the ignition delay data:

The ignition delay times as a function of the external flux are given in Table 1.

Table 1. Ignition delay times

$\phi_{ext}(\text{kW/m}^2) \rightarrow$	18	25	34.5	44
$t_{ig}(\text{sec}) \rightarrow$	472	70	37	22

Since  $\phi_{net}$  is constant for each run, then according to Eq(19), a plot of  $\phi_{ext}$  versus  $t_{ig}^{-1/2}$  should yield a straight line whose intercept is the critical flux,  $\phi_{crit}$ . When this is done, however, the result is not a straight line. More generally, then, we assume that the relationship has the form

$$\Delta\phi \equiv \phi_{ext} - \phi_{crit} = A t_{ig}^{-p} \quad (71)$$

Only the correct choice for  $\phi_{crit}$  will yield a straight line in a logarithmic plot of  $\Delta\phi$  vs  $t_{ig}$ . When that is obtained, the slope of the line is -p; it was found that  $\phi_{crit} \cong 16.9 \text{ kW/m}^2$  and that  $p \cong 1.087$ , with A varying from 757 to 816; the average value is 798. If we take  $p = 1$ , A increases slowly with  $\phi_{ext}$ .

The fact that  $p \approx 1$ , rather than  $1/2$ , indicates that the substrate behaves like a thermally thin material; that, in turn, suggests that it is principally the fabric which is involved in the heating and ignition. If we assume that the principal cooling mechanism is radiation, then  $\phi_{crit} \cong 16.9 \text{ kW/m}^2$  implies that if the radiative absorption coefficient of the fabric is  $\alpha = 0.9$ , then  $T_{ig} = 759 \text{ K} \approx 485^\circ\text{C}$  -- a remarkably high value. Even with  $\alpha = 1.0$ ,  $T_{ig} = 739 \text{ K} = 466^\circ\text{C}$ , considerably greater than the  $400^\circ\text{C}$  measured independently. This shows that there is substantial convective cooling during the heating/ignition process.

#### 4b. Material Data

In order to see whether the program can calculate  $t_{ig}$  correctly, it is necessary to calculate the surface temperature under the heater. In order to do that, however, it is necessary to have correct input data; among these data are the thermophysical data,  $\kappa\rho c$ .

##### 4b.1 Fabric

First, consider the fabric. The fabric that was used in the experiment was #12 cotton duck. Material data for cotton, especially as a function of temperature, are surprisingly difficult to find, even though it is a common and long-used material.

In Appendix E, we find that reasonable values for the thermophysical constants for this particular cotton fabric (#12 cotton duck) are

$$\rho = 620 \text{ kg/m}^3$$

$$\kappa(T) = 0.28505 \kappa_s(T) + 0.84554 \kappa_{gas}(T) \quad \text{W/m-K} \quad (72)$$

where

$$\kappa_s(T) = \kappa_s(T_o) (T/T_o) = 1.242 \times 10^{-3} T \quad \text{W/m-K} \quad (73)$$

(with T in Kelvins) and

$$\kappa_{\text{gas}} = 1.7 \kappa_{\text{air}}, \quad \text{with}$$

$$\kappa_{\text{air}} = \frac{a \sqrt{T}}{1 + \frac{b \times 10^{-cT}}{T}}, \quad (74)$$

The constants are  $a = 2.6464 \times 10^{-3}$ ,  $b = 245.4$ , and  $c = 12$ . Then  $\kappa(25^\circ\text{C}) = 0.1435 \text{ W/m-K}$  and  $c(T) = \kappa(T)/\rho\alpha \approx 7819\kappa(T)$ ; thus,  $c \approx 1122 \text{ J/kg-K}$  at 300 K.

#### 4b.2 Char

The cotton decomposes and pyrolyses to char. According to Parker [15], [16], the specific heat of char is just about that of **carbon**:

$$c_c(T) = 1.43 + 3.55 \times 10^{-4} T - 7.32 \times 10^{-4} / T^2 \quad \text{J/g-K}, \quad \text{with T in K} \quad (75)$$

The thermal diffusivity of wood char is approximately constant:

$$\alpha_c \approx 2.1 \times 10^{-7} \text{ m}^2/\text{s} \quad (76)$$

The density of the char depends on whether the fibers contract while pyrolyzing, or not. Finally, the thermal conductivity of char is found from

$$\kappa_c(T) = \alpha_c \rho_c c_c(T). \quad (77)$$

#### 4b.3 Reaction kinetic parameters

When the analysis of a pyrolyzing material is carried out, it is done for a thin layer, in order to ensure uniformity of temperature and of oxygen concentration throughout the sample. It is then simplest to find the reaction rate in the form

$$k_d = \frac{d(W_d/W_o)}{dt} = A_d \left( \frac{W_d}{W_o} \right)^{n_d} \exp(-E_d/RT) \quad \text{min}^{-1} \quad (78)$$

for the degradation reaction, rather than as in Eq(20); here  $W_d = W_d(t)$  is the (instantaneous) weight of the remaining (virgin) material = weight of sample minus weight of char and ash, and  $W_o$  is the original weight. Note that A is commonly given in reactions/minute. The actual reaction rate is given by

$$R_d = \rho_o k_d.$$

The relationship between (20) and (78) is simple: since  $\rho_d = W_d/V_d$  and  $\rho_o = W_o/V_o$ , then as long as  $V_o/V_d = \text{const}$ ,  $W_d/W_o = \rho_d/\rho_o$ , and, as in Eq.(20),

$$R_d = A'_d \rho_d^n \exp(-\dots)$$

where

$$A'_d = A_d \rho_o^{1-n}$$

(in the appropriate units). T.J. Ohlemiller (private communication, 10/91) found that for pyrolysis in pure nitrogen,

$$A_d = 7.49 \times 10^{14} \text{ min}^{-1}, \quad n = 0.60, \quad \text{and} \quad E_A = 43,600 \text{ cal/mole} = 182.4 \text{ kJ/mole}$$

Instead of these parameters, however, we shall use the results of Kashiwagi and Nambu [6] for a cellulosic paper pyrolyzed in air; that will maintain internal consistency in the reaction set. The global kinetic constants given by Kashiwagi and Nambu for the thermal degradation reaction of their cellulosic paper are

$$\begin{array}{ll} E_d = 220 \text{ kJ/mole} & n_d = 1.8 \\ A_d = 1.2 \times 10^{19} \text{ min}^{-1} & H_d = -570 \text{ J/g} \end{array}$$

The parameters for the other two reactions are given in their Tables 1 and 2, reproduced below. For the oxidative pyrolysis reaction,

$$k_{op} = A_{op} X_{ox}^{n_{op}} \left( \frac{W_d}{W_o} \right)^{n_{fop}} \exp\left( -\frac{E_{op}}{RT} \right) \quad (79)$$

where  $X_{ox}$  is the volume fraction of oxygen. The kinetic constants are

$$\begin{array}{ll} E_{op} = 160 \text{ kJ/mol} & n_{op} = 0.5 \\ A_{op} = 1.5 \times 10^{14} \text{ min}^{-1} & n_{fop} = 1.3 \end{array}$$

and  $H_{op} = 5.7 \text{ kJ/g}$

For the char oxidation reaction,

$$k_c = A_c X_{ox}^{n_{co}} \left( \frac{W_c}{W_o} \right)^{n_c} \exp\left( -\frac{E_c}{RT} \right) \quad (80)$$

with the kinetic constants

$$\begin{array}{ll} E_c = 160 \text{ kJ/mol} & n_{co} = 0.78 \\ A_c = 3.4 \times 10^{11} \text{ min}^{-1} & n_c = 1.0 \\ \text{and} & H_c = 25 \text{ kJ/g} \end{array}$$

The fraction of ash which remains is 9% by mass. Eqs.(79) and (80) transform to the standard form in the same way that (78) does. Thus

$$A'_{op} = A_{op} \rho_o^{1-n_{op}} \rho_a^{-n_{op}}$$

$$A'_c = A_c \rho_o^{1-n_c} \rho_a^{-n_{co}}$$

#### 4b.4 Heats of combustion

Brandrup and Immergut (ref [17]) give the heat of combustion from several measurements; as expected, the results vary:

$$\begin{aligned} H_c(\text{cotton}) &\approx 18850 \text{ J/g} \\ H_c(\text{fabric1}) &\approx 15450 \text{ J/g} \\ H_c(\text{fabric2}) &\approx 16700 \pm 250 \text{ J/g} \quad (\text{fabric weight was } 180 \text{ g/m}^2) \end{aligned}$$

Note: as material pyrolyzes, we should take  $c(T)$  and  $\kappa(T)$  for the combination of materials; for the sake of simplicity, however, we assume that the virgin fuel, the pyrolyzed material, the char, and even the ash, all have the same specific heat. Then the appropriate density to use in Eq.(12), for example, is the density of the solid,  $\rho_s$ , which is the sum of the bulk densities of all the components of the solid (see Eq(25d)). As pyrolysis and combustion proceed,  $\rho_s$  decreases monotonically (assuming no fabric shrinkage).

#### 4b.5a Foam

For the padding component of the substrate, we have PU foam, for which we have the following data (T.J. Ohlemiller, private communication, 12/91):

$$\rho = 0.032 \text{ g/cm}^3 = 32 \text{ kg/m}^3 \quad (81a)$$

$$c_p = 1.46 \text{ J/g-K} \quad (81b)$$

$$\text{and } \kappa(T) = 0.03613 + 2.003 \times 10^{-4} T, \quad (81c)$$

with T in °C.

There is one other datum for PU foam:  $\langle \kappa \rho c \rangle$ , the mean value of the thermal inertia, was measured in the LIFT apparatus (see [5], [18], and [19]) by Quintiere and Harkleroad [19]. However, the foam melts before it ignites, so that  $\rho$  (and, consequently,  $\kappa$ ) go up substantially; moreover, the measurement entails all the other model approximations. Hence the measurement is not directly useful.

#### 4b.5b PU Foam kinetic parameters

The first pyrolysis reaction, which results in the collapse of the foam structure, yields 0.7 g of liquid and 0.3 g of vapor, for every gram of foam which pyrolyzes. The reaction rate,  $RR_1 \equiv (\text{mass gasified/min})/(\text{mass of foam})$ , is given by

$$RR_1 = 0.30 B \left( \frac{\rho - \rho_R}{\rho_o - \rho_R} \right)^m \exp \left( -\frac{E_B}{RT} \right) \quad (82)$$

where  $m = 1.5$                       Also,  $\rho_o =$  starting density,  
 $B = 3.36 \times 10^{17}$ , and                       $\rho =$  current density, and  
 $E_B = 44,700 \text{ cal/mole.}$                        $\rho_R =$  density of residue  $\approx 0.70\rho_o$ .

These densities are those of the **solid phase** ( $\rho_o$  of order  $1 \text{ g/cm}^3$ ), rather than that of the foam ( $\rho_o \approx 0.03$

g/cm<sup>3</sup>). The total heats of pyrolysis of PU foams range between 100 and 200 cal/g; for this foam, it is closer to the upper value. Assuming it varies linearly with the mass loss, we can estimate 30% of 200, or

$$H_p \sim 60 \text{ cal/g} \approx 240 \text{ J/g}$$

Finally, for the diffusion coefficient for O<sub>2</sub> in the fabric, see Eq.(28).

## 5. RESULTS AND DISCUSSION

Rather than give the final results immediately, it was decided to describe the evolution of our thinking, including some of the false steps we took, because a good deal can be learned that way, and it could be instructive for anyone else who might work on this problem in the future. With that in mind, we first consider the results of calculations made assuming an inert substrate:

### 5a. Inert Case

First, the computer program was used to calculate the peak surface temperature under the heater as a function of time, for several peak fluxes. The results are shown in figure 7.

The ignition temperature of cotton was measured to be 390-400°C (T.J. Ohlemiller et al, private communication). According to figure 7, if  $T_{ig} \approx 400^\circ\text{C}$ , then ignition is attained for the 44 kW/m<sup>2</sup> exposure at  $t \approx 18$  sec, and for the 34.5 kW/m<sup>2</sup> exposure at  $t \approx 50$  sec. These values are to be compared with experimental values of 22 and 37 sec, respectively; this is fairly good agreement. On the other hand, ignition is not attained at all for the 25 and 18 kW/m<sup>2</sup> cases; a conceivable reason might be that the ignition temperature given above was overestimated. In order to intersect the  $\phi = 18$  kW/m<sup>2</sup> curve at  $t \approx 472$  sec, the ignition temperature would have to have been about 290°C; it is very unlikely that such a large error in the measurement of  $T_{ig}$  would have been made. Even if it were, that would yield ignition times of 7, 12, and 25 sec, respectively -- much shorter than the measured times of 22, 37, and 70 sec.

Three possible reasons for the calculated ignition times being so short are:

- (a) Endothermic pyrolysis takes place, which slows the temperature rise.
- (b) There is significant radiative heat transfer within the material, so that the flux is absorbed in depth, rather than mainly at the surface.
- (c)  $T_{ig} = 290^\circ\text{C}$  and the estimates of  $\kappa\rho c(T)$  were in error, the actual value being larger.

Now, if we consider endothermic pyrolysis, then we must also consider exothermic pyrolysis. Second, the effect of radiative heat transfer will be small when  $T$  is near  $T_a$ , and small in comparison with the effects of pyrolysis when  $T \gg T_a$ . Finally, consider item (c): If  $\kappa\rho c$  were larger, then the rate of rise of  $T_s$  would be smaller, as can readily be seen from Eqs(17)-(19). The final temperature, however, is independent of  $\kappa\rho c$ . Hence not only would  $T_{ig}$  have to be much smaller, but the estimates of  $\kappa\rho c$  would have to have been 9 times too small. This is all possible, but extremely unlikely.

### 5b. Results with pyrolysis

On the other hand, we know that pyrolysis must take place; Figure 8 shows the effect of including pyrolysis, for the  $Q = 25$  kW/m<sup>2</sup> case. Curve A indicates what the temperature of the fabric surface would be if the fabric (and foam) were inert. Curve B is the result of "turning on" the (endothermic) degradation reaction. Note that although the rate of growth of temperature is slowed down quite

perceptibly, as expected, the temperature the surface reaches asymptotically is exactly the same (assuming the same surface absorptivity/emissivity as before).

However, the exothermicity of the oxidative pyrolysis and of char oxidation are far greater than the endothermicity of thermal decomposition, and should overwhelm it. We cannot, therefore, consider thermal decomposition alone: if we consider pyrolysis, we must include all the major reactions. Another way of seeing this is to note that in order to have ignition, we must have a "thermal runaway," where exothermic pyrolysis heats up the material faster than heat diffusion and surface losses can carry the heat away.

Curve c indicates what takes place when the oxidative pyrolysis reaction is included, as well: it is exothermic, and adds a great deal more energy than the degradation reaction removes. The result is that the temperature rises, rather than falling. Indeed, it rises so rapidly that it begins to appear like a thermal run-away. However, the temperature reaches a peak, then declines. The reason is simple: the fuel is rapidly exhausted; once that happens, the heat source is reduced to the original external flux. This is clearly depicted in Figure 9, which shows the fuel density as a function of time: The ordinate is temperature, in °C, and density in kg/m<sup>3</sup>. The curves marked  $T_0$  and  $\rho_0$  correspond to the cell with the highest temperature. Those marked  $T_1$  and  $\rho_1$  correspond to the (laterally) adjacent cells, and those marked  $T_2$  and  $\rho_2$  to the next ring of cells. These calculations were carried out assuming no char oxidation. We see that as the reaction accelerates,  $T_s$  "runs away" and the density plummets from its virgin value to that of char. Most significantly, the peak temperatures develop just after the density falls.

Finally, curve d of Figure 8 shows the result of adding the char-oxidation reaction as well: that additional heat source takes the pyrolysis "over the top": the temperature continues to run away (we have arbitrarily cut off the calculation at 600°C, here). The question then arose: why is (was) there an oscillation in  $T_s$ ? The explanation is qualitatively clear: if a cell is (too) large, then the surface/volume ratio is small, and the heat cannot diffuse away rapidly enough. This is confirmed by Figure 10: with a cell size taken to be a bit less than half as large, the amplitude of the oscillation declined considerably, and with the cell size halved again, the oscillations have almost disappeared.

Presumably, as we continue to decrease the cell size, the numerical errors should become progressively smaller, until a further decrease in cell size would make no further difference in the results. However, it was found that the results were apparently not converging with decreasing  $\Delta x$ , and that the sensitivity varied with  $Q$ . Investigation of the reason for this great sensitivity revealed that it lay in our use of a variable grid size: whereas for grids of constant spacing, the numerical approximations are correct to second order in  $\Delta x$ , that accuracy drops to somewhere between first and second order. Indeed, if the numerical error is proportional to  $(\Delta x)^n$ , then  $n$  is given by a complex formula (see ref [20], pp.43 and 51). The "flavor" of that expression is given by  $n \sim (2+a)/(1+a)$ , where  $a \equiv \partial \Delta x / \partial x$ . That is, the accuracy depends inversely on the rate of growth of the grid size. An explicit calculation is given in Appendix A; see Table A1 there.

By reducing the rate of increase of grid size, therefore, the accuracy was increased, and the results made to converge better. Moreover, it was decided to switch from an explicit solution method to Larkin's semi-implicit method (see Section 3). After those changes, we arrived at the results shown:

The results of four calculations are shown in Figure 11: these were made with an assumed heat transfer coefficient  $h = 20$ , and an assumed oxygen concentration of 20%. For initial fluxes with peak values of 25 and 34.5 kW/m<sup>2</sup>, calculations are first made assuming that the substrate is inert, and then pyrolysis is "turned on." We see that for the 34 kW case, the asymptotic temperature lies at about 430°C, and that a thermal runaway begins at about 300°C, at  $t \approx 20$ , and is completed at  $t \approx 25$  sec; that would then

be the ignition time. It is difficult to state precisely what "the ignition temperature" is, in this case (but see below).

For the 25 kW case, the asymptotic temperature lies at about 360°C; the first perceptible deviation of the curve for the reactive case from that for the inert material occurs at  $T \approx 280^\circ\text{C}$ , and is clearly established at 300°C. The thermal runaway takes place at  $t \approx 48$  sec. These times may be compared with the experimentally-established ignition times, which were about 22 and 70 sec, respectively. Thus we have achieved semi-quantitative agreement. In Figure 12, on the other hand, we see that a thermal runaway -- and therefore ignition -- apparently did not take place for the 18 kW case. Here, the asymptotic temperature is about 290°C; this is apparently not high enough to produce a runaway.

Wherein lies the difficulty? Most likely, one or more of the input values is incorrect. Altering  $\kappa\rho c$  would principally change the time scale. Fig.13 shows the effect of changing the assumed oxygen concentration: the highest curve reproduces the upper curve in Fig.12. The next two curves show what happens when  $\langle Y \rangle$  is assumed to be 0.15 and 0.11, respectively. Finally, the bottom curve (again) corresponds to the inert case. Thus, it is not  $[\text{O}_2]$  having been chosen too low that prevents ignition, and one or more of the kinetic parameters is probably in error. Refer to Figure 14: curves a and b again reproduce Fig.12 (on a different scale). For curve c, the char-oxidation rate was doubled. It is apparent that the curves overlap completely. A preliminary conclusion inferred from this was that the observed result was due to all the char that is produced already being oxidized. Observation of the kinetic constants for oxidative pyrolysis and char oxidation, however, makes it clear that the latter is three orders of magnitude slower than the former. Therefore merely doubling the char-oxidation rate will only perturb the energy output slightly -- so slightly that it will not even show up in the figure.

For curve d, the oxidative pyrolysis rate was doubled (the preexponential factor A was doubled), doubling the char-production rate through this branch; this indeed produced a thermal runaway. Curves e and f are the results of increasing A by 20% and 10%, respectively. Thus, a quite modest increase in A produces (predicts, that is) ignition, although at 230 sec, rather than the measured 472 sec). Such an increment is not only well within experimental error, but -- more to the point -- is entirely plausible, when the likely differences between the cellulosic paper and a cotton fabric (with different impurities) are considered. On the other hand, it was assumed that  $y = 0.20$ . For  $y = 0.15$ , A must be increased by 30% in order to get ignition (the resulting  $T(t)$  curve is very similar to the "best" one). Although this is greater than the 10% increase found above, it is still entirely plausible.

We have so far considered the sensitivity of the results to the oxygen concentration, the thermophysical constants of the fabric, and its kinetic parameters. Surprisingly, there are two other significant parameters: first, if we use  $h = 22$  for the heat transfer coefficient in Eq.(69) (as suggested by the results of Appendix D, shown in Table D1), rather than the assumed  $h = 20$ , the "asymptotic" temperature (that at  $t = 500$  sec) reaches only 272°C, rather than 292°C, and there is not the faintest possibility of achieving ignition, unless  $E_A$  is substantially smaller than 160 kJ/gm. One solution is to assume that  $h=20$  is the correct value to use, since the theoretical calculations in Appendix D could easily be off by 10% or more. Another resolution is possible, too: the second parameter which is important in this threshold region ("threshold," because 18 kW/m<sup>2</sup> is close to the critical flux, 16.9 kW/m<sup>2</sup>) is the thermal conductivity of the foam padding. In all the runs made above, it was assumed that  $\kappa = 0.056$  J/m-K and  $c = 1.9$  J/g-K, for the foam at  $T = 20^\circ\text{C}$ . If it were assumed that  $\kappa = 0.096$ , instead, then the foam would act as a more efficient heat sink, and the surface temperature could be expected to drop; indeed, a calculation showed that the peak surface temperature at  $t = 500$  s fell to 272°C for the inert fabric. In fact, however, the value 0.056 for the thermal conductivity was for a foam of density 48 kg/m<sup>3</sup>! Transforming that for a 32 kg/m<sup>3</sup> foam, according to Eq.(62), yields 0.036, almost exactly what is given

in the present test (see Eq.(81c)). This reduces the heat sink, and must yield an increased asymptotic surface temperature. Using the foam parameters given by Eqs.(81), and  $h = 20$ , the  $t=500$  temperature indeed rises, from  $292^{\circ}\text{C}$  to  $300^{\circ}\text{C}$ ; with  $h = 22$ , it is  $294^{\circ}\text{C}$ , and we only need to increase  $A$  by 10% to get runaway.

The "best" set of parameters, then, is that given in sections 4b.1 and 4b.3 for the fabric, and 4b.5a for the foam. For the heat transfer coefficient, use the values in Table D1. With that set, we obtain the curves shown in Fig.15. The corresponding calculated ignition times are given in Table 2. Thus, the calculated values are all about half the measured values.

Note that the polyurethane foam begins to melt and recede from the fabric when its temperature reaches about  $300^{\circ}\text{C}$ , thereby decreasing the heat-sink effect of the padding, and accelerating the heating of the fabric; this effect has not been included in the model, however.

Table 2. Calculated vs experimental ignition delay times for the four fluxes

Q (kW/m <sup>2</sup> )	Ignition delay, $t_{ig}$ (in sec)	
	Calculated	Measured
18	209	472
25	37.2	70
34.5	19.0	37
44	12.6	22

It has been suggested that we might avoid the necessity of explicitly including the pyrolysis reactions by choosing some effective ignition temperature. This is not, in fact, feasible: if we take the measured ignition times and mark them on the four curves in Figure 7, corresponding to the inert assumption, we find that they intersect these curves at widely varying temperatures; see Table 3. It is apparent that this "ignition temperature" is a strong function of the external flux.

Table 3. Surface temperatures which would be attained by the substrate at the measured ignition times if the substrate had been inert

$\phi_{ext}$ (in kW/m <sup>2</sup> ) =	18	25	34.5	44
$T_{ig}$ (in $^{\circ}\text{C}$ ) =	291	342	380	400
$T_{ig}$ (in $^{\circ}\text{K}$ ) =	564	615	653	673

On the other hand, if we define "the ignition temperature" as the point on the  $T_s(t)$  curve where the temperature is rising at some rapid rate -- say,  $100^{\circ}\text{C}/\text{sec}$  -- then from Figs.11 and 13 we see that that gradient is attained at the approximate temperatures shown here:

$$\phi_{\text{ext}} \text{ (in kW/m}^2\text{)} = 18 \quad 25 \quad 34.5$$

$$T_{\text{max}} \text{ (in } ^\circ\text{C)} = 390 \quad 390 \quad 380$$

$$T_{\text{max}} \text{ (in } ^\circ\text{K)} = 663 \quad 663 \quad 653$$

These calculated temperatures are close to each other, and close to the 390-400°C which has been measured.

## 6. SUMMARY

We have created several computer programs, of which the central one is TMPSUB2. This program calculates the temperature history at every point in a substrate which is subjected to a strongly localized heating flux on its top surface. The (solid) substrate consists of two layers, the top one being a fabric and the lower a foam pad; there may be a thin intervening air gap. The substrate is taken to be a rectangular parallelepiped, and it is broken up into several thousand cells. There is a user-friendly front end for the input, described in Section 3. The program runs well on a 386-level computer with a math coprocessor, or a 486-chip computer.

As stated in the introduction, this program serves to calculate the temperature of the upholstered furniture as a function of time and position, when it is exposed to a prescribed heating flux. This flux can be highly peaked at a point, vary with time, and move at a constant (specified) rate over the top surface of the furniture, assumed to be horizontal. The radiative and convective heat losses from the surface are given correctly. If and when the temperature rate of rise at a given location suddenly "accelerates" to a value high enough that the surface glows (that is,  $T > 500^\circ\text{C}$  or so), we can say that smoldering ignition has occurred. The ambient oxygen level can be set at whatever value one wishes. The program will not tell us whether **flaming** ignition takes place. It also does not treat the case where the flux is applied in a crevice, such as is formed between the seat cushion and the seat back. The program does not take into account the effect(s) of the foam possibly melting and receding away from the fabric. Finally, it also does not take oxygen diffusion within the cushion explicitly into account; hence in certain threshold situations, where a small change in oxygen concentration determines whether ignition does or does not take place, the results are ambiguous and not to be trusted. Note that it is often difficult to obtain the needed kinetic and/or thermophysical parameters for the material; or, when available, to know how accurately they are known. Therefore this caveat must also be made: even if the program were **perfect**, its results are only as good as the input parameters which are supplied. On the other hand, it should accurately reproduce (or predict) trends.

When the flux to which the substrate is exposed is near the critical flux, the result (i.e., ignition does or does not take place) is sensitive to most of the parameters, such as the ambient oxygen density, the heat transfer coefficient, the thermal conductivity of the foam as well as that of the fabric, etc.

The way  $T(r,t)$  is found is by solving the PDE which describes the diffusion of heat in a solid, Eq.(12), numerically. The solid is subjected to a nonuniform and time-varying heating flux at its top surface, and (simultaneously) experiences convective and radiative heat losses. Moreover, the solid can undergo pyrolytic reactions; we consider three, here: one endothermic step (thermal degradation to char), one oxidative pyrolysis to char, and oxidation of the char (to ash).

The equation set is very stiff, because of the highly nonlinear form of the (Arrhenius) reactions. We have therefore used a semi-implicit method to solve the equation set.

The way ignition is seen to be achieved (in a cell) is that the temperature undergoes a "thermal runaway." This does not occur abruptly as a particular temperature is reached, so that the "ignition temperature" is not well defined. When the transition region between "inert" heating and thermal runaway is narrow, the concept is adequate. According to this model, the transition region is rather broad, and so it is not so useful a concept in this context.

What is and is not in the program is listed in Table 1, section 2.

Note that

- a) We can get a first approximation to the radiative heat transfer within the material by using Kunii's expression, Eq.(14).
- b) The effects of cation concentration can probably be modeled by appropriate changes (not described here) in the kinetic parameters. Finally,
- c) the effect(s) of relative humidity in the ambient can likewise probably also be approximately modeled by making appropriate changes (again, not described here) in  $\rho$ ,  $c$ , and  $\kappa$ .

An experiment was carried out to ignite the substrate. In trying to reproduce those experimental results, it was found that the calculated results are sensitive to the input values chosen, especially the kinetic parameters. It was found that the preexponential factor found by Kashiwagi and Nambu (ref [6]) for the oxidative pyrolysis reaction in a cellulosic paper had to be increased by 10% for the cotton duck fabric in order to get ignition for the lowest of a set of heating fluxes to which the substrate was exposed. The result was semi-quantitative agreement with the observed ignition times.

## 7. REFERENCES

1. Miller, A.L. (1991), "Where There's Smoking There's Fire," NFPA Journal, Jan/Feb 1991, p.86
2. Mitler, H.E. (1988), "Modeling Ignition," Section 5 in **The Effect of Cigarette Characteristics on the Ignition of Soft Furnishings**, by R.G. Gann, R.H. Harris, J.F. Krasny, R.S. Levine, H.E. Mitler, and T.J. Ohlemiller; NBS Technical Note 1241, National Bureau of Standards, Gaithersburg, MD 20899
- 2a. Holman, J.P., **Heat Transfer** (5th ed.), McGraw-Hill, N.Y., 1981
3. Carslaw, H.S., and Jaeger, J.C., **Conduction of Heat in Solids**, 2nd ed; Oxford, 1959
4. Kunii, D., Kagaku Kogaku [Chem. Eng. (Japan)] **25**, 1961, p.891
5. Quintiere, J.G., "The Application of Flame Spread Theory to Predict Material Performance," J. of Res. of Nat'l Bur. of Standards **93**, No.1 (1988) p.61
6. Kashiwagi, T., and Nambu, H., "Global Kinetic Constants for Thermal Oxidative Degradation of a Cellulosic Paper," **Combustion and Flame** **88** (1992) p.345
7. Szekely, J., Evans, J., and Sohn, H., **Gas-Solid Reactions**, Academic Press, 1976
8. Bird, R.B., Stewart, W.E., and Lightfoot, E.N., **Transport Phenomena**, Wiley, 1960
- 8a. Ohlemiller, T.J., "Smoldering Combustion Propagation on Solid Wood," in **Fire Safety Science, Proceedings of the First International Symposium** (Eds., G. Cox and B. Langford); Hemisphere Publishing Co., Washington, D.C. (1991) p.565
9. Muramatsu, M., "Study of Transport Phenomena Which Occur During Unforced Smoldering of Cigarettes," Research Report No.123 of the Japan Tobacco and Salt Monopoly, 1981
10. Treybal, R.E., **Mass-Transfer Operations**, McGraw-Hill, N.Y., 1955
11. Clausing, A.M., "Numerical Methods in Heat Transfer" in **Advanced Heat Transfer**, Ed. B.T. Chao, University of Illinois Press, Urbana IL., 1969
12. Belytschko, T., "An Overview of Semidiscretization and Time Integration Procedures", Chapter 1 in **Computational Methods for Transient Analysis**, edited by T. Belytschko and T.J.R. Hughes, North-Holland, 1983
13. Larkin, B.K., "Some Stable Explicit Difference Approximations to the Diffusion Equation," **Mathematics of Computation** **18** (1964) p.196
14. Conte, S.D. and C. de Boor, **Elementary Numerical Analysis**, McGraw-Hill, New York NY, 1972
15. Parker, W.J., "Prediction of the Heat Release Rate of Wood," Ph.D. Thesis, George Washington University, Washington, D.C., 1988

16. Parker, W.J. (1985), "Prediction of the heat release rate of wood," *Fire Safety Science - Proceedings of the First International Symposium* (Eds., C.E. Grant and P.J. Pagni); Hemisphere Publishing Corp, pp.207-216
17. Brandrup, J., and Immergut, E.H., eds., **Polymer Handbook**, 3d ed. (Wiley, 1989)
18. Quintiere, J.G., Harkleroad, M.F., and Walton, W.D., "Measurement of Material Flame Spread Properties," *CST* 32 (1983) 67-89
19. Quintiere, J.G., and Harkleroad, M.F., "New Concepts for Measuring Flame Spread Properties," NBSIR 84-2943, National Bureau of Standards, Gaithersburg, MD 20899, 1984. Also published as **Fire Safety Science and Engineering**, ASTM STP 882, T.Z. Harmathy, ed., American Society for Testing and Materials (ASTM), Philadelphia, PA (1985) pp.239-267
20. Torrance, K.E., "Numerical Methods in Heat Transfer", **Handbook of Heat Transfer Fundamentals**, 2nd Ed., Eds. W.M. Rohsenow, J.P. Hartnett, & E.N. Ganic, McGraw-Hill, New York, 1985.
21. Croft, D.R., and Lilley, D.G., **Heat Transfer Calculations Using Finite Difference Equations**, Applied Science Publishers Ltd., London, 1977
22. Özisik, M.N., **Heat Conduction**, Wiley-Interscience, New York, 1980.
23. Thomas, P.H., "Some Conduction Problems in the Heating of Small Areas on Large Solids", *Quart Journ. Mech. and Applied Math.*, Vol. X, Pt. 4, 1957.
24. Schneider, P.J., "Conduction," **Handbook of Heat Transfer**, 1st Ed., Eds. W.M. Rohsenow, & J.P. Hartnett, McGraw-Hill, New York, 1973.
25. Siegel, R., and Howell, J.R., **Thermal Radiation Heat Transfer**, 2nd ed., McGraw-Hill, N.Y. 1981
26. **Handbook of Single-Phase Convective Heat Transfer**, S. Kakaç, R. Shah, and W. Aung, eds.; Wiley/Interscience, N.Y., 1987
27. Cohen, N., "Boundary-layer similar solutions and correlation equations for a laminar heat transfer distribution in equilibrium air and velocities up to 41000 feet per second," NASA Technical Report R-118 (1961)
28. Childs, G.E., Ericks, L.J., and Powell, R.L., "Thermal Conductivity of Solids at Room Temperature and Below," NBS Monograph 131, National Bureau of Standards, Gaithersburg, MD, 20899 (1973)
29. Touloukian, Y.S., Powell, R.W., Ho, C.Y., and Klemens, P.G., **Thermophysical Properties of Matter, Vol.2, Thermal Conductivity, Nonmetallic Solids**, IFI/Plenum, 1970
30. Raznjevic, K., **Handbook of Thermodynamic Tables and Charts**, Hemisphere Pub. Co., 1976
31. Hilsenrath, J., Beckett, C.W., Benedict, W.S., Fano, L., Hoge, H.J., Masi, J.F., Nuttall, R.L., Touloukian, Y.S., and Woolley, H.W., **Tables of Thermal Properties of Gases**, NBS circular 564, National Bureau of Standards, Gaithersburg, MD, 20899, 1955

## FIGURE CAPTIONS

- Figure 1. One-dimensional conduction
- Figure 2. Air gap heat transfer model
- Figure 3. Substrate coordinate system
- Figure 4. Schematic of heat source for ignition tests
- Figure 5. Flux profile from heat source, as measured by a total heat flux gauge
- Figure 6. Time required to ignite the fabric, for different (initial) heat flux exposures. Crosses correspond to the discussion in the text. Filled circles correspond to a different set of experiments.
- Figure 7. Peak surface temperatures of substrate as a function of time, for the four exposures
- Figure 8. Peak surface temperatures of substrate exposed to  $Q = 25 \text{ kW/m}^2$ , as a function of  $t$ , for  
a. Material assumed to be inert      d. Char oxidation also included, as well  
b. Thermal degradation only      e. Only one reaction: oxidative pyrolysis  
c. Oxidative pyrolysis as well
- Figure 9. Temperature and density of central cell (subscript 0), adjacent cells (subscript 1), and cells in next ring around center (subscript 2), as functions of time
- Figure 10. Temperature of central surface cell (i.e., peak temperature) for three different grid sizes: 1.25, 0.50, and 0.25-mm cubes. Char oxidation was purposely left out
- Figure 11. Peak temperature for the 25 and 34.5  $\text{kW/m}^2$  cases, assuming (a) no pyrolysis, and (b) all three pyrolytic reactions
- Figure 12. Peak temperature for the 18  $\text{kW/m}^2$  case, with the same assumptions as in Fig.11
- Figure 13. Peak temperature for the 18  $\text{kW/m}^2$  case, for several values of mean  $\text{O}_2$  mass fraction,  $\langle y \rangle$
- Figure 14. Peak temperature for the 18  $\text{kW/m}^2$  case, with various assumptions for the pyrolysis:  
Curve a, no pyrolysis; curve b, "standard" pyrolysis; curve c, double the char oxidation rate;  
Curve d, double the oxidative pyrolysis rate; Curve e, 1.2 times the oxidative pyrolysis rate;  
Curve f, 1.1 times the oxidative pyrolysis rate
- Figure 15. Peak temperature as a function of time, for all four cases, using the best set of input data
- Figure 16. Total heat flux impinging on gauge, with and without purge flow
- Figure 17. Calculated heat transfer coefficient, as a function of the temperature  $T_g$  of the impinging purge gas jet
- Figure 18. Thermal conductivity of cotton as a function of temperature, as measured by different workers

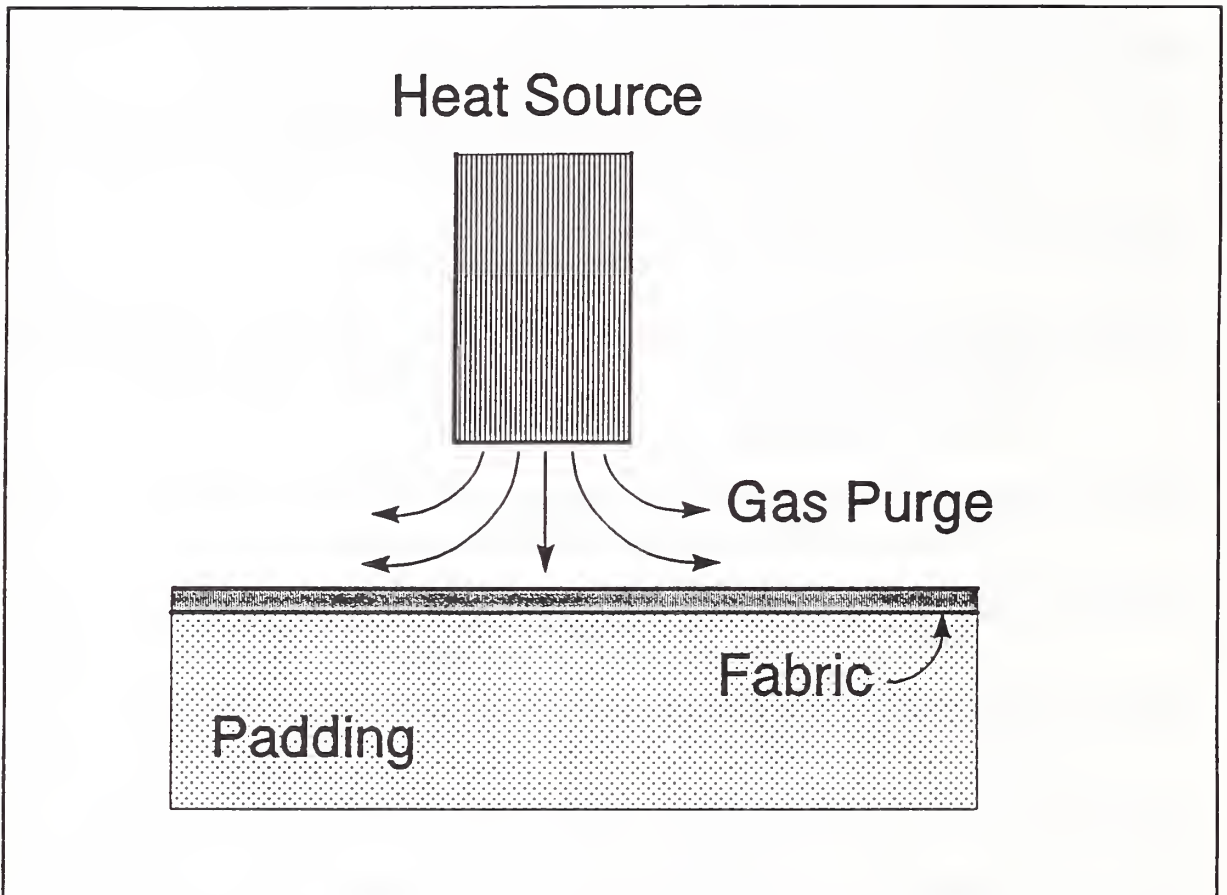


Figure 4. Schematic of heat source for ignition tests

FRONT/BACK HEAT FLUX SCAN  
15 MM LEFT/RIGHT; 5.4 MM VERTICAL

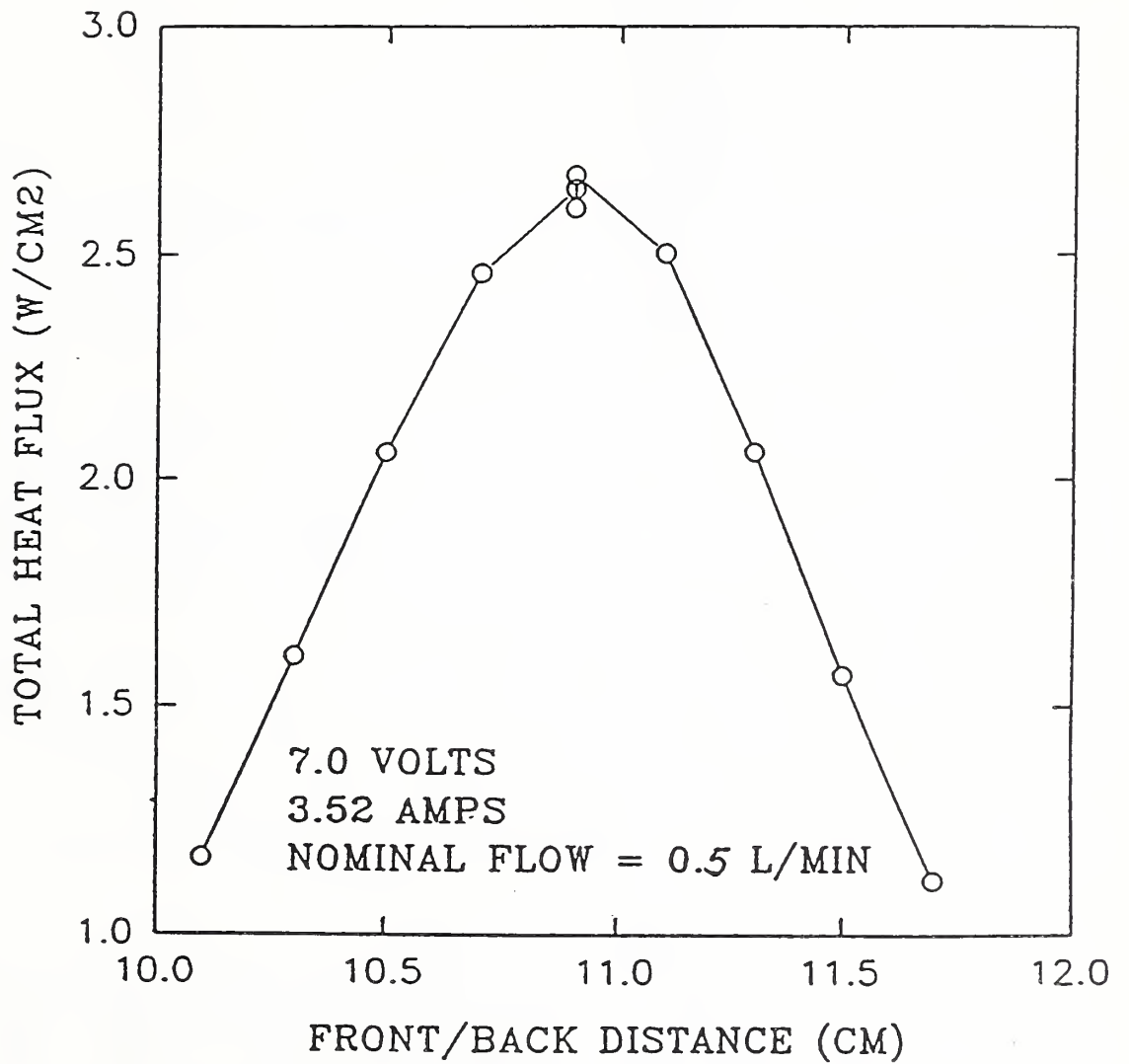


Figure 5. Flux profile from heat source, as measured by a total heat flux gauge

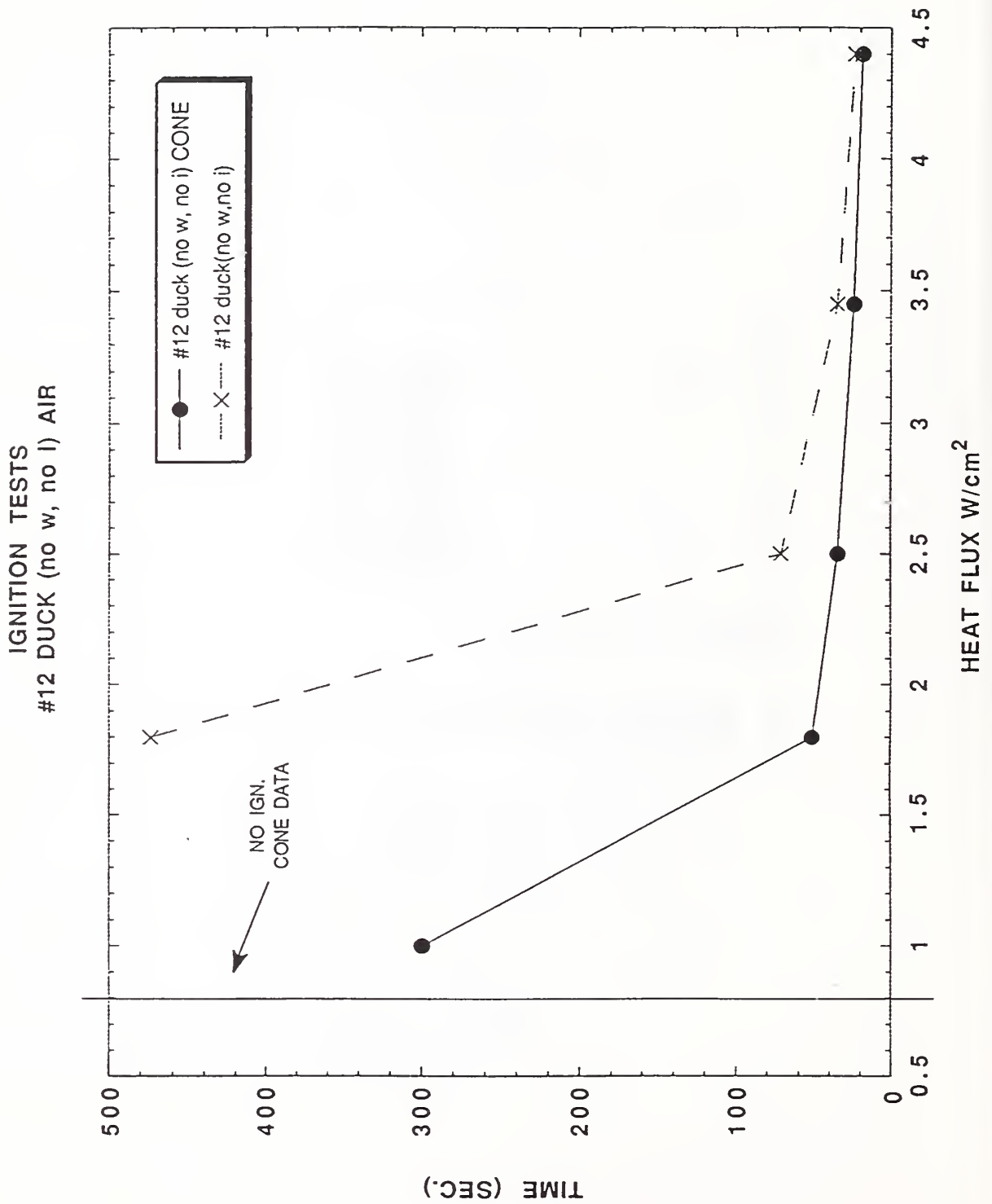


Figure 6. Time required to ignite the fabric, for different (initial) heat flux exposures. Crosses correspond to the discussion in the text. Filled circles correspond to a different set of experiments.

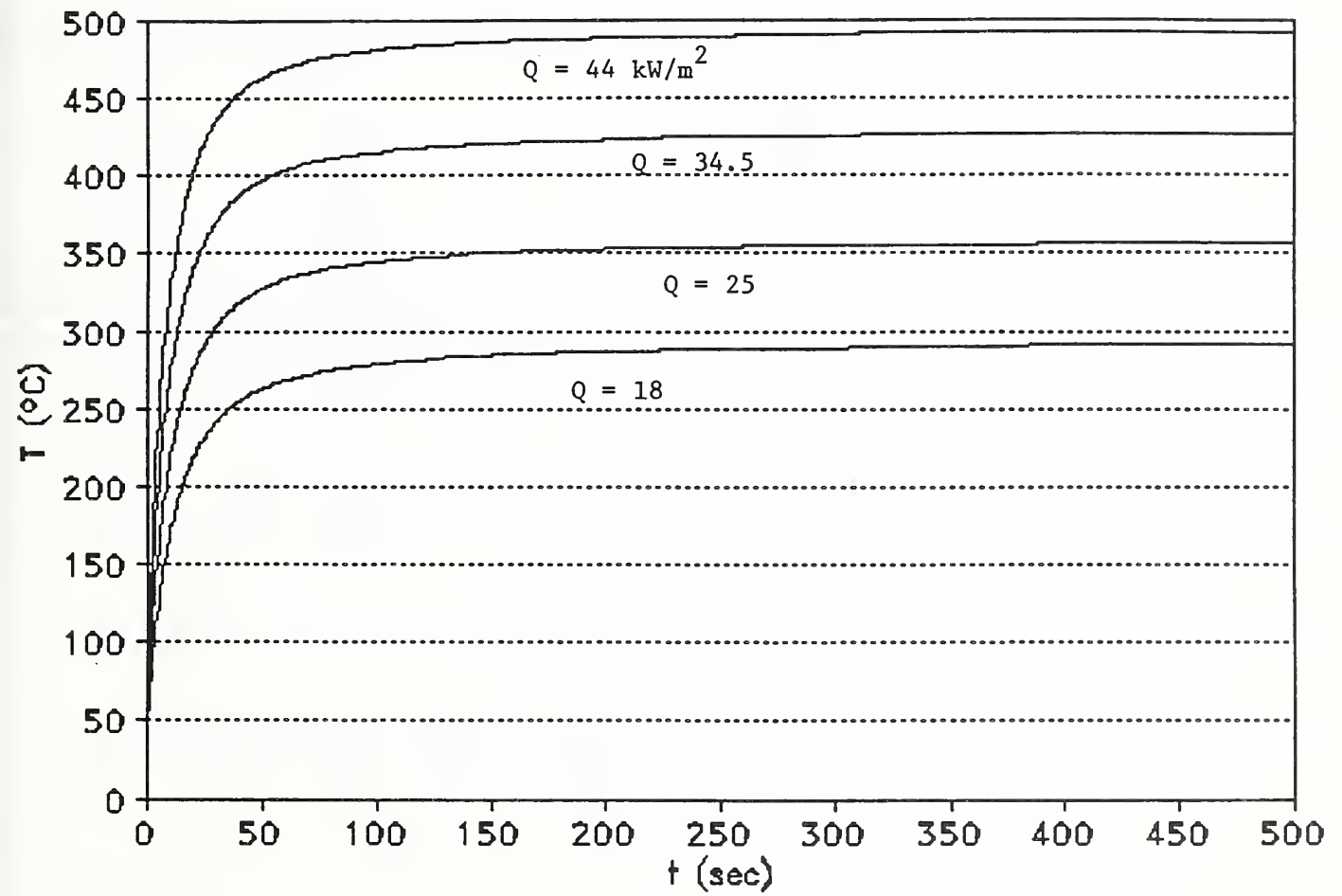


Figure 7. Peak surface temperatures of substrate as a function of time, for the four exposures

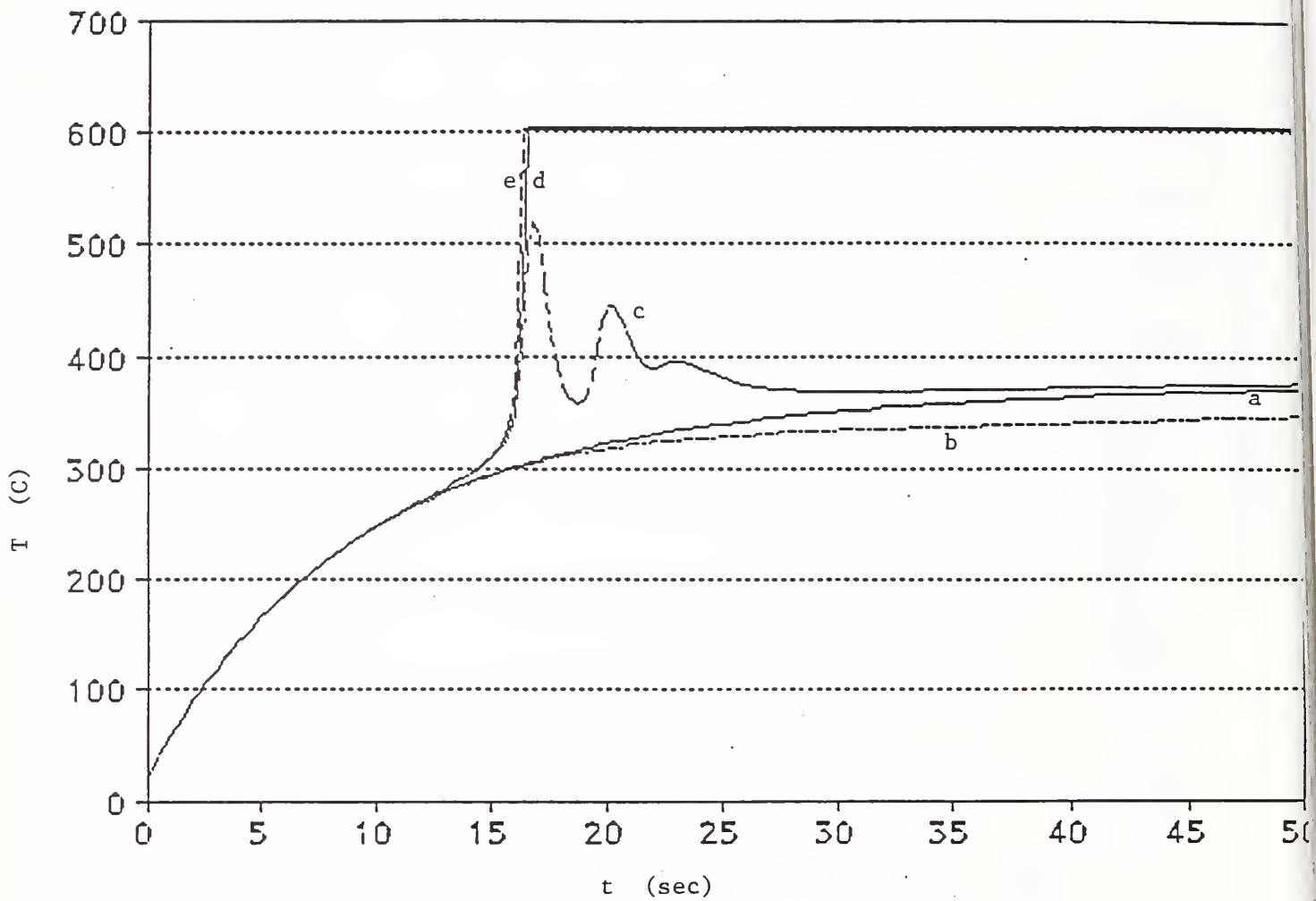


Figure 8. Peak surface temperatures of substrate exposed to  $Q = 25 \text{ kW/m}^2$ , as a function of  $t$ , for

a. Material assumed to be inert	d. Char oxidation also included, as well
b. Thermal degradation only	e. Only <u>one</u> reaction: oxidative pyrolysis
c. Oxidative pyrolysis as well	

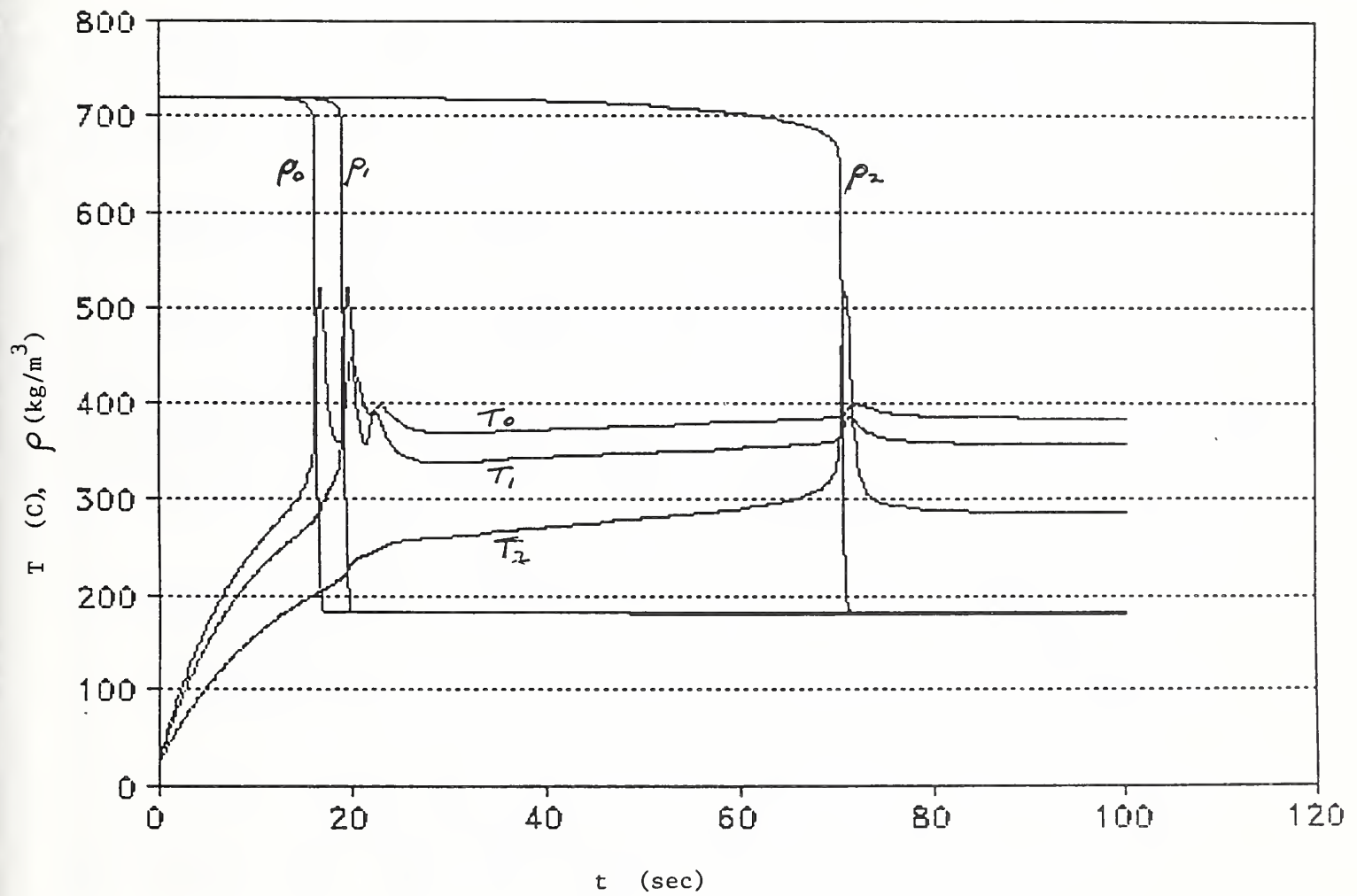


Figure 9. Temperature and density of central cell (subscript 0), adjacent cells (subscript 1), and cells in next ring around center (subscript 2), as functions of time

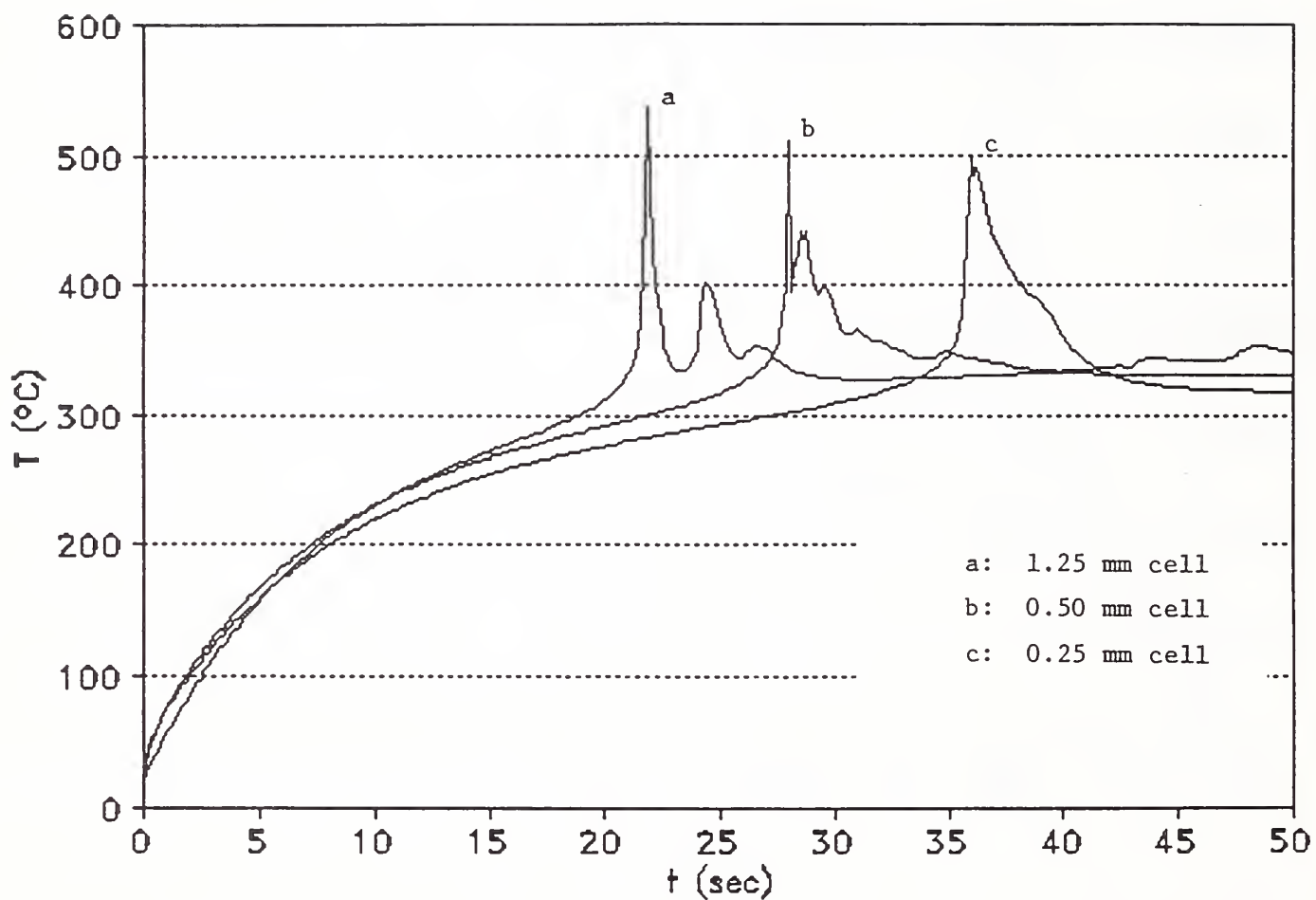


Figure 10. Temperature of central surface cell (i.e., peak temperature) for three different grid sizes: 1.25, 0.50, and 0.25-mm cubes. Char oxidation was purposely left out

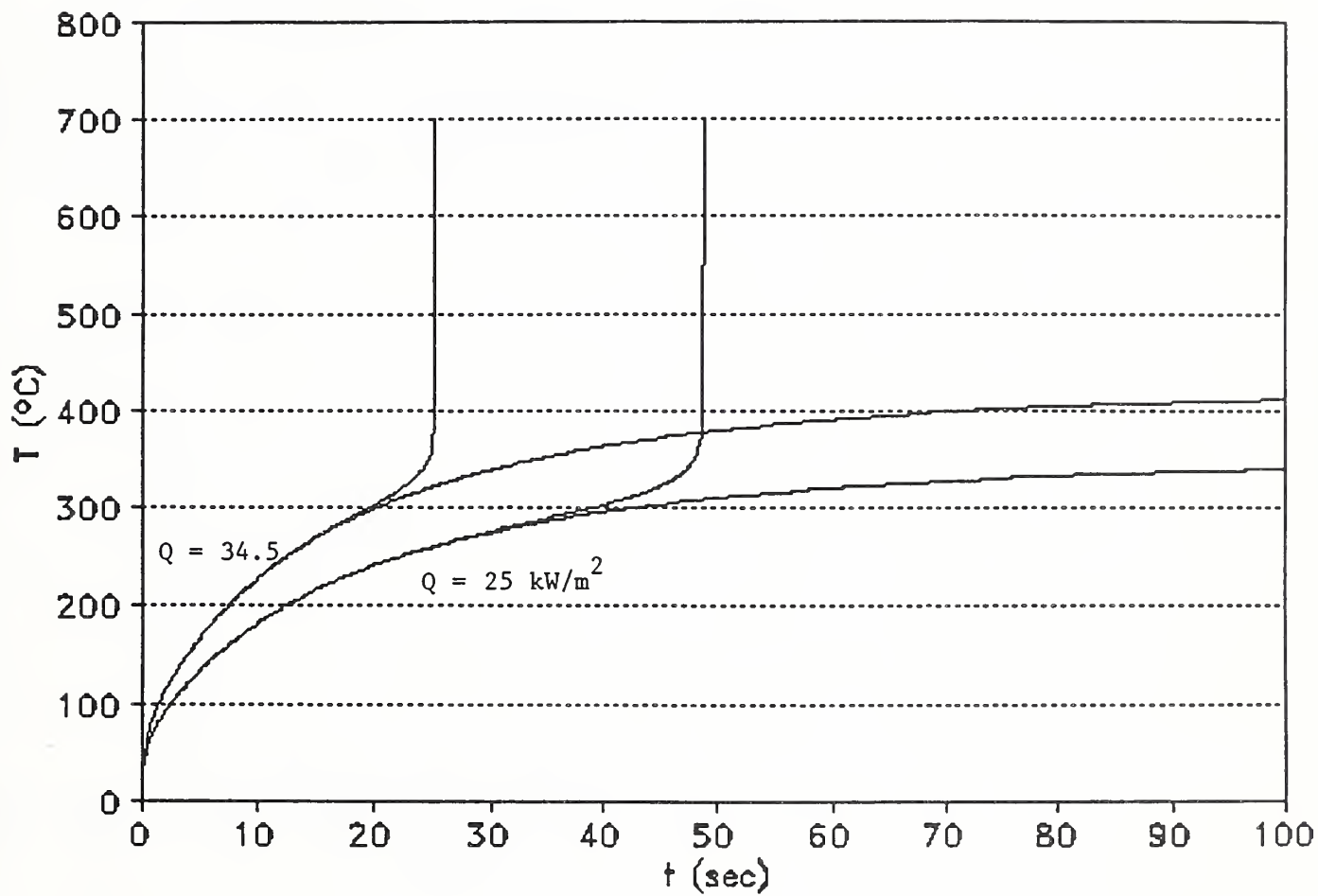


Figure 11. Peak temperature for the 25 and 34.5 kW/m<sup>2</sup> cases, assuming (a) no pyrolysis, and (b) all three pyrolytic reactions

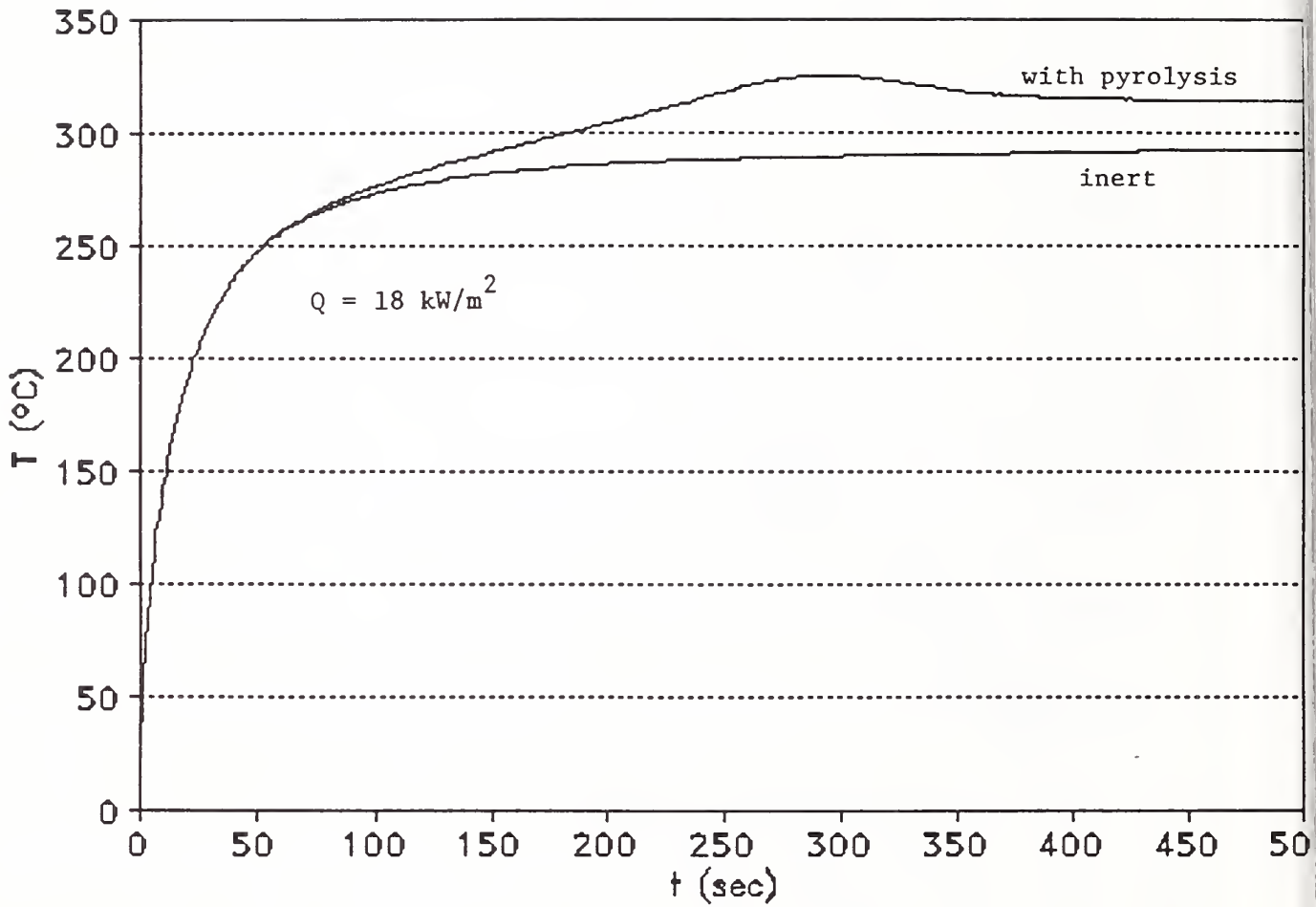


Figure 12. Peak temperature for the  $18 \text{ kW/m}^2$  case, with the same assumptions as in Fig.11

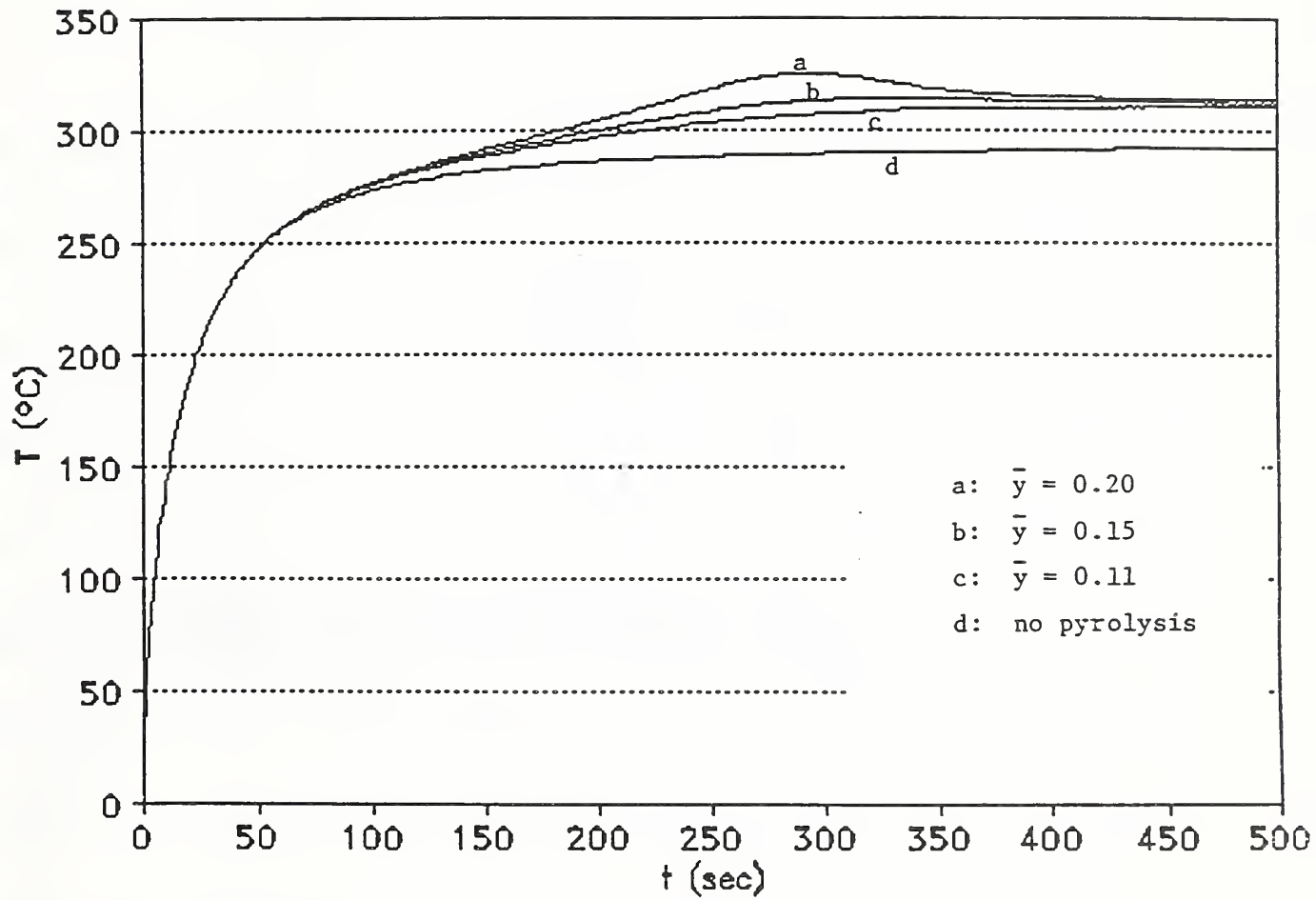


Figure 13. Peak temperature for the 18 kW/m<sup>2</sup> case, for several values of mean O<sub>2</sub> mass fraction,  $\langle y \rangle$

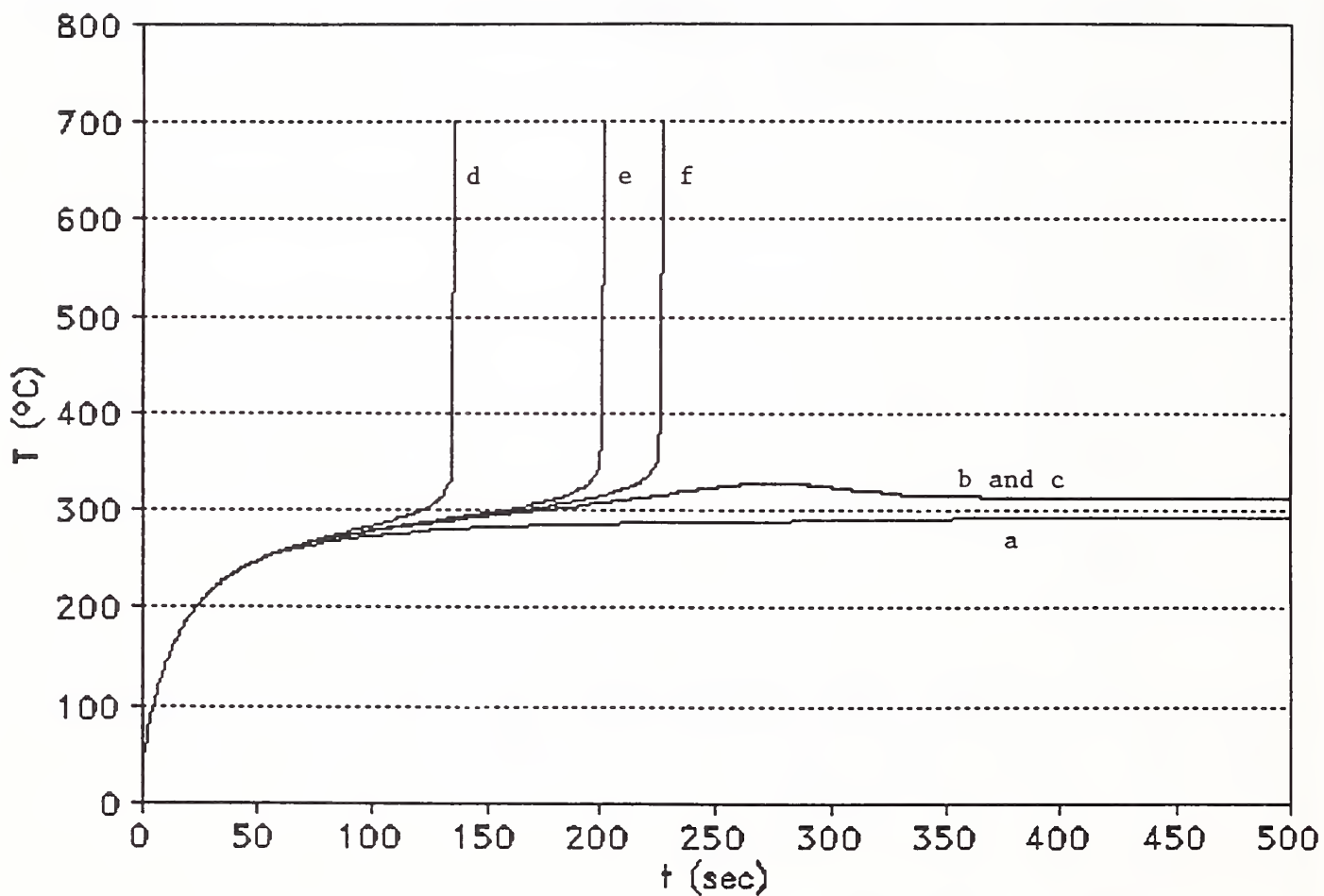


Figure 14. Peak temperature for the 18 kW/m<sup>2</sup> case, with various assumptions for the pyrolysis: Curve a, no pyrolysis; curve b, "standard" pyrolysis; curve c, double the char oxidation rate; Curve d, double the oxidative pyrolysis rate; Curve e, 1.2 times the oxidative pyrolysis rate; Curve f, 1.1 times the oxidative pyrolysis rate

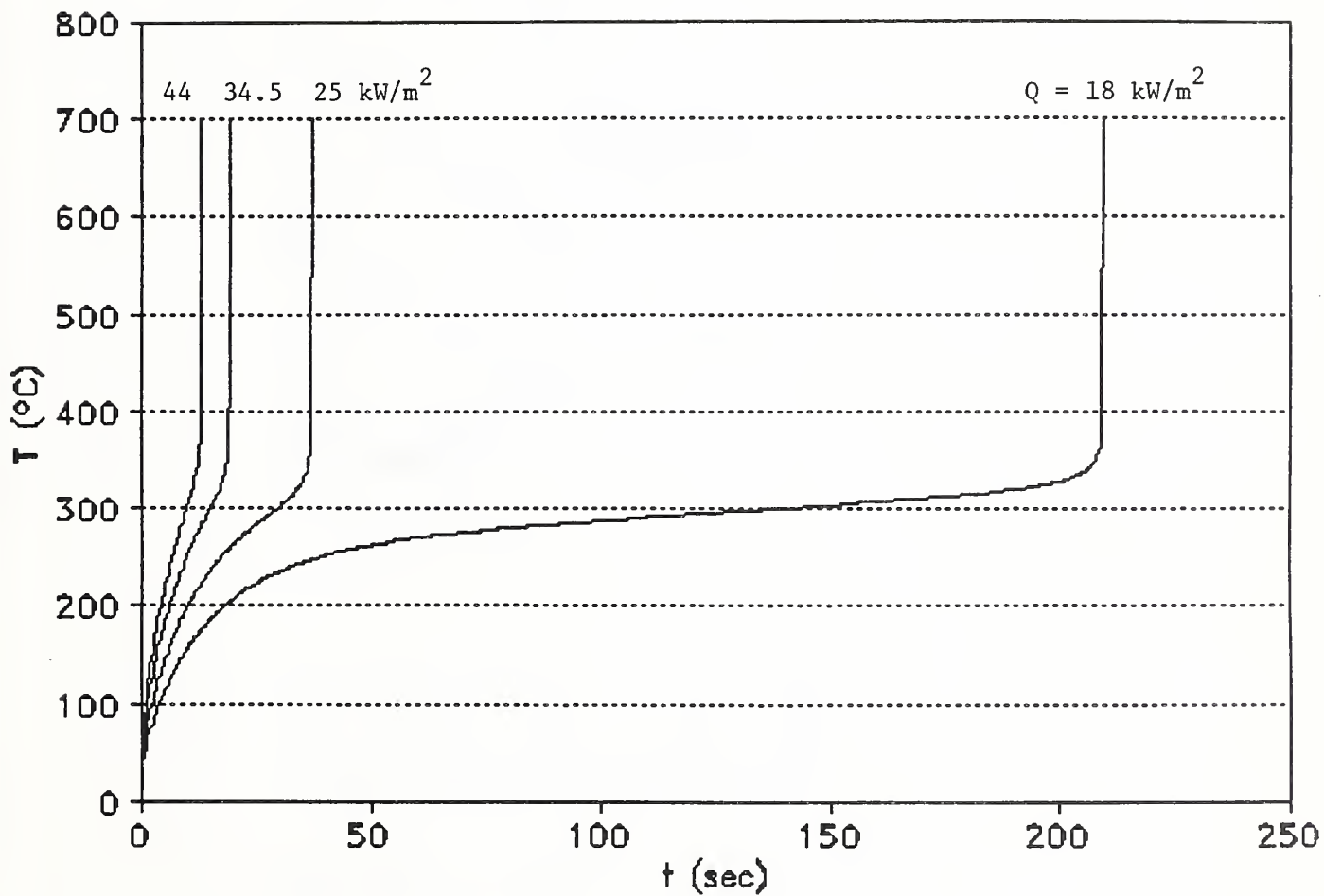


Figure 15. Peak temperature as a function of time, for all four cases, using the best set of input data

EFFECT OF PURGE FLOW ON HEAT FLUX VS HEATER POWER  
MEASURED AT PEAK POSITION; 5.4 MM BELOW HEAT SOURCE

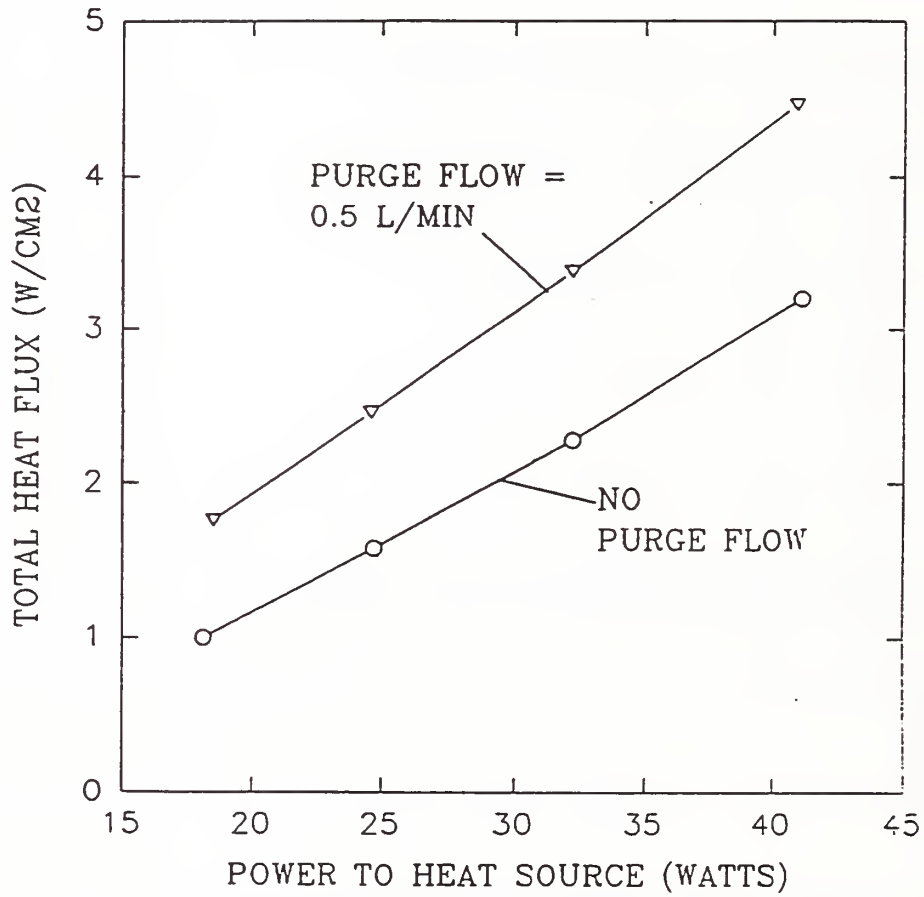


Figure 16. Total heat flux impinging on gauge, with and without purge flow

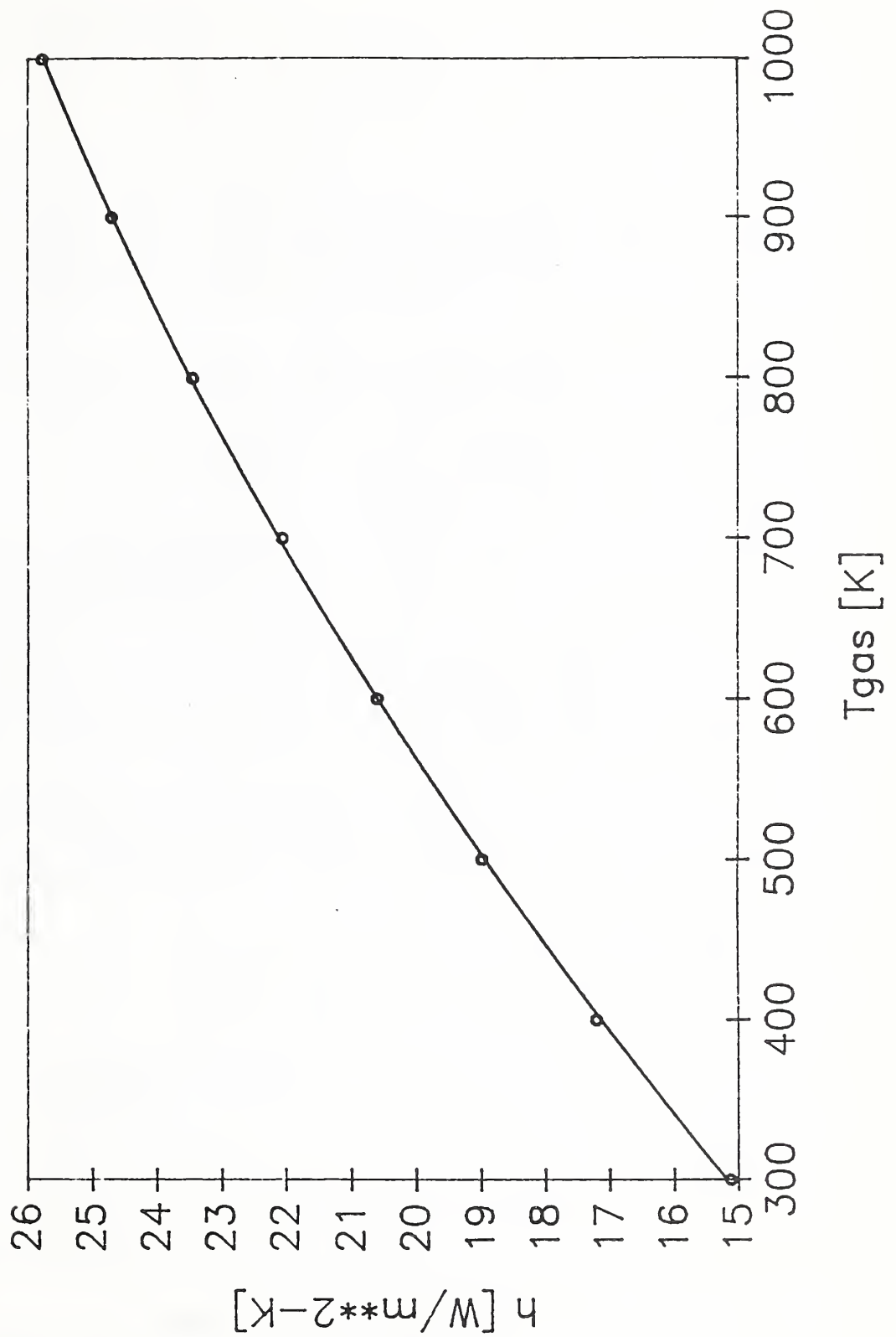


Figure 17. Calculated heat transfer coefficient, as a function of the temperature  $T_g$  of the impinging purge gas jet

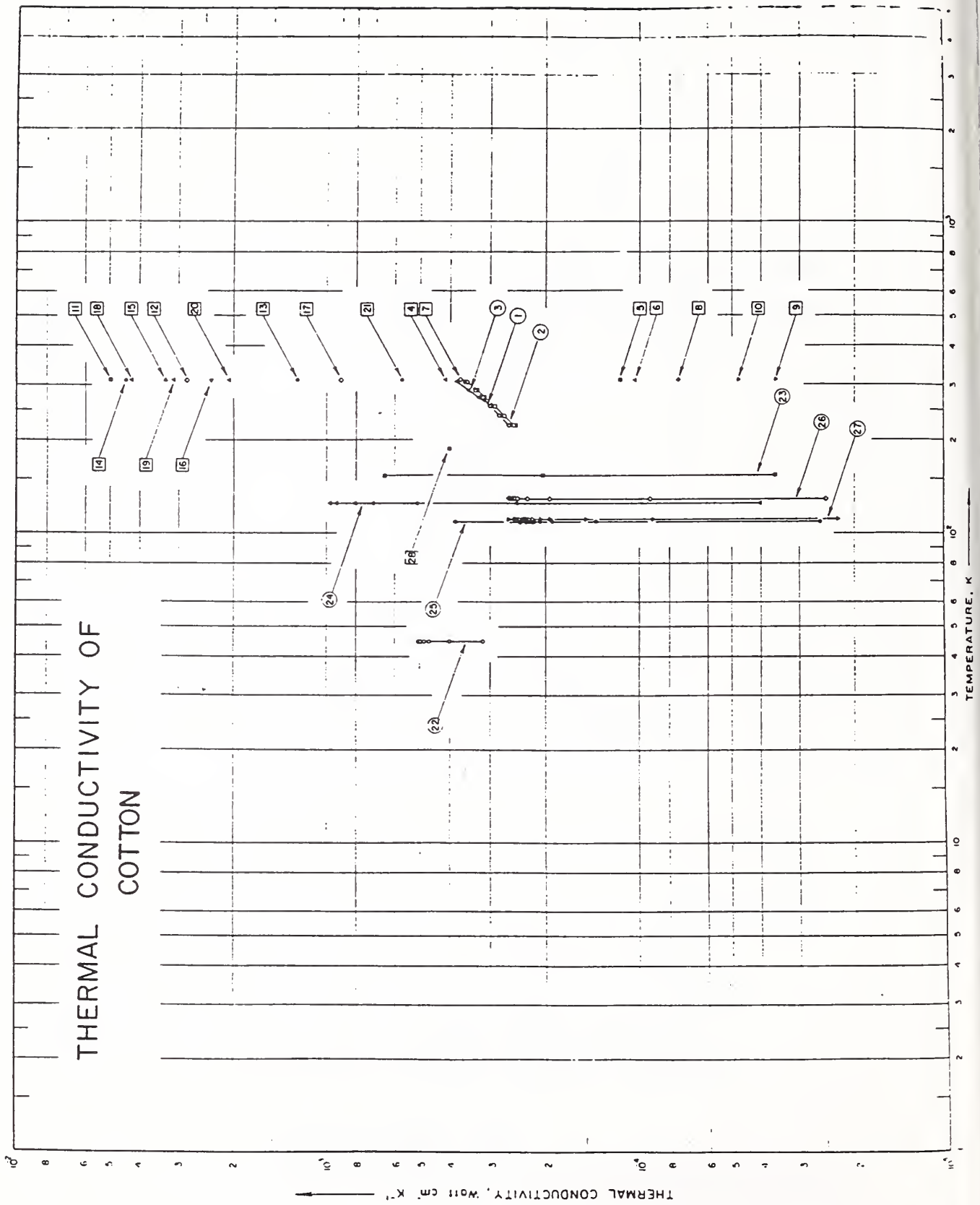


Figure 18. Thermal conductivity of cotton as a function of temperature, as measured by different workers

## APPENDIX A

### Conduction Algorithm Tests

A computer program called TEMPSUB was developed as part of the earlier investigation into the ignition of furnishings by smoldering cigarettes (Gann et al, ref [2]). This program modeled heat transfer in furniture, or in a "substrate," using a simple finite difference approximation (FDA) for a homogeneous substrate with uniform and constant properties. The research indicated that this program would have to be expanded to include a two-layer model (fabric + padding), pyrolysis of each layer, an asymmetric flux input, and a variable grid.

These features have been implemented by using a slightly different approach to the FDA than was used in TEMPSUB. The original approach was to convert the differential equation for heat transfer into an FDA by a Taylor's series approximation. The new approach is based on the conservation of energy within a control volume. It is based on physical reasoning and is usually easy to apply. It is most useful for variable grids, convective boundary conditions, odd-shaped regions, etc. It is more difficult to obtain accuracy estimates for the control volume approach than for the Taylor's series approach. For simple cases involving uniform grids and homogeneous materials the two approaches lead to identical FDAs. See Torrance or Croft & Lilley (refs [21] and [22]) for further details.

Since there is a considerable increase in the desired capabilities of the upgraded program, it was decided to develop a program which would allow extensive testing of the FDA. This program is called CTEST3 (Conduction TEST - 3 dimensional) which has the ability to model simple boundary conditions (constant temperature, heat flux, or convection coefficient) on any of the six faces of the region.

The FDA used in CTEST3, the explicit Euler method, has been checked against several heat transfer problems which have analytic solutions. The first few tests involve various combinations of constant temperature, heat flux, and convection coefficient boundary conditions with analytic solutions from the classic text by Carslaw and Jaeger (ref [3]).

Several of these analytic solutions involve the error function which is defined by

$$\operatorname{erf}(x) = \frac{2}{\sqrt{\pi}} \int_0^x e^{-\xi^2} d\xi \quad (\text{A1})$$

so that  $\operatorname{erf}(0) = 0,$

$$\operatorname{erf}(\infty) = 1,$$

and  $\operatorname{erf}(-x) = -\operatorname{erf}(x).$

The complementary error function is also used. It is defined as

$$\operatorname{erfc}(x) \equiv 1 - \operatorname{erf}(x) = \frac{2}{\sqrt{\pi}} \int_x^{\infty} e^{-\xi^2} d\xi \quad (\text{A2})$$

so that  $\operatorname{erfc}(0) = 1,$

and  $\operatorname{erfc}(\infty) = 0.$

Repeated integrals of the error function are also useful in conduction problems. These are defined by the recursive relationships

$$i^n \operatorname{erfc}(x) = \int_x^{\infty} i^{n-1} \operatorname{erfc}(x) dx \quad n=1,2,\dots \quad (\text{A3})$$

or

$$i^0 \operatorname{erfc}(x) \equiv \operatorname{erfc}(x) \quad (\text{A3a})$$

$$i \operatorname{erfc}(x) \equiv i^1 \operatorname{erfc}(x) = \frac{e^{-x^2}}{\sqrt{\pi}} - x \operatorname{erfc}(x) \quad (\text{A3b})$$

$$2ni^n \operatorname{erfc}(x) = i^{n-2} \operatorname{erfc}(x) - 2xi^{n-1} \operatorname{erfc}(x) \quad n=2,3,\dots \quad (\text{A3c})$$

See Appendix II of Carslaw and Jaeger [3] for further details on error functions. Computer subroutines were written implementing these functions for the computation of the analytic solutions of the heat transfer tests.

#### Test 1: One-dimensional steady-state conduction.

CTEST3 has been tested for steady state conduction (with constant thermal properties and uniform grid spacing). This test consists setting opposite faces on a cubic region to different temperatures and making the remaining faces adiabatic. After a sufficient number of time steps the temperature within the region should vary linearly from the hot to the cold face.

$$T(x) = T(0) + \frac{x}{L} [T(L) - T(0)] \quad (\text{A4})$$

This has been confirmed in all three directions.

#### Test 2: One-dimensional transient conduction, constant heat flux boundary condition.

This test was used in the development of the original substrate model. The analytic case for a constant flux involves a homogeneous solid occupying the semi-infinite region  $x > 0$ . The solid is initially at zero temperature throughout. At time  $t = 0$  a constant heat flux,  $q$ , is applied to the  $x = 0$  surface. The temperature within the region is given by (ref [3], p 75, eq 6)

$$T(x,t) = \frac{q\sqrt{4\alpha t}}{\kappa} \operatorname{ierfc}\left(\frac{x}{\sqrt{4\alpha t}}\right) \quad (\text{A5})$$

Preliminary testing (again using a uniform grid and constant thermal properties) indicated that as  $\Delta t$  and  $\Delta x$  decreased, there was a uniform approach to the analytic solution. As for the accuracy to be expected, for  $\Delta x = 1$  mm and  $\Delta t = 0.5$  sec, the error (after the first three time steps) was  $< 1\%$ . We note that the results of test did not agree with results from the original TEMPSUB model. Further investigation indicated an error in the TEMPSUB boundary conditions subroutine. Correcting this error brought results from the two programs into complete agreement.

Tests show that reducing the grid size along with corresponding reduction of the time step cause the FDA solution to approach the analytic solution. Therefore, the FDA is consistent. Reducing the time step without changing the grid size does not improve the accuracy of the solution. In fact, it is best to operate as close to the stability limit as possible for both accuracy and execution time. Use of the variable grid gives results consistent with the uniform grid at the surface. The error in the calculated surface temperature goes down as time increases.

**Test 3:** One-dimensional transient conduction, constant convection coefficient boundary condition.

This test represents a slab of a homogeneous solid of thickness  $2L$  in the  $x$  direction and infinite extent in the  $y$  and  $z$  directions which is initially at unit temperature throughout. At time  $t=0$  the temperature of the fluid on both sides of the slab is changed to zero and heat is convected from the slab through a constant convection coefficient. Because of symmetry this problem is equivalent to a slab of thickness  $L$  with one adiabatic surface at  $x = 0$  and a convective surface at  $x = L$ . The temperature within the region is given by (ref.[3], p 122, Eq(12))

$$T(x,t) = \sum_{n=1}^{\infty} \frac{2B \cos(\delta_n x/L)}{[B^2 + B + \delta_n^2] \cos \delta_n} e^{-\delta_n^2 F} \quad (A6)$$

where  $B = hL/\kappa$  (Biot number),

$F = \alpha t/L^2$  (Fourier number), and

$\delta_n$  are the solutions of the transcendental equation  $\delta_n \tan \delta_n = B$ .

In order to check the calculation of this complicated analytic solution, the solution to a related problem was also computed. This is the temperatures in a semi-infinite slab with the convective boundary condition (ref.[3], p 72, eq(5))

$$T(x,t) = \operatorname{erfc}\left(\frac{x}{\sqrt{4\alpha t}}\right) - \exp\left(\frac{h}{\kappa}(x+\alpha ht/\kappa)\right) \operatorname{erfc}\left(\frac{x}{\sqrt{4\alpha t}} + \frac{h}{\kappa}\sqrt{\alpha t}\right) \quad (A7)$$

where  $x$  is now the distance from the convective surface into the region. There is good agreement between the FDA and analytic solutions. Again, the error in the calculated temperature goes down as time increases.

**Test 4:** Three-dimensional transient conduction, constant surface temperature boundary condition.

This test represents a block of a homogeneous solid in the region defined by  $-a < x < a$ ,  $-b < y < b$ , and  $-c < z < c$  which is initially at unit temperature throughout. At time  $t=0$  the temperatures of the surfaces of the block are reduced to zero, and the block begins to cool. The temperature within the region is given by (ref[3], p 184, Eq(5))

$$T(x,y,z,t) = \frac{64}{\pi^3} \sum_{l=0}^{\infty} \sum_{m=0}^{\infty} \sum_{n=0}^{\infty} \frac{(-1)^{l+m+n}}{(2l+1)(2m+1)(2n+1)} \times \\ \cos\left[\frac{(2l+1)\pi x}{2a}\right] \cos\left[\frac{(2m+1)\pi y}{2b}\right] \cos\left[\frac{(2n+1)\pi z}{2c}\right] \times \\ \exp\left\{-\frac{\kappa\pi^2 t}{4} \left[\frac{(2l+1)^2}{a^2} + \frac{(2m+1)^2}{b^2} + \frac{(2n+1)^2}{c^2}\right]\right\} \quad (A8)$$

This expression requires the summation of many terms at small values of time, but only a few terms at large values of time. The implementation of this complicated equation had to be checked against simpler analytic cases. The first case represents a homogeneous solid occupying the semi-infinite region,  $x > 0$ . The solid is initially at unit temperature throughout. At time  $t = 0$  the temperature at  $x = 0$  is instantly reduced to zero. The temperature within the region is given by (ref[3], p 59, eq(3))

$$T(x,t) = \operatorname{erf}\left(\frac{x}{\sqrt{4\alpha t}}\right) \quad (\text{A9})$$

The second case involves a solid which occupies the region  $x > 0, y > 0, z > 0$ . It is initially at unit temperature and at time  $t = 0$  the temperature at the  $x = 0, y = 0,$  and  $z = 0$  surfaces is instantly reduced to zero. The temperature within the region is given by (ref[3], p 184, Eq(1))

$$T(x,y,z,t) = \operatorname{erf}\left(\frac{x}{\sqrt{4\alpha t}}\right) \operatorname{erf}\left(\frac{y}{\sqrt{4\alpha t}}\right) \operatorname{erf}\left(\frac{z}{\sqrt{4\alpha t}}\right) \quad (\text{A10})$$

The temperatures near the corners of the block should be very similar to this.

There was good agreement (error  $< 1\%$ ) for a test with  $a=30$  mm,  $b=20$  mm,  $c=10$  mm using a 1 mm uniform grid. The original variable grid model was found to be insufficiently accurate at points where the grid size changed. It was therefore replaced by the current uniformly increasing grid at a cost of some increase in code complexity; although the results are not quite as accurate as for the uniformly-spaced grid, the difference is very minor (see Section 3d).

**Test 5:** One-dimensional transient conduction, two different materials.

This test consists of one material in the region 1 ( $0 < z < L$ ) initially at unit temperature and another material in region 2 ( $z > L$ ) initially at zero temperature. The boundary at  $z = 0$  is adiabatic. At time  $t=0$  heat begins to be conducted between the two regions. The temperatures in the two regions are given by (Özisik, ref[23], p.328, Eq 8-109)

$$\begin{aligned} T_1(x,t) &= 1 - \frac{1-\delta}{2} \sum_{n=0}^{\infty} \delta^n \left\{ \operatorname{erfc}\left[\frac{(2n+1)L-x}{\sqrt{4\alpha_1 t}}\right] + \operatorname{erfc}\left[\frac{(2n+1)L+x}{\sqrt{4\alpha_1 t}}\right] \right\} \\ T_2(x,t) &= \frac{1+\delta}{2} \sum_{n=0}^{\infty} \left\{ \operatorname{erfc}\left[\frac{2nL+\mu(x-L)}{\sqrt{4\alpha_1 t}}\right] - \operatorname{erfc}\left[\frac{(2n+2)L+\mu(x-L)}{\sqrt{4\alpha_1 t}}\right] \right\} \end{aligned} \quad (\text{A11})$$

where

$$\mu = \sqrt{\frac{\alpha_1}{\alpha_2}}, \quad \beta = \frac{\kappa_1}{\kappa_2 \mu}, \quad \delta = \frac{\beta-1}{\beta+1}.$$

There was good agreement between the FDA and analytic solutions. It even worked well when the first layer was only one-half of a grid thick. This may be useful for thin fabric coverings.

**Test 6:** Three-dimensional transient conduction, constant heat flux impinging on a circular area (disk) on a semi-infinite region.

The impinging flux is  $q$ , there is convective cooling from the surface,  $h(T_s - T_a)$ , and the disk radius is  $R$ . The temperature at the center of the heated area is given by (Thomas ref[24], Eq 5)

$$T(t) = \frac{qR}{\kappa} \left\{ \sqrt{\frac{4\alpha t}{\pi R^2}} \left[ 1 - \exp\left(-\frac{R^2}{4\alpha t}\right) \right] + \operatorname{erfc}\left(\frac{R}{\sqrt{4\alpha t}}\right) \right\} - \frac{2q}{h} \int_{\omega=0}^{\frac{h}{\kappa}\sqrt{\alpha t}} \left[ 1 - \exp\left(\frac{-h^2 R^2}{4k^2 \omega^2}\right) \right] \omega e^{-\omega^2} \operatorname{erfc}(\omega) d\omega \quad (\text{A12})$$

The first part of the above expression is the center point temperature if there is no convective cooling. Tests indicate that the accuracy of the FDA for this test is primarily dependent on how accurately the circular flux pattern is represented on the rectangular surface grid. A small grid and assigning cell heat gain according to the portion of the cell that is within the circle improve accuracy.

Note that tests 1 through 6 involve a step change, which should be the worst condition to simulate with the FDA. In all cases the maximum errors occurred at the first time step, and the error declined as time increased.

**Test 7:** Three-dimensional transient conduction, uniformly moving point-source heat flux.

This test consists of a point source of power  $Q$  moving in an infinite body at a constant velocity  $v$  in the  $x$  direction (Schneider, ref[25], pp.3-86, Eq 78)

$$\frac{\kappa r}{Q} (T - T_o) = \frac{1}{4\pi} \exp\left[-\frac{v}{2\alpha} (\xi + r)\right] \quad (\text{A13})$$

where  $\xi = x - vt$  and  $r = (\xi^2 + y^2 + z^2)^{1/2}$ . Adjusting for a semi-infinite body with the point source moving along an adiabatic surface is done by replacing  $4\pi$  by  $2\pi$  in (A13). Generally good agreement was achieved for this test. Accuracy was limited by grid size near the point source and the fact this is a quasi-steady case in that movement of the point source does not have a beginning point.

### Larkin's method

The FDA algorithm in CTEST3 was transferred directly into the new substrate model TMPSUB2. The addition of pyrolysis forced the use of a very small grid in the region of peak temperature for a satisfactory solution. This combined with the stability requirement of the explicit Euler method forced a very small time step and therefore a very long execution time. A different FDA algorithm had to be found to achieve a program fast enough to be useful. Larkin's method was chosen because of its simplicity in that it uses the same spatial FDA as the original method while the new temporal FDA does not require the solution of simultaneous equations.

CTEST3 was not rewritten to run all of the test cases, but several tests were made with TMPSUB2 (some using a modified surface boundary condition) which indicate the accuracy of the method for different grid size and time step options. The results of these tests are shown in tables A1, A2, and A3.

Table A1 gives the results of several tests which can be compared to Eq.(A5) to determine the effect of grid spacing. These tests use a region 40 mm thick to simulate a semi-infinite body which is shown to be appropriate by having negligible heat flux at the constant temperature surface at  $Z=40$  mm. Comparisons are made based on the temperature of the surface ( $Z=0$  mm). Test 2a: using a constant 1 mm grid spacing the temperature after 100 seconds (502.543) is 0.33% less than the exact value. Test 2b: using a constant 0.5 mm spacing gives a surface temperature 0.18% below the theoretical value. Tests 2c through 2f use variable grid spacing to reduce the number of cells and execution time at the cost of some loss of accuracy.

Table A2 gives the results of several tests where the parameters that control the time step while maintaining a constant grid spacing, are varied. These parameters are the maximum time step,  $dt_{max}$ , and the maximum temperature change,  $dT_{max}$ . (Whenever  $T_{n+1} - T_n$  exceeds  $dT_{max}$ , the time step is halved.) Obviously the greatest accuracy should be achieved with small values for these two parameters, but execution time is reduced by using large values. There is no obvious optimum; the user must choose values appropriate for results he wishes to achieve.

Table A3 shows tests of different grid spacings for full three-dimensional heat conduction from a stationary spot heat flux. These tests use representative thermal properties for the fabric and padding. Various combinations of cell spacings are used to select the best grid.

Table A1: Grid Spacing Tests

Thermal diffusivity:  $2e-07 \text{ m}^2/\text{s}$   
 Thermal conductivity:  $0.1 \text{ W/mK}$   
 Surface heat flux:  $1e+04 \text{ W/m}^2$   
 Distance from surface:  $0 \text{ m}$

time	Texact	Test2a	Test2b	Test2c	Test2d	Test2e	Test2f
0.000	0.0000	0.000	0.000	0.000	0.000	0.000	0.000
0.125	17.8412	5.000	9.319	9.319	9.319	9.319	9.319
0.250	25.2313	9.643	16.889	16.889	16.889	16.889	16.889
0.375	30.9019	13.970	23.331	23.331	23.331	23.331	23.331
0.500	35.6825	18.298	28.916	28.916	28.916	28.916	28.916
0.625	39.8942	22.252	33.840	33.840	33.840	33.840	33.840
0.750	43.7019	26.206	38.035	38.035	38.035	38.034	38.034
0.875	47.2035	29.838	42.229	42.229	42.229	42.229	42.229
1.000	50.4627	33.469	45.757	45.757	45.757	45.757	45.757
1.250	56.4190	40.170	52.366	52.366	52.366	52.366	52.366
1.500	61.8039	46.383	58.208	58.208	58.208	58.208	58.208
1.750	66.7558	52.167	63.496	63.496	63.496	63.496	63.496
2.000	71.3650	57.577	68.361	68.361	68.361	68.361	68.361
2.250	75.6940	62.656	73.042	73.042	73.041	73.041	73.041
2.500	79.7885	67.445	77.173	77.173	77.173	77.173	77.171
2.750	83.6828	71.859	81.305	81.305	81.304	81.304	81.302
3.000	87.4039	76.273	85.049	85.049	85.048	85.047	85.044
3.500	94.4070	84.279	92.243	92.243	92.242	92.240	92.233
4.000	100.9253	91.625	98.911	98.909	98.908	98.904	98.893
4.500	107.0474	98.433	105.154	105.152	105.149	105.143	105.125
5.000	112.8379	104.796	111.046	111.042	111.038	111.030	111.002
6.000	123.6077	116.456	121.976	121.970	121.962	121.946	121.894
7.000	133.5116	127.018	132.004	131.993	131.981	132.050	131.966
8.000	142.7299	136.650	141.315	141.300	141.283	141.309	141.188
9.000	151.3880	145.711	150.034	150.014	149.991	149.993	149.830
10.000	159.5769	154.229	158.272	158.248	158.219	158.201	157.994
15.000	195.4410	191.150	194.315	194.266	194.208	194.109	193.654
20.000	225.6758	221.986	224.670	224.600	224.514	224.343	223.631
25.000	252.3132	249.025	251.396	251.307	251.195	250.960	249.998
30.000	276.3953	273.438	275.472	275.367	275.235	274.852	273.660
35.000	298.5410	295.758	297.599	297.487	297.339	296.828	295.425
40.000	319.1538	316.566	318.155	318.040	317.879	317.378	315.771
45.000	338.5137	336.042	337.525	337.408	337.234	336.650	334.844
50.000	356.8248	354.491	355.815	355.694	355.509	354.928	352.929
60.000	390.8820	388.738	389.887	389.758	389.550	388.899	386.532
70.000	422.2008	420.206	421.230	421.093	420.862	420.147	417.431
80.000	451.3517	449.479	450.409	450.262	450.010	449.235	446.188
90.000	478.7307	476.960	477.816	477.660	477.388	476.556	473.195
100.000	504.6265	502.943	503.740	503.574	503.282	502.397	498.738
cells:		41	81	35	25	18	12
steps:		153	154	154	154	153	153

TEST2A: dz=1.0mm, nz=41, nc=41, r=1.000, dtmax=1.0, dTmax = 5.0  
 TEST2B: dz=0.5mm, nz=81, nc=81, r=1.000, dtmax=1.0, dTmax = 5.0  
 TEST2C: dz=0.5mm, nz=35, nc=4, r=1.055, dtmax=1.0, dTmax = 5.0  
 TEST2D: dz=0.5mm, nz=25, nc=4, r=1.115, dtmax=1.0, dTmax = 5.0  
 TEST2E: dz=0.5mm, nz=18, nc=4, r=1.234, dtmax=1.0, dTmax = 5.0  
 TEST2F: dz=0.5mm, nz=12, nc=4, r=1.628, dtmax=1.0, dTmax = 5.0

**Table A2: Time Step Control Tests**

Thermal diffusivity:  $2e-07 \text{ m}^2/\text{s}$   
 Thermal conductivity:  $0.1 \text{ W/mK}$   
 Surface heat flux:  $1e+04 \text{ W/m}^2$   
 Distance from surface:  $0 \text{ m}$

time	Texact	Test2b	Test2g	Test2h	Test2J
0.000	0.0000	0.000	0.000	0.000	0.000
0.125	17.8412	9.319	9.093		
0.250	25.2313	16.889	16.685	20.000	20.000
0.375	30.9019	23.331	23.148		
0.500	35.6825	28.916	28.750	31.538	31.538
0.625	39.8942	33.840	33.688		
0.750	43.7019	38.035	38.107	39.690	39.690
0.875	47.2035	42.229	42.125		
1.000	50.4627	45.757	45.801	47.841	47.841
1.250	56.4190	52.366	52.390		
1.500	61.8039	58.208	58.223	58.553	58.553
1.750	66.7558	63.496	63.506		
2.000	71.3650	68.361	68.368	69.264	69.264
2.250	75.6940	73.042	72.899		
2.500	79.7885	77.173	77.158	77.403	77.403
2.750	83.6828	81.305	81.191		
3.000	87.4039	85.049	85.028	85.542	85.542
3.500	94.4070	92.243	92.222		
4.000	100.9253	98.911	98.891	97.831	97.831
4.500	107.0474	105.154	105.136		
5.000	112.8379	111.046	111.029	110.120	110.120
6.000	123.6077	121.976	121.963	120.390	120.390
7.000	133.5116	132.004	131.993	130.660	130.660
8.000	142.7299	141.315	141.312	139.622	139.622
9.000	151.3880	150.034	150.053	148.583	
10.000	159.5769	158.272	158.312	156.621	157.545
15.000	195.4410	194.315	194.402	192.945	
20.000	225.6758	224.670	224.773	223.337	221.615
25.000	252.3132	251.396	251.504	250.229	
30.000	276.3953	275.472	275.656	274.420	
35.000	298.5410	297.599	297.855	296.726	
40.000	319.1538	318.155	318.512	317.415	313.420
45.000	338.5137	337.525	337.900	336.887	
50.000	356.8248	355.815	356.236	355.255	
60.000	390.8820	389.887	390.336	389.440	382.464
70.000	422.2008	421.230	421.690	420.860	
80.000	451.3517	450.409	450.870	450.093	442.530
90.000	478.7307	477.816	478.274	477.541	
100.000	504.6265	503.740	504.191	503.495	495.723
cells:		81	81	81	81
steps:		154	724	106	42

TEST2B: dz=0.5mm, nz=81, nc=81, r=1.000, dtmax=1.0, dTmax = 5.0  
 TEST2G: dz=0.5mm, nz=81, nc=81, r=1.000, dtmax=1.0, dTmax = 1.0  
 TEST2H: dz=0.5mm, nz=81, nc=81, r=1.000, dtmax=1.0, dTmax = 20.0  
 TEST2I: dz=0.5mm, nz=81, nc=81, r=1.000, dtmax=4.0, dTmax = 5.0  
 ( Same results as test2b because  $dT > 2.5$  at  $dt = 1.0$  )  
 TEST2J: dz=0.5mm, nz=81, nc=81, r=1.000, dtmax=4.0, dTmax = 20.0

**Table A3: 3-D Transient Conduction Tests**

time	test3a	test3b	test3c	test3d	test3e
0.00	0.000	0.000	0.000	0.000	0.000
1.00	65.749	70.904	71.046	71.254	71.301
2.00	88.450	91.190	91.381	91.660	91.723
3.00	104.807	106.828	107.053	107.382	107.455
4.00	118.536	120.437	120.692	121.060	121.140
5.00	130.745	132.693	132.974	133.375	133.460
10.00	178.269	180.414	180.785	181.287	181.377
15.00	211.444	213.792	214.214	214.765	214.850
20.00	236.140	238.668	239.121	239.692	239.766
30.00	269.762	272.068	272.539	273.119	273.173
40.00	291.304	293.512	293.988	294.550	294.585
50.00	305.937	308.182	308.659	309.201	309.219
60.00	316.279	318.588	319.064	319.589	319.594
70.00	323.830	326.195	326.670	327.180	327.176
80.00	329.498	331.903	332.376	332.876	332.865
90.00	333.853	336.285	336.757	337.248	337.233
100.00	337.271	339.718	340.188	340.673	340.654
cells:	18081	18081	18081	19176	18375
steps:	152	154	154	154	154
time:	303.08	316.37	316.10	338.90	346.32

TEST3A: dx=0.5mm, nx=41, ny=21, nz = 21, nc = 4, yw=zw = 40,  
rx=ry=1.167, rz=1.187, dtmax=1.0, dTmax = 5.0

TEST3B: dx=0.25mm, nx=41, ny=21, nz = 21, nc = 4, yw=zw = 40,  
rx=ry=1.240, rz=1.240, dtmax=1.0, dTmax = 5.0

TEST3C: dx=0.25mm, nx=41, ny=21, nz = 21, nc = 4, yw=zw = 30,  
rx=ry=1.210, rz=1.210, dtmax=1.0, dTmax = 5.0

TEST3D: dx=0.25mm, nx=47, ny=24, nz = 17, nc = 4, yw=zw = 30,  
rx=ry=1.161, rz=1.326, dtmax=1.0, dTmax = 5.0

TEST3E: dx=0.25mm, nx=49, ny=25, nz = 15, nc = 4, yw=zw = 30,  
rx=ry=1.149, rz=1.431, dtmax=1.0, dTmax = 5.0

## APPENDIX B

### TMPSUB2 User's Guide

#### General Information

TMPSUB2 and two helper programs are available on a diskette for IBM PC compatible computers. The distribution diskette includes both executable and source code for TMPSUB2, executable code for the other two programs, and sample input files. The general relationship of programs and files is illustrated in figure B1. The TSDATA program is used to prepare data files for TMPSUB2 which in turn creates two types of output files. The plot file is used by the TSPLIT program to display contour plots of substrate temperatures. The list file includes a step-by-step record of the highest temperature in the substrate.

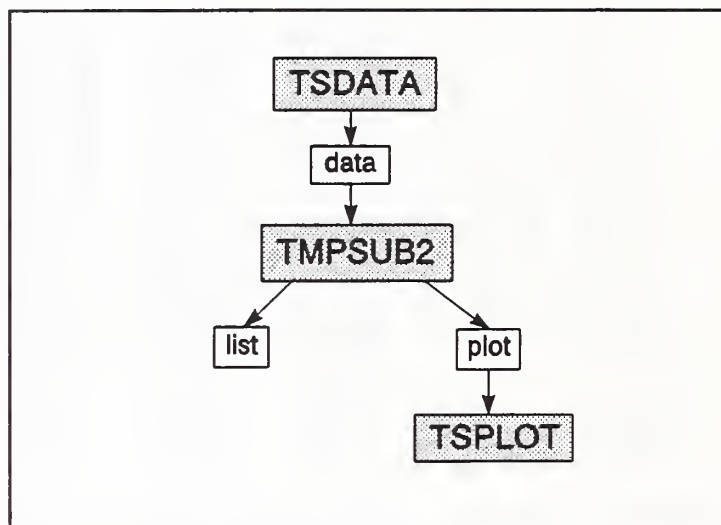


Figure B1. TMPSUB2 Programs and Files

TSDATA and TSPLIT must be run using MS-DOS on IBM PC compatible computers with VGA graphics. TMPSUB2 requires a 386 class PC with math coprocessor or 486 class PC (no graphics needed) in order to achieve satisfactory performance. Typical execution times are 20 to 30 minutes on a 33Mhz 486 computer.

The TMPSUB2 source code (file TMPSUB2.CCC) can be compiled using any ANSI C compiler. All TMPSUB2 input and output files are ASCII files. Therefore, TMPSUB2 can be recompiled and run on a different computer, while still using TSDATA and TSPLIT on a PC and transferring files between the computers. A different computer may allow TMPSUB2 to execute faster and/or handle more cells for more accurate simulation.

Be sure to inspect the README file on the distribution diskette. One way to read this file is to place the diskette in drive A: (or drive B:) and type MORE <A:README (or MORE <B:README). A permanent copy may be made with PRINT <A:README. The README file contains a list of all files on the diskette, instructions for installing the necessary files on your hard disk, and information on any changes or additions to the program.

There should be at least 1,000,000 bytes available on your hard disk. It is best to create a single subdirectory for the executable programs and related data files. This will allow you to easily delete all the files related to this program when you are finished with it. In general, when running on a PC, *keep all files in the current working directory.*

The following sections give details of the operation of TMPSUB2, TSDATA, and TSPLIT.

## TMPSUB2

All input for TMPSUB2 must be placed in a data file. This file is read as the "standard input stream", so TMPSUB2 executes on MS-DOS and UNIX computers by redirecting the input file. For example, if there already exists an input data file -- say, TEST1.DAT -- one can begin a run by typing `TMPSUB2 < TEST1.DAT` Note: TMPSUB2 can be aborted at any time by simultaneously pressing CTRL and C.

### Sample run

If you have not already done so, install the TMPSUB2 program following the instructions in the README file. For example, from the directory on the hard disk where you want TMPSUB2 installed and with the diskette in drive A:, type `A:INSTALL A: .` At the present time you only need to install in response to the first question you will be asked.

During installation a program will determine the "initial unallocated memory". If the required memory is greater than this amount, follow the instructions under memory requirements below before proceeding.

Should you wish to examine the directory at this point, a DIR command should indicate the presence of at least the following files: TMPSUB2.EXE, TEST1.DAT, TEST2.DAT, and MEMREM.EXE. As mentioned above, begin the sample run by typing

```
TMPSUB2 < TEST1.DAT
```

TMPSUB2 will then (1) indicate that it is reading the data file, (2) echo the simulation title to the screen, (3) initialize the data in all cells, and (4) report the amount of unallocated memory. If there is "insufficient memory", an error message will be displayed and the run aborted. See the memory requirements section below for corrective action.

Every time TMPSUB2 completes a time step during the simulation, it displays the time (in seconds) and peak temperature (degrees C) on the screen. This allows you to monitor the progress of the simulation.

This same information is included on the list file, TEST1.LST, thus providing a permanent record of the primary value computed during the simulation. The list file also includes an echo of the input file which helps to identify the simulation and is especially useful in identifying any errors in the input which are also written to the list file.

The plot file, TEST1.PLT, contains all temperatures in the  $Y=0$  and  $Z=0$  planes at the times specified plus data to identify the simulation and the coordinate values.

### Memory requirements

TMPSUB2 has been written to handle an arbitrary number of cells up to some limit imposed by available memory or by the operating system. MS-DOS limits available random access memory (RAM, not disk memory) to 640,000 bytes which is shared by the program, the data in the program, a portion of the operating system, and perhaps various TSR (Terminate & Stay Resident) programs. TMPSUB allocates memory for its data arrays from available RAM. When there is insufficient memory to run a particular simulation, you must either make more memory available or reduce the memory required by the simulation. One way to make more memory available is to remove TSR programs, such as network connections. This usually requires rebooting the computer in such a manner that these programs are not

automatically accessed. MS-DOS 5.0 uses somewhat less memory than previous versions. See you PC consultant for assistance. Run MEMREM to determine approximately the memory available for data.

The memory required by the simulation is determined primarily by the total number of cells which in turn is determined by the values on line 4 of the data file (see below). The total number of cells can be reduced to an arbitrarily small value, but accuracy will suffer. If you must search for the number of cells than can be run on your machine, begin with a relatively small number and increase it until the unallocated memory reported by TMPSUB2 is small.

With minimal other uses of memory, TMPSUB2 is limited to less than 20,000 cells under MS-DOS. The only way to simulate more cells is to recompile TMPSUB2 for a different operating system and/or a different computer.

### Contents of TMPSUB2 Data File

line	variables	brief description
1	LIST	Name of the output file
2	PLOT	Name of the plot file
3	TITLE	Project title; echoed to output
4	NX NY NZ	number of cells in the X, Y and Z directions ( total number of cells = NX × NY × NZ )
5	NCX DX0 XW X0	X-coordinate data <sup>1</sup> : NCX number of constant length nodes in both directions from X0 DX0 length [mm] of constant length nodes XW total length [mm] of X axis X0 location of center of region of constant length nodes = initial position of peak flux from cigarette
6	NCY DY0 YW	Y-coordinate data <sup>1</sup> : NCY number of constant width nodes from Y = 0 DY0 width [mm] of constant width nodes YW total width [mm] of Y axis
7	NCZ DZ0 ZW FT	Z-coordinate data <sup>1</sup> : NCZ number of constant depth nodes from Z = 0 DZ0 width [mm] of constant depth nodes ZW total depth [mm] of Z axis FT fabric thickness [mm] <sup>2</sup>
8	SEP	Width of air gap between fabric and padding [mm]
9	E TM NCF	Fabric data: E emittance TM maximum temperature <sup>3</sup> [°C] NCF number of data points for T, K, C (NCF ≤ 10)
10	T K C	Fabric thermal properties <sup>4</sup> : T temperature [°C] K conductivity [W/mK] C specific heat [kJ/kgK] Repeat line 10 up to NCF times.

11 DV DC DA Densities:  
 DV virgin material [kg/m<sup>3</sup>]  
 DC char [kg/m<sup>3</sup>]  
 DA ash [kg/m<sup>3</sup>]

12 A N1 N2 T H Fabric non-oxidative pyrolysis data:  
 A reaction rate coefficient [1/min]  
 N1 fabric mass exponent  
 N2 oxygen concentration exponent (must be zero)  
 T activation temperature [K]  
 H heat of pyrolysis [kJ/kg]

13 A N1 N2 T H Fabric oxidative pyrolysis data:  
 A reaction rate coefficient [1/min]  
 N1 fabric mass exponent  
 N2 oxygen concentration exponent  
 T activation temperature [K]  
 H heat of pyrolysis [kJ/kg]

14 A N1 N2 T H Fabric char pyrolysis data (similar to 13)

15 E TM NCP Padding data:  
 E emittance  
 TM maximum temperature<sup>3</sup> [°C]  
 NCP number of data points for T, K, C (NCP <= 10)

16 T K C Padding thermal properties<sup>4</sup>:  
 T temperature [°C]  
 K conductivity [W/mK]  
 C specific heat [kJ/kgK]  
 Repeat line 16 up to NCP times.

17 DV DC DA Densities:  
 DV virgin material [kg/m<sup>3</sup>]  
 DC char [kg/m<sup>3</sup>]  
 DA ash [kg/m<sup>3</sup>]

18 A N1 N2 T H Padding non-oxidative pyrolysis data (similar to 12)

19 A N1 N2 T H Padding oxidative pyrolysis data (similar to 13)

20 A N1 N2 T H Padding char pyrolysis data (similar to 13)

21 BC TA TO OX Boundary & initial conditions:  
 BC 0 = adiabatic outer boundaries<sup>5</sup>,  
 1 = constant temperature outer boundaries  
 TA ambient temperature [°C]  
 TO initial substrate temperature [°C]  
 OX oxygen concentration [fraction]

22 QO V Y X+ X- Moving radiant flux distribution on surface:  
 QO peak flux [kW/m<sup>2</sup>]  
 V velocity [mm/min]  
 Y standard deviation in Y direction [mm]  
 X+ std dev in positive X direction [mm]  
 X- std dev in negative X direction [mm]

23 HC HG Heat transfer coefficients<sup>6</sup>  
 HC for quiescent air [W/m<sup>2</sup>K]  
 HG for impinging air [W/m<sup>2</sup>K]

24	dt DT TT	Simulation control: dt maximum time step [s] DT maximum temperature change [°C] TT total simulation time [s]
25	LIST I J K	Debug reports (TMPSUB2 compiled with DEBUG defined): LIST 1 = activate data dumps (default 0) I J K are the indices of the cell to be studied
26	PLOT	Time at which to write temperatures to the plot file; repeat line 26 up to 10 times.

Notes:

<sup>1</sup> The relationship between the number of nodes, number of constant size nodes, size of constant size nodes and total length of an axis must be such that the variable width nodes are increasing in size.

<sup>2</sup> The fabric thickness and the depth of the constant depth cells are related: the fabric/padding boundary must be halfway between two cells. Therefore, the fabric thickness must be 0.5, or 1.5, or 2.5, etc., times the depth of the constant depth cells, or the constant depth cells must be 2, or 2/3, or 2/5, etc. times the thickness of the fabric. The boundary between the fabric and padding must be within the region of constant depth cells.

<sup>3</sup> When the temperature of any fabric (or padding) cell reaches the "maximum" fabric (or padding) temperature, the simulation is terminated.

<sup>4</sup> The way that  $k(T)$  and  $c(T)$  are input is by entering the values for each at a number of temperatures; the program then carries out a cubic spline fit to those points, to obtain the values at any other temperature. Even if  $k(T)$  and  $c(T)$  are given by explicit equations, this is still the way that the program "knows" the values.

<sup>5</sup> The "outer boundaries" of the substrate consist of the  $X=0$ ,  $X=XW$ ,  $Y=YW$ , and  $Z=ZW$  planes (see items 5, 6, & 7).

<sup>6</sup> These coefficients refer to cases A and B in section 2f. When using HC set HG to zero and vice versa.

The contents of the data file are described further in the description of the TSDATA program. It will generally be easier to check a data file by processing it with TSDATA, than to compare it line by line with the description given above.

## TSDATA

The TMPSUB2 data file can be created with any ASCII line editor. However, the contents of the file are quite cryptic and thus prone to error; far better is to use TSDATA. TSDATA is an interactive program for creating data files. Because it is interactive, it uses certain commands which restrict its operation to IBM PC compatible computers. It includes extensive checking of the input data. TSDATA is especially useful for creating a data file which is only slightly different from another data file. This is useful in performing the parametric studies for which TMPSUB2 was designed.

Two special files are used by TSDATA. The help file, TSDATA.HLP, contains the text of the interactive help messages. Help is activated by pressing the F1 function key. If the help file is not available in the current working directory, no interactive help will be available. The configuration file, TSDATA.CFG, sets the colors of the display. The file included on the distribution diskette assumes that a standard VGA monitor is being used. If the configuration file is not in the current working directory, a set of default colors will be used. A new configuration file can be made by using the MAKECFG program. See the README file for instructions.

The operation of TSDATA is explained on the following pages which show the messages and input screens which will appear as the program is run. After reading through these pages, try using TSDATA with one of the sample data files. Begin the program by typing TSDATA. Abort the program by pressing CTRL and C.

### Sample Runs

At this point the following files should be available in the current working directory: TSDATA.EXE, TSDATA.HLP, TSDATA.CFG, and TEST1.DAT. If they are not, use the INSTALL procedure.

First use TSDATA to view the contents of the TEST1.DAT file. Type TSDATA. Press ENTER until the main menu appears; press ENTER again to set up the file information. Enter TEST1.DAT as the name of the previous data file. Press ENTER to cycle through file names (respond Y to the warning message about a duplicate file). Press ESC to return to the main menu. Press ENTER to view each section of data in turn; press ESC to return. When you reach the Save option, press CTRL and C to abort the program. This process will not have changed TEST1.DAT.

Now create a new data file, TEST3.DAT, similar to TEST1.DAT but with a peak flux of  $20\text{kW/m}^2$ . Proceed as above until you reach "Name of new data file:". At this point move the cursor to the "1" in the file name and press 3 and then press ENTER. Revise the other two file names and the title accordingly. Press ESC to return to the main menu, and move to the boundary conditions option. Press ENTER and move (using cursor keys) to the peak heat flux. Change the value to 20, press ENTER, press ESC. Now enter the save option, and respond Y to save the file TEST3.DAT. Then enter the exit option, respond Y to exit, and respond Y to create a batch file. After this you should have exited TSDATA. Now type RUN to start TMPSUB2 using TEST3.DAT as input data.

## TSDATA Input Screens and Help Messages

Standard title page with disclaimer at start of TSDATA program.

=====

TSDATA -- interactive program to prepare data files for TMPSUB2  
Version 1.0

Developed at the National Institute of Standards and Technology.  
Program author: George Walton

This program is furnished by the government and is accepted by any recipient with the express understanding that the United States Government makes no warranty, expressed or implied, concerning the accuracy, completeness, reliability, usability, or suitability for any particular purpose of the information and data contained in this program or furnished in connection therewith, and the United States shall be under no liability whatsoever to any person by reason of any use made thereof. This program belongs to the government. Therefore, the recipient further agrees not to assert any proprietary rights therein or to represent this program to anyone as other than a government program.

=====

### General description of input process:

=====

This program assists you in preparing input data files for the TMPSUB2 program. It operates best by reading an existing TMPSUB2 data file which is then modified to create a new data file. A sample data file is distributed with the program. It can also be used to enter data from scratch. Several data files can be created in one TSDATA session.

Data are processed interactively through a system of data entry menus. Keyboard input is required from the user whenever the cursor is in a data entry field. A data entry field is designated by a special color as is shown in the lower right corner of this screen. This is a standard pause allowing the user to read the screen. Pressing any key in response will allow the program to continue.

While the cursor is in a data entry field, it will often be possible to get help by pressing the F1 function key. Help is intended to give additional information about the data. For help to work, the TSDATA.HLP file must be in the same directory as the TSDATA.EXE file. Program execution may be terminated when the cursor is in a data entry field by pressing CTRL and C simultaneously.

=====

General description (continued):

=====  
There will usually be several data entry fields on a single screen. The field may be blank or it may present a default response. The contents of a data entry field (even all blank) may be edited. That is, characters may be overwritten, deleted, or inserted. It may or may not be necessary to make an entry depending on context.

These fields are ordered from top to bottom and left to right. Pressing the tab key or the down-arrow key moves the cursor to the next field to the right/down; The shifted-tab or up-arrow moves to the previous field to left/up. Control-home or page-up moves the cursor to the first field on the screen. Control-end or page-down moves to the last field. Movement between fields can be done only if an entry is not required and no other keys have been pressed.

Data entry begins in the exchange mode, i.e. the value of the key pressed replaces the character at the cursor. Pressing the insert key will switch to the insert mode (and from insert to exchange). The delete key will remove the character at the cursor. Control-x will clear the entire data entry field. Move the cursor left with the left-arrow, control-left-arrow, or home keys. Move the cursor right with the right-arrow, control-right-arrow, or end keys. When the data is satisfactory, press the ENTER key.

=====  
Various checks are usually made on each data entry. These may produce a warning or error message at the bottom of the screen. The first line of this message indicates the nature of the problem. The second line indicates the severity of the problem, the file and line in the TSDATA source code where the error message originated, and whether some help may be available by pressing the F1 key.

Most errors will return you to the data entry field to correct the input. Such errors include invalid characters or numeric values outside certain situation-dependent limits.

Some problems may generate a question:

Question? (y/n) █

The user can press the Y and then ENTER keys to indicate a positive (yes) response or N and then ENTER to indicate a negative (no) response.

Some errors are fatal causing the program to terminate.  
=====

Screen 1: (primary menu)

=====

TMPSUB2 data preparation:

- █ File information
- █ Geometry description
- █ Fabric data
- █ Padding data
- █ Boundary conditions
- █ Simulation control
- █ Save this data file
- █ Exit data preparation

Use cursor keys to move between menu selections.  
Press ENTER to activate the menu selection at the X.  
Press ESC to return from a selection. Press F1 for help.

=====

General help message:

This program assists you in preparing input data files for the TMPSUB2 program.

This is the main menu. It directs you to the different data preparation subsections.

Begin each data file by entering the "file information".

Data relating to the geometry, fabric, padding, or boundary conditions may be entered or changed in any order.

The data file is not created until you "save this data file".

Multiple data files can be created in one interactive session. Terminate the session by entering "exit data preparation".

Note:

An X appears in the selection designator: █.



## Help messages in response to error messages:

### (1) could not open file:

The file which you specified was not found. A typing error is the most likely problem, or the file is not in the current directory.

### (2) duplicate file names:

This message indicates that a file name matches one in the local directory, or one previously set in this session, or that you have not pressed ENTER at each of the file names to complete the check of file names.

If you have copied an existing data file, the "new" file names are the ones that appeared in the existing data file.

Files should generally have different names. For example, consecutive TMP SUB2 runs with the same plot file names will save only the plot file from the last run (which will have replaced the previous plot files). Use identical names if you definitely want to replace existing files, including data files.

You may use a duplicate file name by responding 'Y' to the question about writing over the previous file.

## Notes:

An entry for the previous data file causes its data to be copied.

The new data file will be created when "save this data file" is executed at the main menu. This save adds the new data, list and plot file names to the list displayed at the bottom of this screen.

There should be no duplicate file names. That would cause files to be overwritten during simulation. The program checks for duplicates.

The simulation title is echoed in the output files.

Note that upon entering the "Title for this simulation," the cursor jumps back to the first box and blanks it out. This is done only so that if the user has changed his mind (or an error has been made), new (or corrected) entries can be made immediately. If there has been no error, then simply press ESC.

Screen 3:

```

=====
Geometric description:                press ESC when done;  press F1 for help.

Fabric thickness:  [ ] mm
Width of air gap:  [ ] mm

X-coordinate data:
  Number of grid points: [ ] Rx = 1.xxx
  Total length of substrate: [ ] mm
  Size of constant length cells: [ ] mm
  Number of constant length cells: [ ]

Y-coordinate data:
  Number of grid points: [ ] Ry = 1.xxx
  Half-width of substrate: [ ] mm
  Size of constant width cells: [ ] mm
  Number of constant width cells: [ ]

Z-coordinate data:
  Number of grid points: [ ] Rz = 1.xxx
  Total depth of substrate: [ ] mm
  Size of constant depth cells: [ ] mm
  Number of constant depth cells: [ ]
                                     cells: xxxxx
=====

```

General help message:

The substrate consists of a thin fabric, padding, and possibly an air gap between them. An air gap width of 0.0 indicates no gap.

The X direction is along the cigarette; the Y direction is along the fabric; the Z direction is into the padding.

A variable grid is used. It consists of several constant width cells near the point of peak incident heat flux followed by increasingly larger cells out to the boundaries of the substrate. For example:



Each variable width cell is R times longer than the preceding cell. Simulation is most accurate when R is only slightly greater than one. A value of R less than about 1.25 should be sufficiently accurate. Simulation will generally involve a trade-off of accuracy and run time.

The fabric thickness and the depth of the constant depth cells are related: the fabric/padding boundary must be halfway between two cells. Therefore, the fabric thickness must be 0.5, or 1.5, or 2.5, etc., times the depth of the constant depth cells.

Other help messages:

For the X-axis the following conditions should apply:

$$4 * NCX < NX \quad \text{and} \quad (NX - 1) * DX0 \leq XW$$

where NX = number of grid points, XW = total length of substrate,  
DX0 = size of const length cells, & NCX = number of const length cells.

For the Y-axis the following conditions should apply:

$$2 * NCY < NY \quad \text{and} \quad (NY - 1) * DY0 \leq YW$$

where  $NY$  = number of grid points,  $2YW$  = total width of substrate,

$DY0$  = size of const width cells, &  $NCY$  = number of const width cells.

Because of the assumed bilateral symmetry of the flux, it is only necessary to make calculations between  $y = 0$  and  $y = YW$  (half the width). The number of constant-width cells is that in the half-width section.

For the Z-axis the following conditions should apply:

$$2 * NCZ < NZ \quad \text{and} \quad (NZ - 1) * DZ0 \leq ZW$$

where  $NZ$  = number of grid points,  $ZW$  = total depth of substrate,

$DZ0$  = size of const depth cells, &  $NCZ$  = number of const depth cells.

The fabric thickness and the depth of the constant depth cells are related: the fabric/padding boundary must be halfway between two cells. Therefore, the fabric thickness must be 0.5 or 1.5 or 2.5 etc., times the depth of the constant depth cells, or the constant depth cells must be 2 or 2/3 or 2/5 etc. times the thickness of the fabric.

The boundary between the fabric and padding must be within the region of constant depth cells.

Notes:

" $R_x$ ", " $R_y$ ", and " $R_z$ " are the geometric progression rates. The sample problems have a relatively high value in the Z direction. Tests have indicated this is satisfactory because the low conductivity of the padding permits less heat transfer in this direction.

"cells:" gives the total number of cells used to model the substrate. It equals  $NX \times NY \times NZ$ . This value is critical to the total memory required for a simulation.

The following figure illustrates the substrate coordinate system and the variable grid:

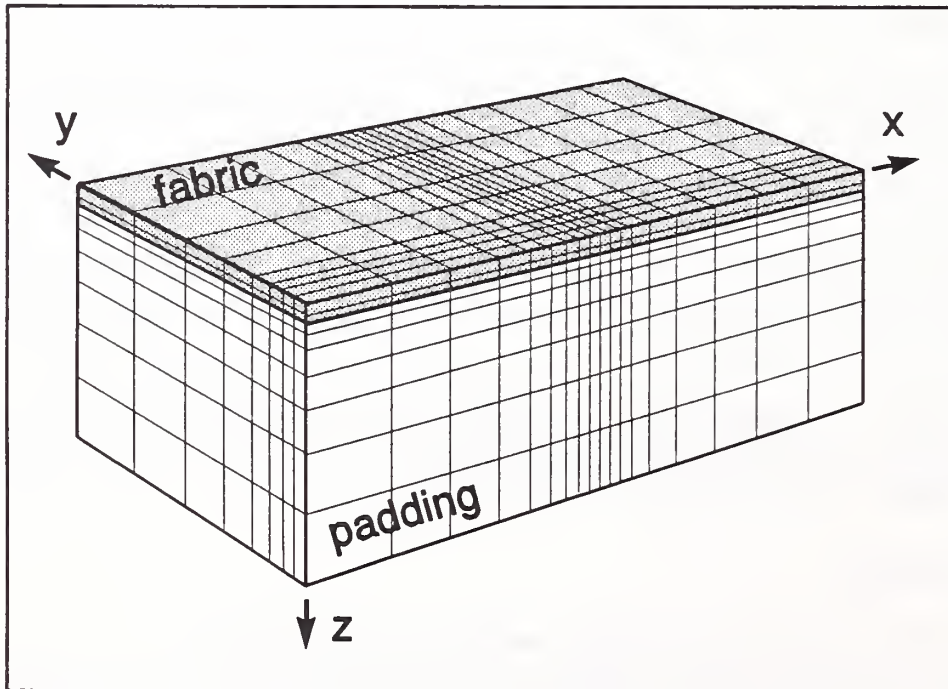


Figure B2. Substrate Coordinate System and Variable Grid

Screen 4:

```
=====
Fabric Properties:                press ESC when done;  press F1 for help.
Emittance: [REDACTED]           Maximum temperature: [REDACTED] °C

#      T [°C]      K [W/m-K]      C [kJ/kg-K]
1      [REDACTED]  [REDACTED]      [REDACTED]
2      [REDACTED]  [REDACTED]      [REDACTED]
3      [REDACTED]  [REDACTED]      [REDACTED]
4      [REDACTED]  [REDACTED]      [REDACTED]
5      [REDACTED]  [REDACTED]      [REDACTED]
6      [REDACTED]  [REDACTED]      [REDACTED]
7      [REDACTED]  [REDACTED]      [REDACTED]
8      [REDACTED]  [REDACTED]      [REDACTED]
9      [REDACTED]  [REDACTED]      [REDACTED]
10     [REDACTED]  [REDACTED]      [REDACTED]

Densities: ( kg/m3 )
Virgin material: [REDACTED]   char: [REDACTED]   ash: [REDACTED]

Reactions:
#      A      n1      n2      Ta      Hc
1      [REDACTED]  [REDACTED]  [REDACTED]  [REDACTED]  [REDACTED]
2      [REDACTED]  [REDACTED]  [REDACTED]  [REDACTED]  [REDACTED]
3      [REDACTED]  [REDACTED]  [REDACTED]  [REDACTED]  [REDACTED]
=====
```

General help message:

Emittance is used in computing radiant heat loss from the fabric to ambient and radiant heat transfer across the air gap.

The simulation stops when the temperature of any fabric cell reaches the prescribed maximum temperature.

Thermal conductivity (K) and heat capacity (C) can be specified at up to 10 temperatures. TMPSUB2 uses a cubic spline curve fit for K and C. As fabric mass is lost by pyrolysis, K is also reduced in proportion to the current density. Values are required at least two temperatures even if K and C are constant.

A two-stage, three-reaction pyrolysis model is used: the virgin material is converted to char in stage 1 and then to ash. The char density is the value for completely converting the virgin material to char with no conversion to ash. The ash density is what's left after total pyrolysis.

The pyrolysis equations are of the form:

$$R = A * Dm^{n1} * Cx^{n2} * \exp( Ta/T ) \quad \text{and} \quad Q = R * Hc$$

where

- R = rate of pyrolysis
- A = reaction coefficient [1/min]
- Dm = density of material (virgin or char )
- n1 = related exponent
- Cx = oxygen concentration
- n2 = related exponent
- Ta = activation temperature [°K]
- T = current cell temperature [°K]
- Hc = heat of pyrolysis [kJ/kg]

The first reaction is thermal degradation (n2 = 0 and Hc < 0) of virgin material. The second reaction is oxidation of the virgin material. These two reactions produce char. The third reaction is oxidation of the char to produce ash.

Help message in response to error message:

Temperatures must be given in increasing order.  
The lowest temperature should be several degrees less than any possible substrate temperature. The highest temperature should be several degrees higher than the maximum temperature.

```
=====
Screen 5:
=====
Padding Properties:                press ESC when done;  press F1 for help.
Emittance: ██████████             Maximum temperature: ██████████ °C

#      T [°C]      K [W/mK]      C [kJ/kgK]
1      ██████████ ██████████ ██████████
2      ██████████ ██████████ ██████████
3      ██████████ ██████████ ██████████
4      ██████████ ██████████ ██████████
5      ██████████ ██████████ ██████████
6      ██████████ ██████████ ██████████
7      ██████████ ██████████ ██████████
8      ██████████ ██████████ ██████████
9      ██████████ ██████████ ██████████
10     ██████████ ██████████ ██████████

Densities: ( kg/m³ )
Virgin material: ██████████ char: ██████████ ash: ██████████

Reactions:
#      A      n1      n2      Ta      Hc
1      ██████████ ██████████ ██████████ ██████████ ██████████
2      ██████████ ██████████ ██████████ ██████████ ██████████
3      ██████████ ██████████ ██████████ ██████████ ██████████
=====
```

Padding help messages are similar to fabric messages.

Screen 6:

```
=====
Boundary Conditions:                press ESC when done;  press F1 for help.
At X=0, X=Xmax, Y=Ymax, Z=Zmax: ( ) adiabatic
                                ( ) constant temperature

Initial substrate temperature: [ ] °C
Ambient temperature:           [ ] °C
Oxygen mass fraction:          [ ]

Heat transfer coefficients:
  Quiescent air: [ ] W/m²K
  Impinging air:  [ ] W/m²K

Moving heat flux pattern from the cigarette:
  Peak heat flux: [ ] kW/m²
  Initial X position of peak: [ ] mm
  +X velocity: [ ] mm/min
  ±Y standard deviation (A): [ ] mm
  +X standard deviation (B): [ ] mm
  -X standard deviation (C): [ ] mm
=====
```

General help message:

Select the condition of the outer boundaries (X=0, X=length, Y=width, Z=depth) by pressing ENTER in the appropriate place.

The incident heat flux from the cigarette is represented by a moving flux distribution on the surface of the substrate. This distribution has the shape of non-symmetric Gaussian curve which is described by 6 parameters:

- (1) the X coordinate at the peak of the curve at the start of the simulation { the initial position of the peak is (Xo, 0, 0) },
- (2) the speed, S, at which the peak moves along the X axis { the position P of the peak at time t is (Xo+S\*t, 0, 0) },
- (3) the maximum heat flux at the peak { at position (P, 0, 0) },
- (4) the width of the curve in the Y direction { at position (P, ±A, 0), the heat flux is 0.37 times the flux at the peak },
- (5) the width of the curve in front of the peak { at position (P+B, 0, 0), the heat flux is 0.37 times the flux at the peak }, and
- (6) the width of the curve behind the peak { at position (P-C, 0, 0), the heat flux is 0.37 times the flux at the peak }.

Screen 7:

```
=====
Simulation Control:                press ESC when done;  press F1 for help.

Maximum time step: ██████████ s
Maximum temperature change: ██████████ °C
Total simulation time: ██████████ s

Plot times (s):
1 ██████████ s
2 ██████████ s
3 ██████████ s
4 ██████████ s
5 ██████████ s
6 ██████████ s
7 ██████████ s
8 ██████████ s
9 ██████████ s
10 ██████████ s
=====
```

General help message:

TMPSUB2 uses a variable time step which is chosen so as not to exceed the maximum time step given and so that the maximum temperature change in any cell is not greater than the maximum given. This allows the program to run quickly when the temperatures are not changing rapidly. Smaller values for these two parameters will lead to more accurate simulations at the cost of longer execution times.

The simulation will stop at the total simulation time unless it has already stopped by exceeding a maximum fabric or padding temperature.

Plot times are entered in increasing order. When the simulation reaches a plot time, substrate temperatures are copied to the plot file. Leave later positions blank if you do not want to use all 10 times. A plot is automatically written when the simulation stops. The last plot time should be greater than the simulation time to satisfy a requirement in the TMPSUB2 program.

Screen 8:

```
=====
Save this data file? (y/n) █
display any error message(s).
=====
```

General help message:

If you entered this area accidentally and are not ready to stop preparing the current data file, respond 'N' to this question. This will return you to the main menu.

Help messages in response to error message:

(1) check data.

Data in the indicated section may be incomplete or incorrect. Enter that section and check the data.

(2) temperature problem.

The lowest temperature for fabric or padding thermal properties must be several degrees lower than either the initial or ambient temperature. You need to change (at least) one of those values.

(3) files limit.

No more TMPSUB2 data files can be created in this session. You probably should exit TSDATA now. You may replace one of the data files already created.

Screen 9:

```
=====
Exit data preparation? (y/n) █ (1)
display error messages, if applicable (2)
prepare DOS batch file to run all cases (y/n)? █ (3)
=====
```

Help messages:

(1) initial message.

If you entered this area accidentally and are not ready to stop preparing data files, answer 'N' to this question.

(2) error messages.

This warning indicates that TSDATA may have data which you have not saved. If you respond 'Y' to the question about checking this data file, you are returned to the main menu where you can check and then save the file. If you respond 'N', you will continue to exit the TSDATA program.

(3) batch file message.

A positive response will create a file RUN.BAT resembling:

```
TMPSUB2 <datafile.1
TMPSUB2 <datafile.2
TMPSUB2 <datafile.3
TMPSUB2 <datafile.4
```

This file can be used to run TMPSUB2 on computers using MS-DOS.

Notes:

Message (1) appears automatically.

Error message (2) may appear.

Message (3) appears after a Y to question (1).

## TSPLOT

The TSPLOT program will display contour plots of substrate temperatures on the screen. It is an interactive program which uses the plot file from TMPSUB2 as input. Because it is interactive and graphic, it uses certain commands which restrict its operation to IBM PC compatible computers. A plot file contains the substrate surface ( $Z = 0$  plane) and center-plane ( $Y = 0$  plane, see fig B2) temperatures at various times set in the input data file.

Three special files are used by TSPLOT. The CHRSET.VGA file contains the bit patterns for the graphic display. This file is required. The help file, TSPLOT.HLP, contains the text of the interactive help messages. Help is activated by pressing the F1 function key. If the help file is not available in the current working directory, no interactive help will be available. The configuration file, TSPLOT.CFG, sets the colors of the display. The file included on the distribution diskette assumes that a standard VGA monitor is being used. If the configuration is not in the current working directory, a set of default colors will be used. These colors may not provide satisfactory contour plots. A new configuration file can be made by using the MAKECFG program. See the README file for instructions.

The operation of TSPLOT is briefly explained on the following page. Because the screen interface is similar to TSDATA and relatively few options are available, a detailed description should not be necessary. After reading this description, try using TSPLOT with the sample plot files. Begin the program by typing TSPLOT. Abort the program by pressing CTRL and C.

### Sample Run

At this point the following files should be available in the current working directory: TSPLOT.EXE, CHRSET.VGA, TSPLOT.HLP, TSPLOT.CFG, TEST1.PLT, and TEST2.PLT. If they are not, use the INSTALL procedure. If you ran TEST1 or TEST2 and aborted before completion, use INSTALL to replace the plot files with the original complete versions.

Type TSPLOT. Press ENTER until the main menu appears; press ENTER again to get the plot file. Enter TEST1.PLT as the name of the plot file. After returning to the main menu, press ENTER to display the next plot. Note that this plot is for  $t = 1$  second, and the pattern is rather small. After viewing this plot, press any key to return to the main menu. Move (use cursor keys) to the set display parameters option and press ENTER. Change the Xmin value from "0" to "10", press ENTER, change Xmax from "60" to "50", press ENTER, and press ESC. Now press ENTER to display the prior plot. The limits of the display have been changed, and the heated area appears larger. Press ENTER to alternate between the main menu and the next plot. In the later plots note the discontinuity in the profiles in the padding caused by the air gap. After the last plot you will arrive at the exit option. Instead of exiting, move to the get plot file option, press ENTER, and enter TEST2.PLT as the name of the plot file. Return to the main menu and display the next plot which is the first plot from TEST2.PLT. Note that the limits of the X-axis have not been reset for this new plot. As you continue by displaying successive plots note how the point of peak temperature is moving along the X-axis. When you reach the exit option, press ENTER, and respond Y to exit the program.

## TSPLOT Main Menu

This is the main menu screen. It directs you to the different options.

```
=====
TSPLOT program:
  █ Get plot file
  █ Display next plot
  █ Redisplay
  █ Set display parameters
  █ Exit
```

Use cursor keys to move between menu selections.  
Press ENTER to activate the menu selection at the X.  
Press ESC to return from a selection. Press F1 for help.  
=====

The first option is "Get plot file". You must get a (enter the name of an existing) plot file before any plots can be displayed.

The plot file is read sequentially. You may display the data at the next plot time (option two), or you may redisplay the last plot shown (option three).

The graphic display consists of three parts: the temperature scale (in °C) to the right, the substrate surface temperature contours in the upper left of the screen, and the center-plane temperatures in the lower left. In other words, the temperature contours for the  $Z=0$  and  $Y=0$  planes are displayed together as if they have been folded along the X-axis so as to both be flat on the screen. The display also shows the time and the X-axis with coordinates at the left and right edges and tic marks every millimeter.

The fourth option lets you reset the display parameters. You may set the coordinates of the left and right edges of the display. These values change both the position and the scale of the regions being displayed thus enlarging or shrinking the plot. The initial limits of the X-axis are for the entire region simulated. You may also change the temperature contours which are initially set at 25°C intervals. Changes must be made so that each temperature is always less than the one above and more than the one below. You will then probably want to redisplay the last plot.

After displaying one set of plots, you may get a new plot file without exiting this program. This is the only way to go back in time on the plot file: get the plot file again and start at the beginning.

When you reach the end of the plot file, TSPLOT automatically takes you to the exit option.

## APPENDIX C

### Analysis of numerical errors produced by having a runaway reaction rate

We have made an effort to make a fine grid in the region where the fluxes and flux gradients are high. Nevertheless, when the reaction rates become very high, the gradients will become so steep that the approximation of constant temperature and constant reaction rate within a cell becomes questionable. In this appendix, we examine the magnitude of the errors thus committed by discretization. This analysis can also serve to make appropriate corrections in the program; this has not been done here, partly because the analysis should first be generalized to the non-symmetric case (see the assumptions made just below Eq.(C1)).

Consider the heat diffusion equation, Eq.(12). Suppose we have the (correct) temperature distribution  $T(x,y,z,t)$ , with a peak at  $(x_o, y_o, z_o)$ ; the reaction rate is given by an expression such as (20) or (22). Let us simplify this form and assume that

$$R_p = R_\infty \exp(-T_A/T(r)) \quad (C1)$$

where all the preexponential factors are lumped together as the factor  $R_\infty$  and  $r \equiv (x,y,z)$  is the position vector. Consider the terms in Eq.(12); we simplify the analysis by assuming that the temperature peak lies at the cell center (i.e., at  $r_o$ ), and that the distribution is symmetric fore-and-aft. Then, since calculating  $R_p$  in that cell means calculating it at the center, and therefore the peak, that means we overestimate the reaction rate, since the rate falls off at the faces of the cell.

Symmetry implies that

$$\nabla \cdot (\kappa \nabla T) \approx \kappa \left( \frac{\partial^2 T}{\partial x^2} + \frac{\partial^2 T}{\partial y^2} + \frac{\partial^2 T}{\partial z^2} \right) \approx 3\kappa \frac{\partial^2 T}{\partial x^2} \quad (C2)$$

A second-order approximation to this derivative is

$$\nabla \cdot (\kappa \nabla T) \approx 3\kappa \frac{T_{i-1} - 2T_i + T_{i+1}}{(\Delta x)^2} \quad (C3)$$

Because of the assumed symmetry,  $T_{i-1} = T_{i+1}$ , so that we finally have

$$\nabla \cdot (\kappa \nabla T) \approx 6\kappa \frac{T_{i-1} - T_i}{(\Delta x)^2} \quad (C4)$$

Inserting this into Eq.(12), that equation becomes

$$\rho c \frac{\Delta T_{i,j,k}}{\Delta t} \approx H_c R_p(r) - 2\kappa \frac{T_{i,j,k} - T_{i-1,j,k}}{(\Delta x)^2} - \dots \quad (C5)$$

minus similar terms in  $\Delta y$  and  $\Delta z$

(as indicated by the ellipsis). Suppose further, for the sake of simplicity, that the temperature profile is Gaussian:

$$\theta(x,y,z,t) = \theta_m \exp \left[ - \frac{(x-x_o)^2 + (y-y_o)^2 + (z-z_o)^2}{\sigma^2} \right] \quad (C6)$$

where  $\theta \equiv T - T_a$

and  $T_a =$  ambient (reference) temperature.

If we redefine the origin to be at  $(x_0, y_0, z_0)$ , then

$$\theta(x, y, z, t) = \theta_m \exp(-r^2/\sigma^2) \quad (C7)$$

where  $r^2 \equiv x^2 + y^2 + z^2$ .

Then if  $x^2/\sigma^2 \ll 1$  everywhere within the cell, we can expand (C7): at the center of the cell,

$$\theta_i = \theta(r_0) = \theta_{\max} \equiv \theta_m \quad (C8)$$

and

$$\theta_{i-1} = \theta_m \exp[-(\Delta x/\sigma)^2] \approx \theta_m [1 - (\Delta x/\sigma)^2]. \quad (C9)$$

Define  $\xi = (\Delta x/\sigma)^2$ . Then

$$T_i - T_{i-1} = \theta_i - \theta_{i-1} \approx \theta_m \xi \quad (C10)$$

so that Eq.(C5) becomes

$$\rho c \frac{\Delta \theta}{\Delta t} \approx H_c R_p - \frac{2\kappa}{(\Delta x)^2} \left[ \theta_m \frac{(\Delta x)^2}{\sigma^2} \right] - \dots \quad (C11)$$

Assuming three-fold symmetry, the other two terms in (C11) are the same, and thus

$$\rho c \frac{\Delta \theta}{\Delta t} \approx H_c R_p - 6\kappa \frac{\theta_m}{\sigma^2} \quad (C12)$$

Note that the dependence on  $\Delta x$  has dropped out. Indeed, the last term is the exact diffusive loss rate, resulting from the distribution (C7).

Now let us examine the magnitude of the error made by using a finite value of  $\Delta x$ : from Eq.(C7),

$$\Delta \theta \equiv \theta_i - \theta_{i-1} = \theta_m [1 - \exp(-\xi)] \quad (C13)$$

Then expanding to the next higher order than was done in (C9),

$$\Delta \theta \approx \theta_m \xi (1 - \xi/2) \quad (C14)$$

and the second term in (C5) becomes

$$\frac{2\kappa \Delta \theta}{(\Delta x)^2} \approx \frac{2\kappa \theta_m}{\sigma^2} (1 - \xi/2) \quad (C15)$$

Thus the numerical calculation underestimates the loss rate. Since the correct heat loss rate is

$$\mathcal{L} = 6\kappa \theta_m / \sigma^2 \quad (C16)$$

and we have

$$L \equiv \frac{6\kappa \theta_m}{(\Delta x)^2} [1 - \exp(-\xi)], \quad (C17)$$

we evidently must multiply  $L$  by the ratio

$$F = \frac{\xi}{[1 - \exp(-\xi)]} \approx \frac{1}{1 - \xi/2} \quad (C18)$$

in order to get the correct loss rate  $\mathcal{L}$ .

As the temperature "runs away," the distribution becomes increasingly peaked, and  $\sigma$  declines. As it does so,  $\xi$  increases, and so, therefore, does  $F$ ; this helps to slow down, or moderate, the runaway.  $\xi$  is readily found to be

$$\xi = \ln(\theta_i/\theta_{i-1}) \quad (C21)$$

Next, consider the source term in Eqs (C5) and (C12), again. Define

$$f(x,y,z) = \exp[-T_A/T(x,y,z)] \quad (C22)$$

The correct power output in the elemental volume  $\Delta V$  is, from Eq. (C1),

$$R_p \Delta V = 8 R_m \int_0^{\Delta x/2} dx \int_0^{\Delta y/2} dy \int_0^{\Delta z/2} f(x,y,z) dz \quad (C21)$$

where we have again translated  $(x_0, y_0, z_0)$  to be at the origin, and have taken advantage of the 3-fold reflection symmetry. Again assume Eq.(C7) to hold. If  $\xi \ll 1$ , then within the cell we can Taylor expand and write

$$f(x,y,z) = \exp(-T_A/T_m) + x \left( \frac{\partial f}{\partial x} \right)_0 + \frac{x^2}{2} \left( \frac{\partial^2 f}{\partial x^2} \right)_0 + \dots \quad (C22)$$

plus similar terms in  $y$  and  $z$ .

Since the peak is at the origin,

$$\left( \frac{\partial f}{\partial x} \right)_0 = \left( \frac{\partial f}{\partial y} \right)_0 = \left( \frac{\partial f}{\partial z} \right)_0 = 0, \quad (C23)$$

and dropping the higher-order terms,

$$f(x,y,z) \approx \exp(-T_A/T_m) + \frac{x^2}{2} \left( \frac{\partial^2 f}{\partial x^2} \right)_0 + \frac{y^2}{2} \left( \frac{\partial^2 f}{\partial y^2} \right)_0 + \frac{z^2}{2} \left( \frac{\partial^2 f}{\partial z^2} \right)_0 \quad (C24)$$

We find that

$$\left( \frac{\partial^2 f}{\partial x^2} \right)_0 = -\frac{2T_A}{T_m^2} \frac{\theta_m}{\sigma^2} \exp(-T_A/T_m) \quad (C25)$$

Thus

$$f(x,y,z) \approx \exp(-T_A/T_m) \left[ 1 - \frac{T_A \theta_m}{T_m^2 \sigma^2} r^2 \right] \quad (C26)$$

and integration over the cell yields

$$R_p \Delta V \approx (\Delta x)^3 R_- f(0) \left[ 1 - \frac{T_A \theta_m}{4 T_m^2} \xi^2 \right] \quad (C27)$$

This is only valid for  $\Delta x/\sigma \ll 1$ . In that limit, however, (C26) is well approximated by

$$\bar{R}_p \approx R_- \exp(-T_A/T_m) \exp\left[-\frac{T_A \theta_m}{4 T_m^2} \xi^2\right] \quad (C28)$$

which is a reasonable first approximation to the correct integral, even when  $\Delta x/\sigma$  is not very small!

The numerical approximation is

$$R_p = R_p(r_0) \approx R_- \exp(-T_A/T_m) \quad (C29)$$

Thus (C28) shows that we must multiply this approximation by  $\exp\left[-\frac{T_A \theta_m}{4 T_m^2} \xi^2\right]$  in order to get a still better approximation to the source term.

## APPENDIX D

### Analysis of Ignition Experiment

Among the things we wish to extract from this experiment, is the heat transfer coefficient to the surface,  $h$ . Fig.16 shows the radiative and total heating fluxes to the gauge, as a function of the power input. Thus, consider the  $18 \text{ kW/m}^2$  case. Without purge flow,  $\phi_{\text{rad}}^* \approx 10 \text{ kW/m}^2$ ; with the purge flow on,  $\phi_{\text{tot}} \approx 18 \text{ kW/m}^2$ , suggesting that the convective flux is  $\phi_{\text{con}} = \phi_{\text{tot}} - \phi_{\text{rad}} = 18 - 10 = 8 \text{ kW/m}^2$ . However, when the purge flow is turned on, it cools off the heating element somewhat. How much it does so, however, is unknown. Assume that the purge flow reduces the hot-surface temperature such that  $\phi_{\text{rad}}$  is reduced to some fraction  $F$  of the original. Then

$$\phi_{\text{rad}} \approx 10F \quad (\text{D1})$$

and

$$\phi_{\text{con}} \approx 18 - 10F \quad (\text{D2})$$

At the point P, on the heater axis but at the surface being heated (5.4 mm below), the heater subtends a solid angle such that the view factor is  $\Omega$ . Hence the impinging radiative flux is

$$\phi_{\text{rad}} = \Omega \epsilon_d \sigma T_d^4 + (1 - \Omega) \sigma T_a^4 \quad (\text{D3})$$

where  $\epsilon_d$  is the emissivity of the device surface. For the particular case that was carried out, the standoff distance is 5.4 mm, while the diameter of the glowing filament is 13 mm. According to Siegel and Howell (ref [25], Appendix C), the view factor for a disk of radius  $R$ , at a point a distance  $H$  along the axis normal to the disk, is

$$\Omega = \left( \frac{H^2}{R^2} + 1 \right)^{-1} \quad (\text{D4})$$

Hence  $\Omega = 0.592$ . We also assume that  $T_a = 25^\circ\text{C} \approx 298 \text{ K}$ , and that  $\epsilon_d \approx 0.85$ . It follows from Eqs(D1) and (D3) that

$$T_d^4 = \frac{10F}{\Omega \epsilon_d \sigma} - \frac{(1 - \Omega) T_a^4}{\Omega \epsilon_d \sigma} \quad (\text{D5})$$

If  $F = 1$ , this yields  $T_d \approx 493^\circ\text{C}$ , while  $F = 0.9$  yields  $T_d = 472.5^\circ\text{C}$ . The device surface cannot be much colder than  $500^\circ\text{C}$ , since it is observed to glow red. If  $T_d = 472.5^\circ\text{C}$ , then

$$\phi_{\text{rad}} \cong 9 \text{ kW/m}^2.$$

We will assume that the factor  $F$  remains constant for all irradiations. Thus for the case  $\phi_{\text{tot}} = 25 \text{ kW/m}^2$ ,  $\phi_{\text{rad}}^* \approx 16 \text{ kW/m}^2$ , and Eq.(D5) implies that  $T_d = 840.3 \text{ K} = 567.1^\circ\text{C}$ .

We proceed the same way for all four cases, and obtain the values in the first six columns of Table D1 (with fluxes given in  $\text{kW/m}^2$ ). Column 6, marked  $\phi_c$ , is the convective flux, found as the difference between  $\phi_{\text{tot}}$  and  $\phi_{\text{rad}}$ . These values of  $\phi_c$  are plotted vs  $\phi_{\text{tot}}$  and a smooth curve passed through these points, including the point at the origin. That yields the smoothed convective fluxes  $\phi_c$ , given in Col.7.

Table D1. Measured and inferred quantities from the ignition experiments.

$\phi_{\text{tot}}$	$\phi_{\text{rad}}/F$	$T_d(\text{K})$	$T_d(^{\circ}\text{C})$	$\phi_{\text{rad}}$	$\phi_c$	$\bar{\phi}_c$	hf	$T_g(\text{K})$	h	f
18	10	745.7	472.5	9.0	9.0	8.9	19.67	698	22.0	0.893
25	16	840.3	567.1	14.4	10.6	10.7	19.56	760	22.9	0.854
34.5	23	921.0	647.8	20.7	13.2	13.0	20.71	837	23.9	0.865
44	32	1000.9	727.7	28.8	15.2	15.2	21.48	907	24.8	0.866

The convective flux can be written in the form

$$\phi_c = h(T_g - T_c) \quad (\text{D6})$$

where  $T_g$  is the purge gas temperature, and  $T_c$  is the (cold) gauge temperature. In order to make progress we make one further plausible assumption: the purging gas takes up a (constant) fraction of the total energy delivered to the device. We can express this as

$$\theta_g = f\theta_d \quad (\text{D7})$$

where  $\theta$  is the temperature, referred to the gauge temperature:

$$\theta_i \equiv T_i - T_c \quad (\text{D8})$$

Thus, eqs (D6) and (D7) yield

$$\phi_c = h\theta_g = fh\theta_d \quad (\text{D9})$$

Since we have  $T_d$  (col. 4) and  $\phi_c$  (col. 7), we readily infer the factor fh from Eq.(D9). This is given as col. 8.

Next, we must find the heat transfer coefficient h for stagnant flow. The purge air comes down, strikes the fabric, and must move away radially. This configuration is approximated by the standard problem of stagnant flow. The heat transfer coefficient for this case is given in Kacaç et al (ref. [26]) ref [26].

Their Eq.(2.176), on page 2-59, gives the Nusselt number:

$$\left( \frac{Nu}{Pr^{0.4} \sqrt{Re}} \right)_w = 0.767 \left( \frac{\mu_e \rho_e}{\mu_w \rho_w} \right)^{0.43} \quad (\text{D10})$$

which was found by Cohen (ref. [27]). The subscripts w and e, above, stand for "wall" and "edge" (of the boundary layer), respectively. The second factor on the right-hand side is approximately one, in this case. The Reynolds number is

$$Re = \frac{u_{\infty} \ell_c}{\nu} \quad (D11)$$

where  $\ell_c$  is the characteristic length. One might think that the characteristic length here is the diameter of the opening. In fact, however, Cohen [27] gives  $Re$  in the form

$$Re = \frac{du_{\infty}}{dx} \frac{\ell_c^2}{\nu} \quad (D12)$$

Since the (vertical) velocity goes from  $u_{\infty}$  to zero in the distance  $\delta$ , we may write

$$\frac{du_{\infty}}{dx} \approx \frac{u_{\infty}}{\delta}; \quad (D13)$$

then Eq.(D12) indicates that the proper  $\ell_c$  to use here is  $\delta$ .  $u_{\infty}$  is readily inferred from the volumetric flow,  $dV/dt = 0.5$  liters/min. Thus

$$\dot{V} = \frac{\pi r^2 u_{\infty} \rho_g}{\rho_a} = \frac{\pi d^2 u_{\infty} T_a}{4 T_g} \quad (D14)$$

which yields

$$u_{\infty} = 6.28(T_g/T_a) \quad \text{cm/sec} \quad (D15)$$

The Nusselt number is given by

$$Nu = \frac{h \delta}{\kappa} \quad (D16)$$

where  $\delta$  is the stand-off distance between the heater and the substrate, 5.4 mm. Combining these, and knowing  $\kappa(T)$  and  $\nu(T)$  for air, we obtain  $h(T_g)$ , as shown in Fig.17. Note that this is independent of any estimates of  $F$ , the radiative and convective fluxes, etc.

We now proceed as follows: we guess a value for  $T_g$ ; corresponding to this we have  $h(T_g)$ , and we then find  $h(T_g)(T_g - T_a) \equiv \phi^*$ . We must do this until  $\phi^* = \overline{\phi_c}$ , as given in Table D1. This procedure converges quite rapidly, and we find the values of  $T_g$  and  $h(T_g)$  shown in columns 9 and 10. Finally, dividing  $hf$  by the now-known values of  $h$ , we obtain the values of  $f$  shown in col.11. There are two things to be noted about  $f$ : it is almost as large as it can get (i.e., close to unity), and it is approximately independent of  $\phi_{tot}$ .

## APPENDIX E

### Thermophysical Data for Cotton

The fabric is a weave of cotton fibers. Cotton itself is a flexible, hollow tube of cellulose; the central channel is called the *lumen*, and occupies a fraction  $\eta$  of the total volume. Thus we would expect that the density of cotton is about

$$\rho(\text{cotton}) = (1-\eta)\rho_s,$$

where  $\rho_s$  is the density of the solid (largely  $\alpha$ -cellulose). Measurements yield  $\eta = 0.2 - 0.4$ . However, ref[17] gives the following data on page V-122 (the references given there to the original authors are omitted here for brevity):

Material	Density (g/ml)
Cellulose I	1.582-1.630
Cellulose II	1.583-1.62
Cellulose III	1.61
Cotton	1.545-1.585

Thus, the density of cotton appears to be very nearly the same as that of the solid (cellulose) implying that  $\eta \approx 0$ . We will hereafter ignore the apparently small difference between  $\alpha$ -cellulose and cotton, and take the (mean) density to be  $\rho_s = 1.565 \pm 0.02$  g/ml.

For many polymers, there is only a weak dependence of the thermal conductivity on T, between 100 and 300 K (see Fig.68b, ref [25]). One can get an idea of the variability of the thermal conductivity of cotton and of cotton fabrics from Figs.AA-AC, in ref [26].

Measurements at NIST by J.R. Lawson (private communication) have shown that the density of #10 duck is  $\rho \approx 0.6$  g/cm<sup>3</sup>, that of #6 duck is 0.72 g/cm<sup>3</sup>, and that of all the other cotton duck fabrics measured is

$$\rho_f \equiv \rho(\text{fabric}) = 0.62 \text{ g/cm}^3 = 620 \text{ kg/m}^3.$$

The "void fraction" of the fabric is  $\Phi$ . With  $\rho_s = 1.565$ ,  $\rho_f = 0.62$ , and with  $\rho_a =$  density of air at STP =  $1.774 \times 10^{-3}$  g/cm<sup>3</sup>, the relationship

$$\rho_f = (1 - \Phi)\rho_s + \Phi\rho_a$$

yields  $\Phi = 0.6045$ .

Next, consider the specific heat. Again, the values given in ref [17] are:

Material	Specific Heat (J/g-K)
Cellulose	1.34
Cotton	1.22
	1.15-1.18 (0-34°C)
	1.32 (0-100°C)
	1.327-1.251
	1.273-1.35

Where the temperature range is not listed, it is assumed to be the ambient (20 or 25°C). We will thus not be far wrong if we take

$$c_s = 1.3 \text{ J/g-K},$$

where the subscript "s" stands for "solid" (cotton or  $\alpha$ -cellulose). We expect that, just as was the case for density,

$$c_f \equiv c(\text{fabric}) = \Phi c_{\text{air}} + (1 - \Phi)c_s.$$

Hence

$$c_f \approx 1.122 \text{ J/g-K}, \quad \text{at } T \approx 300\text{K}.$$

This author has not been able to find the temperature dependence  $c_s(T)$ ; we will defer that question for the moment.

Finally, we come to the thermal conductivity,  $\kappa$ . This is a quantity which is notoriously difficult to obtain accurately. Figure 18, from ref [26], shows the large variations in thermal conductivity depending on measuring conditions. Many of the low values (nos. 5, 6, and 8, for example) were measured in a vacuum. Numbers 4 and 9, on the other hand, were similar specimens, measured in air at 25°C; however, #9 had over three times the density of #4 (and would therefore have been expected to have a substantially higher thermal conductivity!).

We list here four sources for the thermal conductivity:

- a. The apparently most consistent data from [26] -- curves 1, 2, and 3, and point 7, give

$$\kappa \approx 0.0365 \text{ W/m-K} \quad \text{at } T = 306 \text{ K} = 33^\circ\text{C}$$

- b. We have the following data for cotton paper, from ref. [17]:

T (°C)	$\kappa$ (W/m-K)
30	0.049
40	0.071
50	0.084
60	0.090

A curve-fit to these points, if extrapolated, would predict that  $\kappa$  vanishes at (and below)  $T \approx 10^\circ\text{C}$ , which is nonsense.

- c. Ref [27] gives:

T (°C)	$\kappa$ (W/m-K)
0	0.056
20	0.058
100	0.067

The density of the material for these measurements is listed as  $81 \text{ kg/m}^3$ ; hence  $\Phi = 0.9493$ . Then Eq.(50) gives

$$\kappa = 0.03408\kappa_s + 0.9828\kappa_g \quad (\text{E1})$$

while the tabular data are reasonably well fitted by

$$\kappa(T) = 0.056 + 1.1 \times 10^{-4} T, \quad \text{with } T \text{ in } ^\circ\text{C} \quad (\text{E2})$$

We have  $\kappa_{\text{air}}(25^\circ\text{C}) = 0.02624 \text{ W/m-K}$ ; now if the data in the table are the conductivities for the light cotton/air mixture, then at  $20^\circ\text{C}$ , with  $\kappa_g = \kappa_{\text{air}}$ , Eq.(E1) yields  $\kappa_s = 0.945$ , which is an unreasonably large value. According to Kunii (ref [4]), the value for the gas-phase thermal conductivity to be used in Eq.(50) is 1.7 times what it is in the ambient. If we use  $\kappa_{\text{gas}} = 1.7 \times 0.02624 = 0.04461$ , the resulting value of  $\kappa_s$  is  $\kappa_s = 0.415 \text{ W/m-K}$ , still very large. If, on the other hand, the listed values are for  $\kappa_s$ , then  $\kappa_s = 0.058$  and  $\kappa_g = \kappa_a$  imply that  $\kappa = 0.0278$ , while for  $\kappa_g = 1.7\kappa_a$ ,  $\kappa = 0.0458$ . Thus none of the combinations is plausible.

d. T.J. Ohlemiller has made measurements of the thermal conductivity of the (#12) cotton duck; the apparatus only works properly when the sample is thermally thick, however. Therefore he carried out a series of measurements, with an increasing number of layers of the fabric. It was then possible to infer the asymptotic value which would be reached if the number of layers had been increased to a very large number: It was assumed that

$$\kappa(n) = \kappa_\infty [1 - \exp(-n\Theta)],$$

where  $\Theta =$  dimensionless thickness of one layer, and  $n =$  number of layers. The data were

n	$\kappa$
0	0
6	0.346
12	0.533
18	0.683

The thermal conductivity is given here in units of  $\text{BTU-in/ft}^2\text{-hr-}^\circ\text{F}$ . The asymptotic value of the series at the left is 0.9. Converted to units of  $\text{J/m-K}$ , that is  $\kappa_\infty = 0.13 \text{ J/m-K}$ .

$\kappa = 0.13$  is about twice the value (0.056) found in the Handbook, as quoted in c., just above. Recall that for this fabric, the void fraction is 0.6045. With  $\Phi = 0.6045$ , Eq.(50) gives

$$\kappa = 0.28505\kappa_s + 0.84554\kappa_{\text{gas}}$$

If we use  $\kappa_{\text{gas}} = \kappa_{\text{air}}$ , we would then infer that  $\kappa_s = 0.378$ , which is an order of magnitude greater than the earlier estimates. If we use  $\kappa_{\text{gas}} = 1.7\kappa_{\text{air}}$ , then  $\kappa = 0.13$  implies  $\kappa_s = 0.324$ , only a little smaller. The latter value is not too different from the 0.415 found in section c., above.

We thus take  
and

$$\begin{aligned} \kappa_a &\equiv \kappa_s(T_a = 25^\circ\text{C}) \approx 0.324 \quad \text{W/m-K} \\ \kappa(T_a) &\approx 0.13 \quad \text{W/m-K} \end{aligned}$$

Assuming that the temperature dependence is like that given by Eq.(E2), we find that

$$\kappa(T) = 0.125 + 2.457 \times 10^{-4} T, \quad (\text{E3})$$

with  $T$  in  $^\circ\text{C}$ . Alternatively, we might use Eq.(50) in its more general form (that is, include the temperature dependence):

$$\kappa(T) = 0.28505\kappa_s(T) + 0.84554(1.7)\kappa_{\text{air}}(T) \quad (\text{E4})$$

For air,  $\kappa(T)$  is given by Eq(52) (see ref [28]). For the solid, a reasonable assumption is that the conductivity is proportional to the absolute temperature, and that it is also proportional to the density. Thus  $\kappa_s(T)$  is given by

$$\kappa_s(T) = \kappa_s(T_a) \rho T / \rho_a T_a \cong 0.3237 \rho T / \rho_a T_a \quad (E5)$$

We now turn to the question of the **temperature dependence** of  $c_f$ . For a number of materials, the thermal diffusivity is relatively insensitive to  $T$ . This is, in particular, the case for **wood** (see [15], [16]) which consists, to a significant extent, of cellulose and related compounds. If we assume that to be the case for cotton, then we could write

$$\kappa(T) = \alpha \rho c(T); \quad (E6)$$

$c(T)$  is generally much easier to measure than  $\kappa(T)$ , and this would be a relatively good way to obtain  $\kappa(T)$ ; the irony is that we do not have  $c(T)$  for cotton or cellulose.

If we take  $\kappa_f = 0.13$  for the fabric at ambient temperature, we now find that

$$\alpha \cong \kappa / \rho c \approx 0.13 / (620)(1122) = 1.87 \times 10^{-7} \text{ m}^2/\text{s}$$

We therefore have, finally,

$$c(T) = \kappa / \rho \alpha \approx \kappa(T) / 620(1.87 \times 10^{-7}) = 8630 \kappa(T) \text{ J/kg-K}$$

where  $\kappa(T)$  is given by Eq(E3) (or by (E4), if preferred).



NIST-114A (REV. 3-90)	<b>U.S. DEPARTMENT OF COMMERCE</b> <b>NATIONAL INSTITUTE OF STANDARDS AND TECHNOLOGY</b>	1. PUBLICATION OR REPORT NUMBER NISTIR 4973 2. PERFORMING ORGANIZATION REPORT NUMBER - 3. PUBLICATION DATE NOVEMBER 1992
<b>BIBLIOGRAPHIC DATA SHEET</b>		
4. TITLE AND SUBTITLE A Computer Model of the Smoldering Ignition of Furniture		
5. AUTHOR(S) Henri E. Mitler and George Walton		
6. PERFORMING ORGANIZATION (IF JOINT OR OTHER THAN NIST, SEE INSTRUCTIONS) U.S. DEPARTMENT OF COMMERCE NATIONAL INSTITUTE OF STANDARDS AND TECHNOLOGY GAITHERSBURG, MD 20899	7. CONTRACT/GRANT NUMBER	
8. TYPE OF REPORT AND PERIOD COVERED		9. SPONSORING ORGANIZATION NAME AND COMPLETE ADDRESS (STREET, CITY, STATE, ZIP)
10. SUPPLEMENTARY NOTES		
11. ABSTRACT (A 200-WORD OR LESS FACTUAL SUMMARY OF MOST SIGNIFICANT INFORMATION. IF DOCUMENT INCLUDES A SIGNIFICANT BIBLIOGRAPHY OR LITERATURE SURVEY, MENTION IT HERE.)  <p>This paper describes a user-friendly computer model, TMPSUB2. This model calculates the temperature field throughout a solid (but porous) substrate which can undergo exothermic pyrolysis, when it is exposed to an arbitrary (localized) heat flux which can move uniformly, such as that of a smoldering cigarette. TMPSUB2 has successfully simulated the thermal runaway signifying smoldering ignition of the substrate when it is exposed to a set of external heating fluxes. The processes taken into consideration are three-dimensional heat conduction in the substrate, pyrolysis of the latter, and the diffusion of air into it at the top surface. TMPSUB2 also takes into account the fact that the substrate consists of two layers (a foam pad covered by a fabric), with the possibility of an air gap between them, up to three pyrolytic reaction steps, and with temperature-dependent thermophysical constants. TMPSUB2 solves the equations describing the physics and chemistry of the heating and ignition process numerically; the results have been compared with a set of ignition experiments, and have been found to be semi-quantitatively correct, both for the ignition temperature and for the time to ignition. Analysis of the experiments indicates that the substrate, which consists of a thin fabric layer over a thick foam padding, behaves as a thermally thin layer. Use of TMPSUB2 shows that smoldering ignition would result from a stationary hot spot of intensity and dimension simulating a quietly smoldering cigarette. A users' guide is included.</p>		
12. KEY WORDS (6 TO 12 ENTRIES; ALPHABETICAL ORDER; CAPITALIZE ONLY PROPER NAMES; AND SEPARATE KEY WORDS BY SEMICOLONS) computer models; furniture fires; ignition; mathematical modeling; pyrolysis; smoldering		
13. AVAILABILITY <input checked="" type="checkbox"/> UNLIMITED FOR OFFICIAL DISTRIBUTION. DO NOT RELEASE TO NATIONAL TECHNICAL INFORMATION SERVICE (NTIS). <input type="checkbox"/> ORDER FROM SUPERINTENDENT OF DOCUMENTS, U.S. GOVERNMENT PRINTING OFFICE, WASHINGTON, DC 20402. <input checked="" type="checkbox"/> ORDER FROM NATIONAL TECHNICAL INFORMATION SERVICE (NTIS), SPRINGFIELD, VA 22161.	14. NUMBER OF PRINTED PAGES 100 15. PRICE A05	

ELECTRONIC FORM





